University of Stavanger

Faculty of Science and Technology

MASTER THESIS

Study program/Specialization: Master of Science in Mechanical Structure and Materials Engineering / Mechanical System	Spring semester, 2021 Open access
Authors: Bishal Bhandari Raju Pant	 …… (Author's signature)
Faculty supervisor: Chandima Ratnayake Mudiyanselage, Co-Supervisor/Advisor: Sachin Bhardwaj External supervisor(s):	
Thesis Title: Thermo-Mechanical Based Residual Stress and Distortion Visualization Using Analytical, Graphical, and FEM Based Numerical Methods	
Credits (ECTS): 30	
Key words: Residual stress Abacus/CAE Weld induced residual stress Finite element analysis Thermo-mechanical analysis Shrinkage strain method	Pages: ……93…… + enclosure: 14 Stavanger, ……15/06/2021…….. Date/year

THIS PAGE IS INTENTIONALLY LEFT BLANK

Acknowledgements

We would like to express our sincere gratitude to Professor Chandima Ratnayake Mudiyanselage and Advisor Sachin Bhardwaj for their guidance and support throughout the thesis process.

It is a privilege to thank Nikolai Westlund for providing solace in this pandemic.

We thank our family and friends for giving us motivation during this period.

Abstract

The arc welding process is the main fusion welding process used in the offshore industry. This thesis attempts to understand the residual stress and distortion issues attributed to welding, and the study aims to bring a sense of value, purpose, and relevancy to academic scholarship and industrial application. Welding-induced residual stresses and distortions are prevalent in welded structures. Therefore, understanding the basic principles and theories behind the measurement of residual stress and distortion is the key to solving the issue attributed to welding. This thesis presents an overview of the welding process used in the offshore industry, general weld metallurgy, a brief introduction to the issue, and a short overview of experimental, analytical, and finite element based residual stress and distortion measurement techniques.

Residual stress and distortion issues are discussed in the simplest yet efficient way using one-bar and a three-bar model. Demonstration of longitudinal and transverse residual stress and distortions using the one-bar and three-bar model is the simplest way to visualize the inherent problem of welding.

Thermo-mechanical-based finite element analysis is performed to analyze the 2D axisymmetric plate when the prescribed temperature field is applied to the simplified quarter plate model using ABAQUS software. The result obtained from thermo-mechanical simulation is compared with the result obtained from the shrinkage strain method.

Yield level tensile residual was found along the welding centerline at the end of the heating cycle, causing a longitudinal expansion along the welding axis. At the end of the cooling process, the compressive residual of yield stress magnitude was obtained, which caused longitudinal shrinkage along the welding centerline. The shrinkage strain method showed an approximate result to that of the thermo-mechanical simulation for the case of residual stresses and shrinkage along the welding centerline. A component of transverse residual stress across the welding plate is one-fourth of the yield stress value; however, another component of stresses across the welding centerline observed was nominal. The lateral expansion was observed by thermo-mechanical simulation contrary to the transverse shrinkage observed in the shrinkage strain method.

Table of Contents

List of Tables

Table of Figures

Abbreviations

FPSO	Floating Production Storage and Offloading
FSRU	Floating Storage Regasification Unit
FSO	Floating Storage and Offloading
FDPSO	Floating Drilling Production Storage and Offloading
HAZ	Heat Affected Zone
SAW	Submerged Arc Welding
SMWA	Shielded Metal Arc Welding
GMAW	Gas Metal Arc Welding
GTAW	Gas tungsten Arc Welding
HSLA	High Steel Low Alloy
PWHT	Post Weld Heat Treatment
FZ	Fusion Zone
CGHAZ	Coarse Grain Heat Affected Zone
FGHAZ	Fine Grain Heat affected Zone
PMZ	Partially Melted Zone
AWS	American Welding Society
CM	Contour Method
HDR	Hole Drilling
HDM	Hole Drilled Material
NDT	Non-Destructive Testing
XRD	X-ray Diffraction

FEA	Finite Element Analysis
FEM	Finite Element Method
VLHS	Variable Length Heat Source
ILHS	Instantaneous Line Heat Source
MHS	Moving Heat Source
NT	Nodal Temperature

List of Symbols

$T_{liquidus}$	Liquidious temperature
$T_{solidus}$	Solidus temperature
α_w	Widmanstätten ferrite
α_a	Fcicular ferrite
α	Ferrite in microstructure, thermal diffusivity (mm^2/s) in heat conduction equation, coefficient of thermal expansion in modelling procedure
T_p	Peak temperature
q	Heat input
r	Distance from fusion boundary at the workpiece surface in mm
T_p	The peak or maximum temperature at a distance Y from the fusion boundary in Kelvin
T_o	Ambient temperature in Kelvin
e	Natural exponent (= 2.71828)
ρ	The density of a medium in kg/m^3
T	The increase in temperature above the surroundings in Kelvin
C_p	Specific heat capacity of a substance in J/KgK
h	The plate thickness of the work piece in mm
μ_x	Decreasing transverse velocity
Q	The heat flux or rate of heat flow per unit area across the surface in W/mm2
T_m	Melting point of the work piece in Kelvin

A_{c1}	Start of Austenite formation temperature
∇	Laplacian operator
A_{c3}	Complete austenite formation temperature
A_w	Cross-sectional area of weld in inch
t	the thickness of plate in inch
d	Root opening in inch
S	Transverse shrinkage
ε_x, ε_y	Elastic strain in X and Y direction respectively
R	Incompatibility function
γ_{xy}	Shear stress in xy Direction
σ_z	Residual stress
$\partial T/\partial t$	The time rate of change of temperature in the moving coordinate system in K/sec
$\partial T/ (\partial x)$	Temperature gradient with respect to distance from the point of irradiation in K/mm
V	Velocity in stressed region
V_0	Velocity in stress free region
σ	Final residual stress
θ	Temperature of the bar
θ_m	Melting point temperature
$\Delta\varepsilon$	Total measurable strain increments
$\Delta\varepsilon_e$	Elastic strain increments
$\Delta\varepsilon_p$	Plastic strain increments
$\Delta\varepsilon_t$	Thermal strain increments
$\Delta\varepsilon_{Tr}$	Phase transformation induced strain increments
S_y	Yield strength as a function of temperature
E	Young's modulus
δ	Deformation
ε	Elastic strain
K	Stress intensity Factor

Q_v	Volumetric heat flux
k	Thermal conductivity in $W.m^{-3}$
q_{conv}	Rate of convective heat transfer
h	Heat transfer coefficient
T_s	Surface temperature in k
T_∞	Surrounding temperature
$\sigma_1, \sigma_2, \sigma_2$	Principle stresses
W_p	Plastic zone size
W_p'	Shrinkage zone size
ΔT_y	Yield point temperature
S11,S22,S33	Residual stress components along, and across weld centreline, and in the shear plane
U1, U2	Displacement components along and across welding centreline
T(x)	Temperature distribution function

1 Introduction

1.1 Background

Offshore structures are widely used to produce renewable and non-renewable energies and transport goods through sea routes. Wind turbines are more focused offshore because of more uniform and high energy production than onshore structures, which have other issues such as noise generation, lower wind speed, and fluctuating wind direction. Although oil and gas production facilities are non-renewable sources, industries are expected to meet the global energy demand. The construction of ships for both the oil and gas industry and wind energy generation is essential for transporting goods to production sites. The welding process is used to join most offshore structures to obtain higher strength in joint connection, ease of fabrication facility, and productivity. Fusion welding is the most commonly used welding process to join oil and gas production, transportation facility, ship construction, and wind power generation. It is employed in the construction of jackets, tension leg platforms, guyed towers, stiffened and curved panels in oil and gas. Transportation and storage facilities such as floating storage and offloading (FSO), floating production storage and offloading (FPSO), floating drilling production storage and offloading (FDPSO), floating storage regasification unit (FSRU) use extensively fusion welding.

With the onset of the new industrial era, offshore industries focus on minimizing the cost of energy production, transportation and increasing the service life of structures. The service life of structures can be improved by using advanced materials and technology for fabrication or ensuring higher quality and meeting the relevant codes and standards. As offshore facilities are subjected to highly dynamic and harsh marine environments such as wind waves, significant pressures, etc., it is essential to either eliminate or reduce the problems associated with the proper operation of structures. Structural welds under continuous, highly fluctuating loading often fail due to fatigue. One of the main issues in offshore construction is residual stresses during manufacturing and fabrication, leading to distortion issues. Residual stress and distortions highly influence the integrity of welded structures and affect the service life of components. Weld-induced residual stress can increase the chances of brittle fracture, decrease

the buckling strength, elevate the stress corrosion cracking issues and reduce the fatigue life. Formation of transverse crack (Figure 1a), corner cracks (Figure 1b), and defects as a result of longitudinal residual stress, and buckling distortions in lightweight ship structure (Figure 1c) are illustrative examples of issues in welding science (Song, 2012). Steel is a major material for the construction of offshore structures. Steels used in offshore facilities require higher strength, toughness, weldability, corrosion resistance, and so on. Therefore, stainless steel, high strength, low alloy steel, P91 steel, and creep strength-enhanced ferritic steel have seen a wide application in offshore construction. Cold cracking in steel due to hydrogen embrittlement in some welded steel is another issue of residual stress due to welding. The distortion caused by welding can result in dimensional inaccuracies resulting in misfits, which means more time needed during fabrication, incurring higher costs. Therefore, detection, prevention, and mitigation techniques for residual stress and distortions are critical in improving weldment performance, i.e., the structure's service life.

Figure 1: (a) Transverse crack in Titanium due to butt welding, (b) Corner cracks in FPSO unit (Song, 2012), (c) Large buckling distortion (Huang et al., 2007). These figures illustrate that the complex and Multiphysics nature of welding generated issues: residual stress and distortion can lead to severe issues and may result in catastrophic failure of the structure.

1.2 Problem Statement

Steel plate is commonly used to fabricate structures offshore. Problems associated with steel weldings like residual stress and distortion are also found in the growing offshore business. Experimental techniques may not always be economically feasible even though they are highly desirable for getting precise values. Thus, analytical and finite element simulation is favored for getting plausible data with limited economic resources. Investigating different ways to determine accurate and acceptable methods of getting residual stress and distortions is necessary.

1.3 Aim and Objectives

The residual stress investigation using different methods and its prevention or mitigation can help in increasing the service life of welded structures. Therefore, we aim to establish profound knowledge on the following objectives.

- Literature review on residual stress measurement technique (experimental and numerical).
- Residual stress analysis using one-bar and three-bar model.
- Demonstration of longitudinal and transverse distortions.
- Thermo-mechanical (elastic-plastic) analysis of residual stress using a case study.
- Comparison of the thermomechanical analysis with shrinkage strain method (Linear elastic analysis).

1.4 Limitations

- The present study does not consider solid-state phase transformation effects on residual stress distribution due to welding. Rate independent material properties are mainly considered in the thermo-mechanical analysis and shrinkage method.
- A 2D axisymmetric analysis is performed for simplicity and to reduce the computational time,

- Only longitudinal and transverse residual stress components are mapped. The orthogonal component of residual stress in through-thickness direction is not considered assuming it is nominal in a simple single-pass butt-welded plate.

1.5 Thesis Outlines

- Chapter 2 aims to explain pertinent theories that are key to understanding residual stress and distortion. The chapter starts with introducing fusion welding processes employed in the offshore industry and the description of welding metallurgy. Following this, an explanation of residual stress generation, its cause and effect, and lastly, an overview of distortion issues caused by welding phenomena are exemplified. Chapter 2 is supplemented by residual stress measurement methods and their limitations.
- Chapter 3 demonstrates the one-bar model, the simplest method used to analyze and understand residual stress development in welded structures. Only one component of stress can be mapped with this model. A graphical explanation of the variation of different strains and stress is provided in the result section. Finally, the significance of those strains and stress plots is discussed.
- Another demonstration of residual stress and distortion is dealt with using the three-bar model in the fourth chapter. The tensile and compressive transverse residual stresses are mapped, and displacement due to these stresses is discussed simultaneously.
- Chapter 5 contains a case study where a temperature field is applied in a symmetrical plate, and residual stress and distortions are discussed. Firstly, thermo-mechanical (elastic-plastic) analysis is performed. Secondly, the shrinkage strain (linear-elastic) method is used to analyze the case study, and at last, the comparison is made between the result obtained from both numerical methods.
- Chapter 6 concludes the thesis, and future research prospects are mentioned.

2 Theory

2.1 Fusion Welding Process

Fusion welding is primarily used welding process in the offshore industry. In this process, the faying surfaces are joined by melting and subsequent solidification, with-or-without the use of filler metal. An electric arc, plasma, laser, electron beam, and combustion of fuel gases can produce the heat required for melting. The weldment mainly consists of three distinct regions: fusion zone, heat affected zone (HAZ), and base-metal zone. The fusion zone undergoes melting and solidification, heat affected zone experiences thermal exposure, and the base metal zone is unaffected by the welding process (DebRoy and David, 1995). Fusion zone and HAZ in steel weld microstructure are subjected to residual stresses and discussed in more detail in the welding metallurgy section. Arc welding is the most practiced welding process that uses an electric arc to heat the metal part to be joined above the melting point, thereby fusing them (Kou, 2002). Gas metal arc welding (GMAW), Submerged arc welding (SAW), Shielded metal arc welding (SMAW), and Tungsten inert gas welding (TIG) are primary fusion welding processes used in joining structures offshore and are briefly explained below.

2.1.1 Submerged Arc Welding (SAW)

Submerged arc welding derives heat from an arc between a bare metal electrode and the workpiece. Unlike other arc welding processes, the arc is covered with a granular flux (Figure 2) that adds protection from atmospheric contamination and prevents the emission of arc radiation, sparks, spatter, and fumes. The slag formed covers the weld area allowing for slow cooling, which aids in shaping the weld contour (Antonini, 2014). SAW is often characterized by a higher deposition rate, higher heat input, and larger weld beads than the gas tungsten arc and shielded metal arc processes (Suman and Biswas, 2020, Natsume et al., 1995) and is extensively used in the offshore industry to join thick steel plates, pipes and pressure vessel, either in single-pass or multi-pass welding (Karaoğlu and Seçgin, 2008). For instance, SAW welding is used to join large steel plates in shipbuilding. Suman and Biswas suggested that, unlike multi-pass submerged arc welding, the single-pass SAW process

demonstrates an even distribution of residual stresses. Therefore, single-pass SAW welding is preferable over multi-pass welding in joining creep strength enhanced ferritic (CSEF) steel. However, large weld beads and high heat inputs can sometimes lead to large nodal displacements in an FE model and require attention while numerical simulation (M.Benson, 2018).

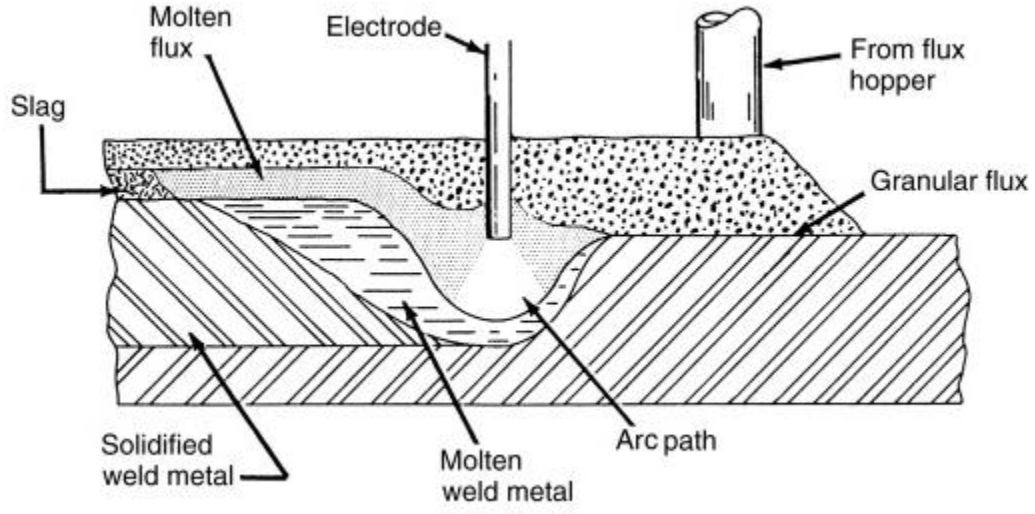

Figure 2: Schematic illustration of SAW process (Antonini, 2014).

2.1.2 Shielded Metal Arc Welding (SMAW)

Shielded metal arc welding (SMAW), also referred to as manual metal arc welding (MMAW) or stick electrode welding, is a low heat welding process. This type of fusion welding was predominant until the beginning of the 1980s. The arc is generated by striking a consumable electrode to the workpiece, and the heat of the arc melts the electrode coating to form a protective slag. The electrode consists of a wire core coated with chemicals, minerals, and iron powder (Weman, 2012). The SMAW process is used for welding steels, including low carbon or mild steels, low-alloy steels, high-strength steels, quenched and tempered steels, high-alloy steels, stainless steels, and many cast irons. Because of the higher power density available in the SMAW process, SMAW can be used to weld thicker sections above 5 mm and is preferred over oxy-fuel gas welding (Wahab, 2014). The schematic illustration of the SMAW process is shown in Figure 3.

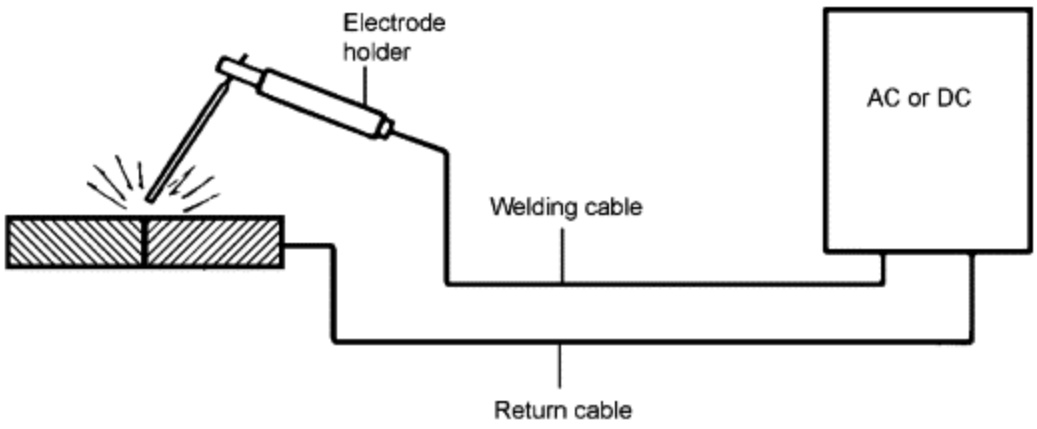

Figure 3: Schematic diagram of Shielded metal arc welding process (Weman, 2012).

2.1.3 Gas Metal Arc Welding

Gas metal arc welding (GMAW) is a high heat input welding process that uses an electric arc to produce heat and incorporates a continuous-feed consumable electrode shielded by an externally supplied gas, as shown in Figure 4 (Naidu et al., 2003). GMAW has higher efficiency than gas tungsten arc welding (GTAW) and SMAW processes due to its high operating factor and deposition rate. Though the achievement of consistent quality has proven difficult in the past, a global trend towards greater use of GMAW due to maximized economic benefits. As a result, the primary focus of growth has been on enhancing control and ensuring consistent quality (Norrish, 2006).

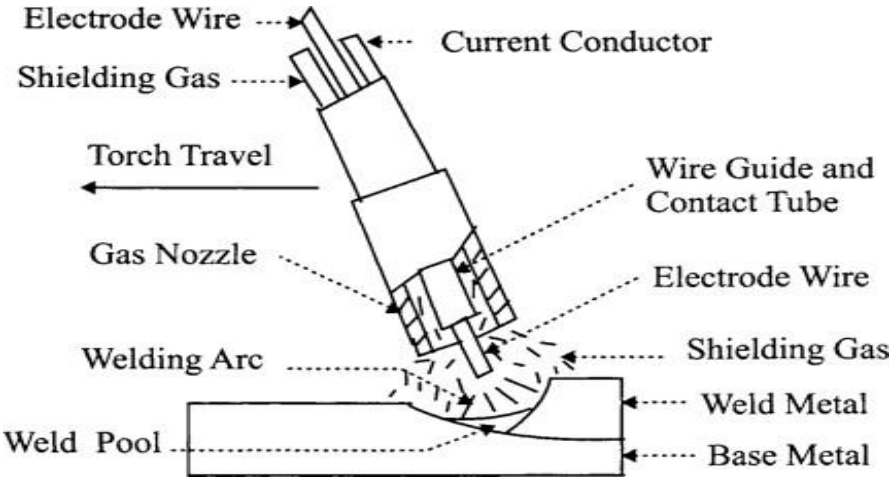

Figure 4: Schematic diagram of Gas metal arc welding (GMAW) process.

2.1.4 Gas Tungsten Arc Welding

Gas tungsten arc welding (GTAW), also called inert tungsten gas (TIG) welding, is an arc welding process where the coalescence of metal is achieved by heating with an arc between a non-consumable tungsten electrode and the base metal. A gas or gas mixture, typically helium, argon, or a combination of the two, provides the shielding in this process (Antonini, 2014). Welding thin pieces of stainless steel and light metals like aluminum, magnesium, and copper alloys are best done with GTAW. The process gives the operator more control over the welding process than other welding methods, resulting in better and more reliable welds. GTAW has the drawback of being more complicated and slower than many other welding methods (Smith, 2007).

2.2 Welding Process Selection

The weld, ideally, should achieve continuity between the part being joined in such a way that the weld joint is indistinguishable from the base metal from which it is joined. However, it is impossible to achieve such an ideal situation, but a satisfactory weld can be produced by choosing a more appropriate welding process and parameters (Khan, 2007). Some of the critical factors which must be duly considered while selecting the welding process are:

- Type of metal and its metallurgical characteristics
- Type of joint, location, and welding position
- End-use of joint and expected performance
- Joint design, accessibility, and accuracy required
- Structural size
- Cost of production

2.3 Selection of Materials

The commonly used material in the offshore application is carbon steel. Even though it has poor corrosion resistance and low service life, it provides a low maintenance cost and is easier to use in construction. The carbon-steel pipes are generally used after epoxy coatings to prevent corrosion, and different heat-treatment methods are performed to enhance their

mechanical properties. Micro alloyed HSLA steels have been widely accepted as the standard for oil and gas extraction and its transmission purpose. Its transformation characteristics in the weld heat-affected zone (HAZ), around the structural steel joint, remain unchanged and have high strength, toughness, and formability (Cochrane, 2012).

The study (Deng, 2009) suggests that residual stress and distortions in low carbon steels are less influenced by solid-state phase transformation. Thus, we have not considered microstructural changes due to welding in the thermo-mechanical analysis.

2.4 Welding Metallurgy

The heat source interactions with the metal lead to areas with differing temperatures, resulting in three distinct regions in the weldment; fusion zone, heat-affected zone, and unaffected base metal zone (David, 2003). The melting and solidification process that occurs in the fusion zone is generally described using a temperature-phase diagram (Figure 5).

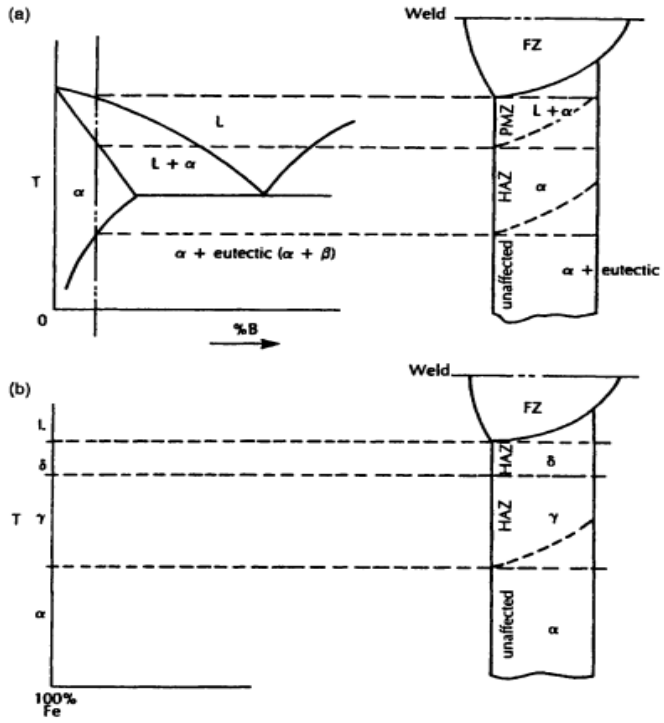

Figure 5: Schematic illustration of various zones in weldment with corresponding phase diagram for (a) alloy and (b) metal(Messler, 2008).

The area around the fusion zone is a heat-affected zone where mechanical and microstructural properties get changed without melting. The unaffected base metal zone is the area outside HAZ (M. Larsson, 2019). The temperature in this region is lower than the temperature required for tempering (Bhadeshia and Honeycombe, 2017).

However, in the case of an alloy, there is another region known as a partially melted zone where the temperature of base metal rises from the liquidus ($T_{liquidus}$) to the solidus ($T_{solidus}$) (Messler, 2008). Figure 5 shows different regions in weldment for (a) alloy (b) pure metal.

2.4.1 Fusion Zone

The welding area in metal is referred to as a fusion zone (FZ). The welding parameters such as welding speed, heat input, and heat source distribution significantly influence the fusion zone's geometry. Welding speed has a prominent effect on residual stress and weldment distortion (Gery et al., 2005, Long et al., 2009). The solidification behavior of the weld pool largely influences the microstructure development in the fusion zone, thereby affecting the shape and size of grains, segregation, and the dispersion of porosity and inclusions (David et al., 2003). The grain structure development in the fusion boundary may grow epitaxially if the base metal and weld metal have the same crystalline structure or non-epitaxially if they have different crystalline structures (Kou, 2002). Low alloy steel weld deposits follow a solidification process with epitaxial growth (Bhadeshia and Honeycombe, 2017). The primary microstructure or as-deposited microstructure in single pass weld consists of grain boundary (allotriomorphic) ferrite (α), acicular ferrite (α_a), and Widmanstätten Ferrite (α_w), as indicated in Figure 6. In addition, microphases can co-exist. Microphases means that traces of martensite, retained austenite, and degenerate pearlite are present in the primary microstructure (Bhadeshia and Svensson, 1993). The multi-pass weld microstructure is more complex as it involves reheating the original microstructure.

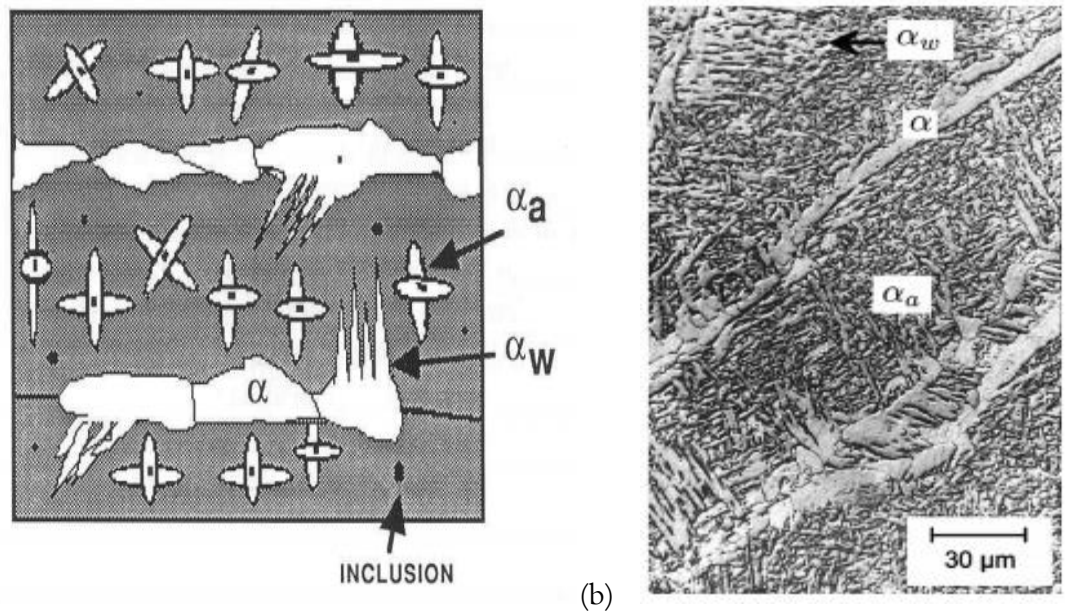

Figure 6: (a) Main constituents of Steel weld deposit (primary microstructure). The size of inclusion is much smaller than the acicular ferritic plates. Hence, inclusion is not lucidly visible on the planer section of the microstructure, (b) Scanning electron micrograph of primary microstructure (Bhadeshia and Honeycombe, 2017).

Low alloy steel, which is prominently used in welding application, has alloying elements such as carbon (C) as a significant constituent, in addition, a small amount of magnesium (Mg), chromium, molybdenum (Mo), manganese (Mn), vanadium (V), Silicon (Si), and nickel (Ni). A higher concentration of carbon (especially above 0.25%) and other alloying elements decreases the weldability of steel and increases HAZ, hardness, brittleness, and changes other properties, requiring post-weld heat treatment (PWHT). The carbon concentration alters the sensitivity of other alloy elements besides the hardenability of steel. Carbon equivalence, CE, is used to define the hardenability of steel. International institute of welding (Fujita and Nomoto, 1971) and Ito and Besseyo formulated two different expressions of CE for steels having carbon content greater than 0.18% wt. and lesser than 0.18% wt. respectively (Bhadeshia and Honeycombe, 2017).

- For carbon content >0.18 % wt. (IIW recommended expression),

$$CE = C + \frac{Mn + Si}{6} + \frac{Ni + Cu}{15} + \frac{Cr + Mo + V}{5} \qquad (2.4.1)$$

- For carbon content <0.18% wt. (Ito and Besseyo recommended expression),

$$CE = C + \frac{Si}{30} + \frac{Mn + Cu + Cr}{20} + \frac{Ni}{60} + \frac{Mo}{15} + \frac{V}{10} + 5B \quad (2.4.2)$$

The letters in the above equations (2.4.1) and (2.4.2) represent the percentage of the weight corresponding to the element (symbol of the element is used for simplicity) in steel.

2.4.2 Heat Affected Zone (HAZ)

HAZ is the area in the workpiece which has not melted. Still, its microstructure and properties are significantly changed due to the heating and subsequent cooling, i.e., the melting and solidification process. The overall weld performance is influenced by the size and shape (to a few extents) of the heat-affected zone (Messler, 2008).

2.4.2.1 Thermal Cycles

Heat input during the welding process significantly impacts the microstructure and mechanical properties of the base metal close to the weldment and heat-affected region. Changes in the microstructure may cause local brittleness in the HAZ (Shi and Han, 2008). As the distance from the fusion boundary increases, the temperature and heating rate decrease, as in Figure 7. The microstructure in the HAZ zone depends on the thermal weld cycle and the base metal chemical composition. The thermal processes in the HAZ are characterized by peak temperature (Tp) and Δt_{8-5} (cooling time required for solid-state phase transformation from austenite to ferrite, which usually occurs in the temperature range of 800 $^{\circ}$C – 500 $^{\circ}$C for many weldable steels). The cooling time and peak temperature increases with increased heat input (q) and is expressed in equation (2.4.3) and (2.4.4)

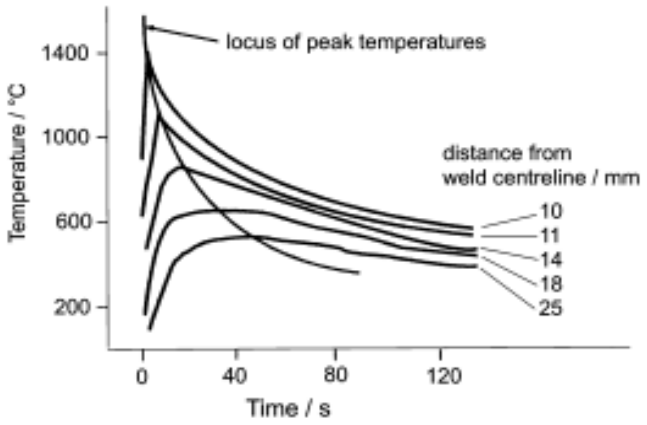

Figure 7: Temperature-time curve for the typical thermal cycle in HAZ

$$T_p \propto \frac{q}{r} \tag{2.4.3}$$

$$\Delta t_{(8-5)} \propto q^n \tag{2.4.4}$$

Where 'q' is heat input and the heat flow is either two-dimensional or three-dimensional depending on the relative thickness.

'r' is the distance from the fusion boundary, and 'n' is a constant, which depends on the thickness ratio of the weld bead to the thickness of the part being joined (Bhadeshia and Honeycombe, 2017).

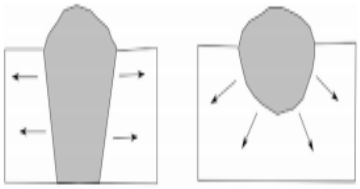

Figure 8: 2D and 3D heat flow in welding (left to right) (Bhadeshia and Honeycombe, 2017).

Equations (2.4.5) and (2.4.6) are helpful to find the size of the HAZ. From both the equation, it is seen that preheating and higher heat input leads to larger HAZ. Peak temperature for thick plate (point source) and thin plate (line source) for single-pass weld can be expressed as (Kumar, 2014):

- For thick plate (3D heat flow)

$$\frac{1}{T_p - T_o} = \frac{\sqrt{2\pi e}}{Q}\frac{\rho C_p h \mu_x r}{1} + \frac{1}{T_m - T_o} \tag{2.4.5}$$

- For thin plate (2D heat flow)

$$\frac{1}{T_p - T_o} = \frac{2\pi e \alpha k}{Q \mu_x} 2 + \left(\frac{\mu_x r}{2\alpha}\right)^2 + \frac{1}{T_m - T_o} \tag{2.4.6}$$

2.4.2.2 Cooling Rate

The cooling rate from the peak temperature during welding is solely responsible for the final weld microstructures in FZ and HAZ. When we move away from the heat source, the time required for cooling and solidification decreases, i. e. the point at the fusion boundary takes longer to cool than the point at the heat-affected zone's outer boundary shown in Figure 9.

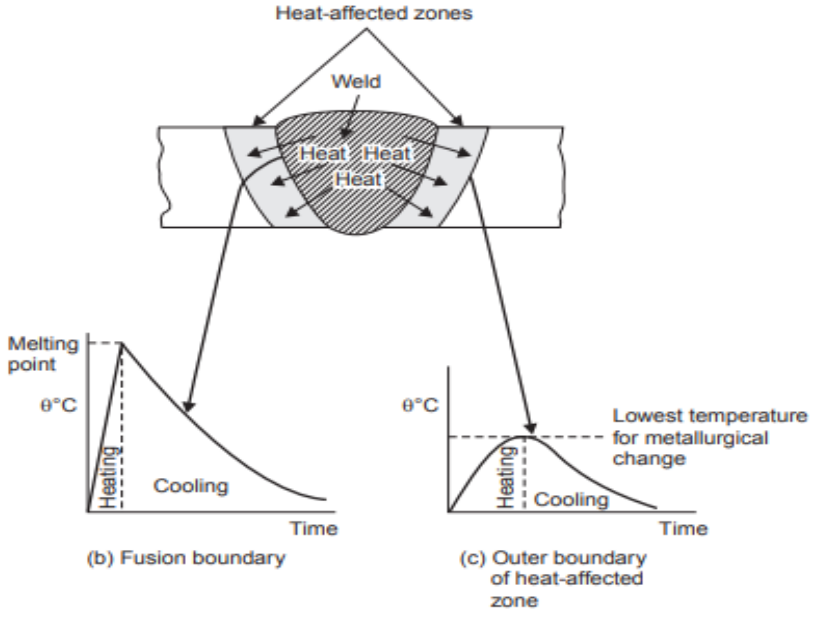

Figure 9: Variation in cooling rate as we move away from fusion boundary (Khan, 2007).

A higher cooling rate may increase susceptibility to hydrogen embrittlement in steels. Therefore, knowledge of the cooling rate is needed. In diffusion-controlled transformations,

the cooling rate influences coarseness and fineness of the final microstructure, homogeneity, and the different phase forms in the microstructure (Messler, 2008). The cooling rate can be reduced by increasing heat input, decreasing transverse velocity (μ_x), preheating or raising the initial temperature of the workpiece, decreasing plate thickness, and using a material with lower conductivity (Kumar, 2014).

2.4.2.3 HAZ Microstructure

The width of the HAZ is very narrow, consisting of several fine-grained regions with different microstructures, which change as the distance from the fusion boundary increases, as seen in Figure 10 (Shi and Han, 2008, Bhadeshia and Honeycombe, 2017). The grain growth and particle dissolution in the HAZ are dependent on the process variables such as heat input, weld speed, preheat, etc. (Ion et al., 1984, Shome, 2007, Shome et al., 2004). A process with higher heat input, such as SMAW, has a higher peak temperature and produces a coarser grain size. "The coarse grain heat-affected zone, CGHAZ, is situated next to the fusion line, and the fine grain heat-affected zone (FGHAZ) located marginally away from the fusion are closely spaced in real welds" (Shome, 2007, Li et al., 2011). Bhadeshia and Honeycombe describe the weld microstructures in the HAZ as summarized below (Bhadeshia and Honeycombe, 2017).

- The adjacent region to the fusion line experiences very high temperatures, resulting in a complete austenite transformation. The austenite formation starts at $A_{c1} \approx 800\ ^{\circ}C$, and the region becomes complete austenitic at $A_{c3} \approx 950\ ^{\circ}C$. This region usually experiences higher temperatures than the A_{c3}, thereby annealing the formed austenite, resulting in a coarser austenitic grain structure. This occurs in the peak temperature range of $1200\ ^{\circ}C$-$1500\ ^{\circ}C$.

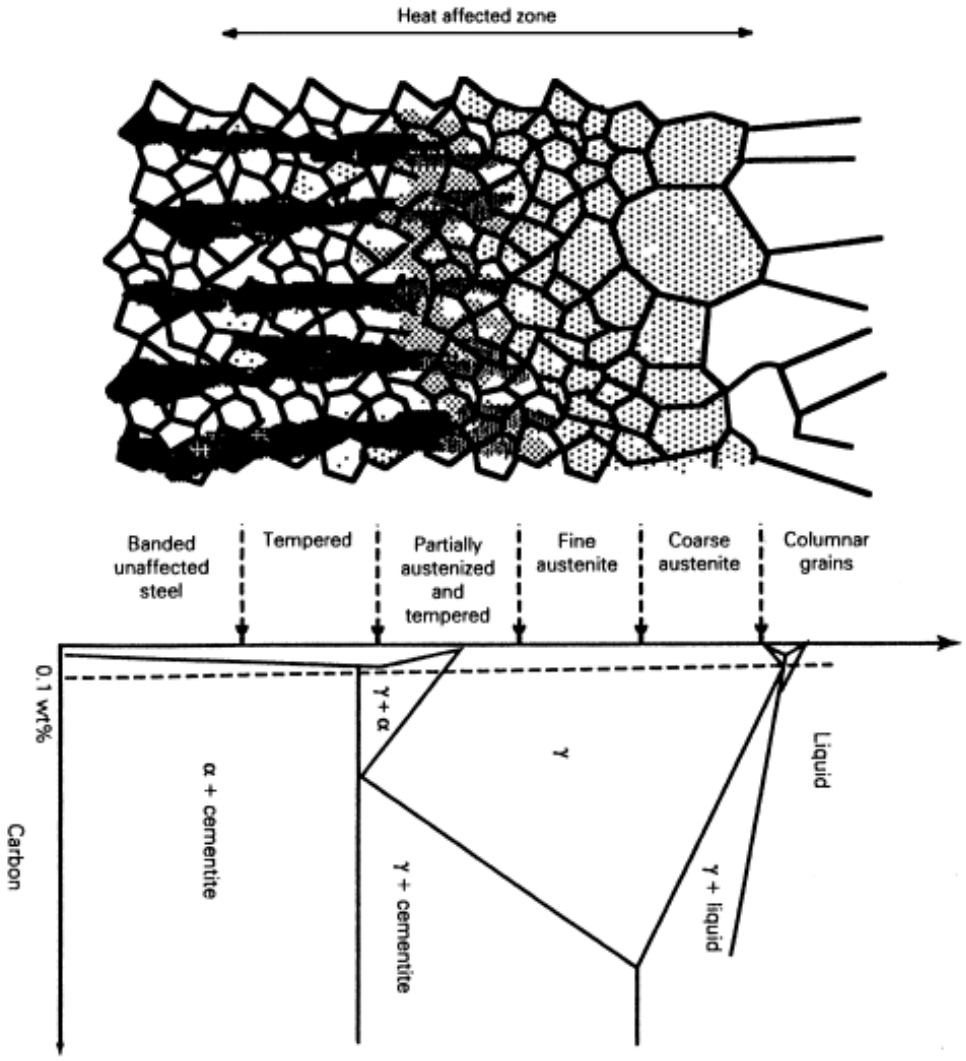

Figure 10: Schematic illustration of various regions in HAZ of steel weld (Bhadeshia and Honeycombe, 2017).

- As the distance from the fusion boundary increases, the austenite grain size decreases sharply, resulting in a fine grain structure with vibrant mechanical properties than the coarser region. Fine-grain austenite forms at 1200 $^{\circ}C > T_P > A_{c3}$.
- At $A_{c3} > T_P > A_{c1}$, a partially austenitic region forms during the heating cycle, and parts resistant to austenite formation get tempered. In this region of decreasing temperature, the austenite has a higher carbon concentration because of increased carbon solubility in γ at lower temperatures.
- If $A_{c1} > T_p$, then tempering becomes the only process. Tempering intensity decreases with an increase in the distance from the fusion boundary.

2.4.3 Partially Melted Zone

A partially melted zone only exists in an alloy where the temperature of the weldment ranges from liquidus ($T_{liquidus}$) to the solidus ($T_{solidus}$). However, there is no PMZ in the weldment of pure metal (Messler, 2008).

2.5 Residual Stresses and Distortions

Stress in a component can arise from mechanical and thermal sources. Mechanical sources can be either internal or external. Examples of external forces are; wind, earthquakes, the weight of vehicles, people on bridges, thrust on a spacecraft's fuselage, etc. The internal forces, which are also called inertial forces, are caused only by the object's weight. The thermal source is the temperature gradient present/applied in a component, leading to thermal stress or thermally induced stress (Messler, 2008). The stress present in an element can either be reaction stress or residual stress. Reaction stress represents the "overall distribution of tensile and compressive stresses" (M. Larsson, 2019). The stress left in a component (locked in stress) after removing an external source causing the stress is referred to as residual stress. The residual stress caused by an unbalanced strain, a by-product of a different process which the material is going through, is unsymmetrical in three orthogonal directions to the weld because of various restraints acting in each direction (Leggatt, 2008). It may be desirable or harmful depending upon the application and the state of the stress. For instance, the tensile residual stresses on the surface of the objects are most often detrimental, either in forming brittle fractures or abetting already formed ones from fatigue. However, compressive stresses at the surface usually increase the component's fatigue strength (Noronha et al., 1973). The tensile and residual compressive stress distribution in a butt-welded plate is shown in Figure 11.

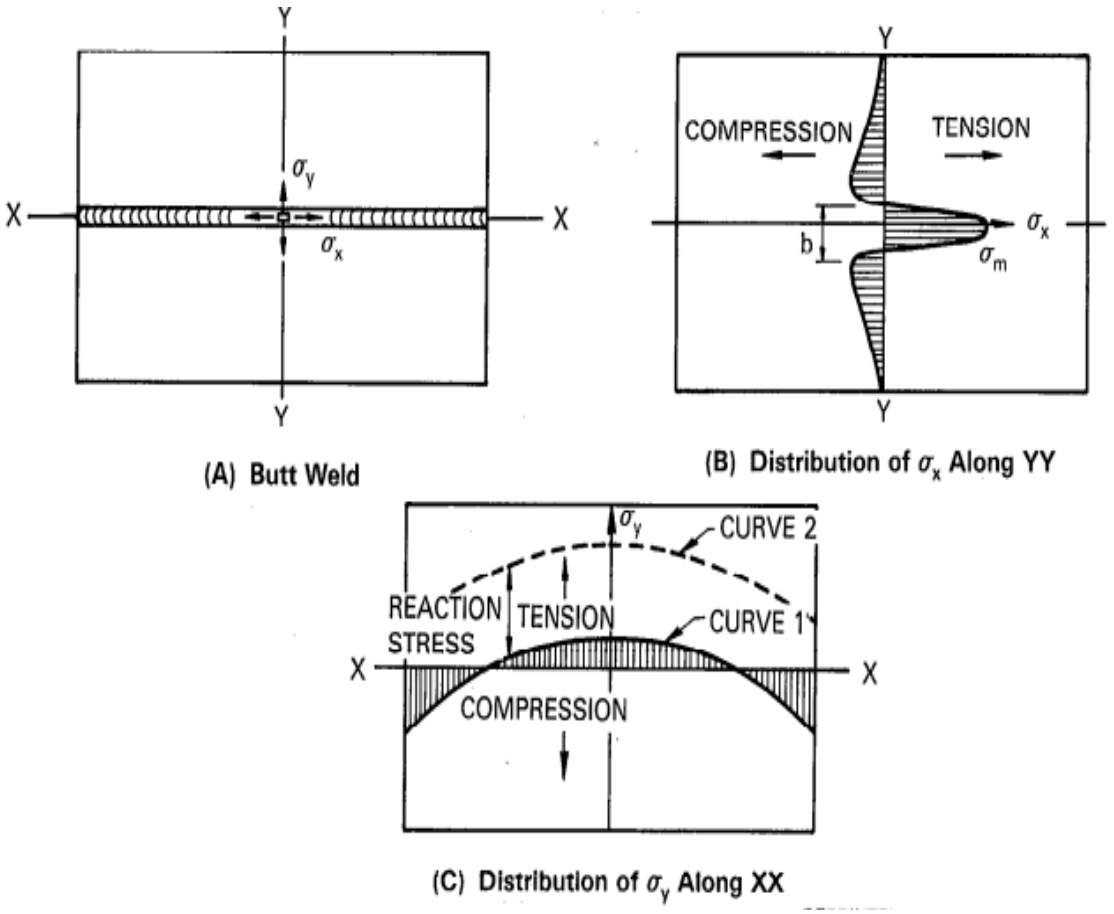

Figure 11: Distribution of residual stresses in the butt-welded plate (Connor et al., 1991).

Structural failure may occur even at lower levels of stress by buckling, caused by compressive stress, and by brittle fractures due to tensile stress. The probability of failure is higher in the presence of residual stress and distortions (Connor et al., 1991).

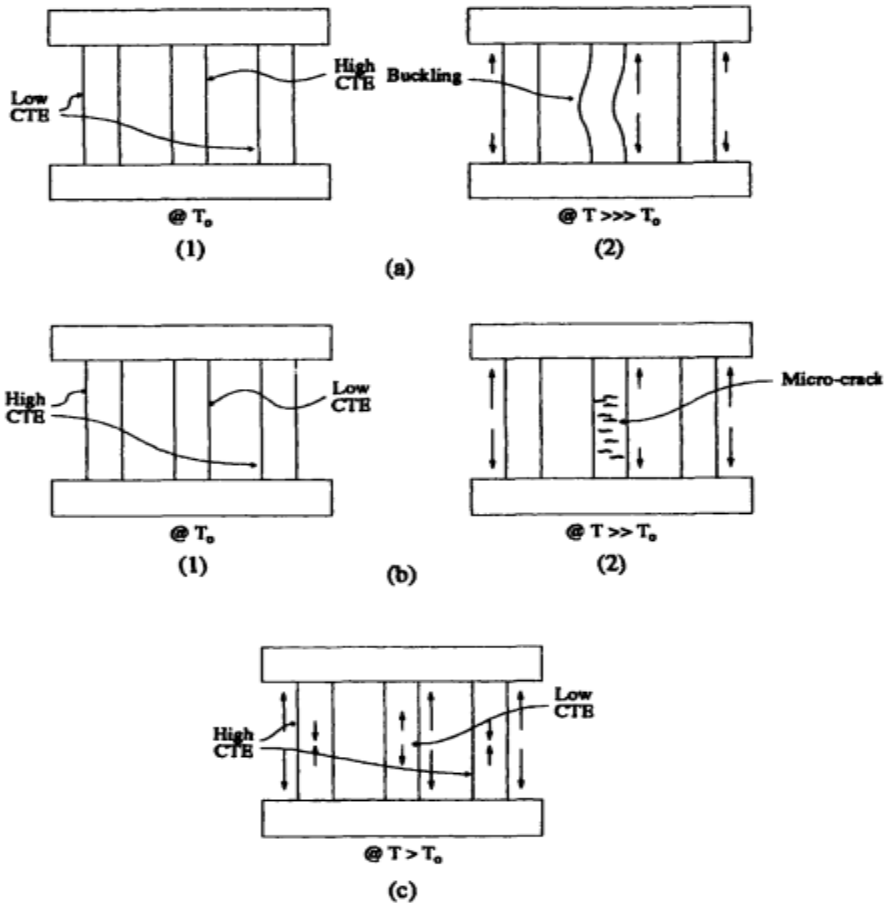

Figure 12: Thermal stresses resulting in (a) macroscopic distortions, (b) microscopic distortions, or (c) residual stresses (Messler, 2008).

Thermally and mechanically induced stress distorts the material. Welding distortion can be in-plane or out-of-plane. Rotational, transverse, and longitudinal distortion are considered in-plane distortion while buckling, angular, and longitudinal bending are considered out-of-plane distortion (Bhide et al., 2006, Pilipenko, 2001). Thermally induced stress distorts the material macroscopically or microscopically by yielding or cracking, elsewise resulting in residual stress (Figure 12). Microscopic distortion, in this case, can relieve the thermal stresses by creep (Messler, 2008). Unbalanced stresses in weld produce longitudinal and transverse shrinkage along with angular distortions, as shown in Figure 12. Longitudinal shrinkage can cause bending if the welding line deviates from the neutral axis of the workpiece. The rotational distortions during welding and the restraining conditions are the two major factors influencing transverse shrinkage in the weld. Transverse shrinkage (S) in

low alloy steel butt-weld can be calculated using the following equation (Connor et al., 1991):

$$S = 0.2 \frac{A_W}{t} + 0.05\, d \tag{2.5.1}$$

Where A_w is the cross-sectional area of weld in inches, 't' is the thickness of plate (inches), and 'd' is root opening in inches.

In fillet weld, transverse shrinkage is lesser than in butt weld and is influenced by the degree of constraints applied at the joint, joint design, root opening, and weld size (Kihara and Masubuchi, 1954, Messler, 2008). Restraining the workpiece can alter the temperature distribution and alter the distribution of residual stresses (Kohandehghan and Serajzadeh, 2011). If the backstep sequence is used in the butt-weld, then the transverse shrinkage along the weld is not uniform with the increasing number of weld passes, transverse shrinkage increases. However, the shrinkage in later passes is always lesser than the shrinkage in the first pass (Kihara and Masubuchi, 1954). A larger root opening has lesser shrinkage, and an increase in the degree of constraint results in lower transverse shrinkage. Rotational distortions caused by welding depends upon the heat input and the welding speed. The low-speed welding process (SMAW) results in the enlargement of the opening between the unwelded portion of the workpiece. In contrast, SAW welding, which has a higher welding speed, causes the opening to decrease (Masubuchi, 1960).

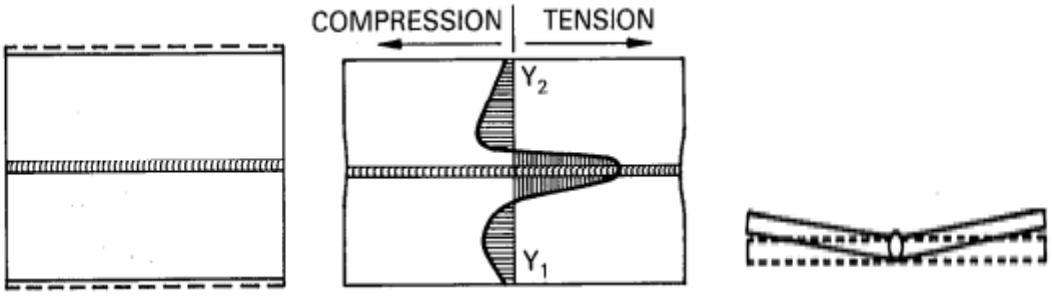

(a) (b) (c)

Figure 13: Transverse shrinkage in butt-weld, (b) longitudinal shrinkage with residual stress distribution in butt-welded plate, (c) angular distortion in butt weld (Connor et al., 1991).

Another type of distortion, buckling distortion, occurs when the length of the workpiece is higher than the critical length for a given thickness of a specific workpiece. This usually happens while welding thin plates. Unlike, buckling distortions may result in many stable deformed shapes (Figure 14).

(d)

Figure 14: Buckling distortion in a thin plate (Connor et al., 1991).

2.5.1 Residual Stresses due to Mechanical Operations and Machining Process

A mechanical operation such as rolling, extrusion, forming, forging, and so on and machining operation like grinding, milling, turning causes non-uniform plastic deformation in the material resulting in residual stresses (Messler, 2008, Cerutti and Mocellin, 2016). Mechanical operations initiate the residual stresses and are redistributed with an increase in magnitude during the machining process resulting in deflections, overcuts, and undercuts in the workpiece (Cerutti and Mocellin, 2016). Initial residual stresses are considered the first order, which causes secondary order residual stresses during machining operations (Yang et al., 2014). These stresses must be considered to obtain good machining quality with desired geometric and dimensional tolerances and minimize finished product distortions (Cerutti and Mocellin, 2016). Cerutti and Mocelin concluded that machining sequence, clamping, and initial residual stresses govern the machining accuracy and quality of the part being machined. The residual stress redistribution can occur smoothly while machining if the lower depth of cut is used and eliminating the chances of deflection. However, (Capello, 2005, Dahlman et al., 2004) Contradicts (Cerutti and Mocellin, 2016) and describes that the depth of cut does not influence residual stresses.

Capello asserts that turning operation can decrease the fatigue life because of residual stresses generated as components are subjected to variable loads. He also concludes that the tool

nose radius, feed rate, and entrance angle (to a few extents) are the critical parameters that can increase the residual stresses in a machined part. Capello concluded that a large nose radius and higher feed rate can lead to higher residual stresses and suggests 90^0 as the optimal entrance angle for the turning process.

Residual stresses in milling operation are highly influenced by the specimen's milling conditions and tensile strength (El-Khabeery and Fattouh, 1989). Feed rate and spindle speed significantly influence residual stresses at higher depth of cut in milling (Masmiati et al., 2016). Tool flank wear resulting from the high-speed milling process significantly affects cutting forces and the temperature fields, increasing the thickness of residual stress (Tang et al., 2009). Figure 15 shows the variation of longitudinal and transverse residual stresses in milling operation with the distance from the milling surface.

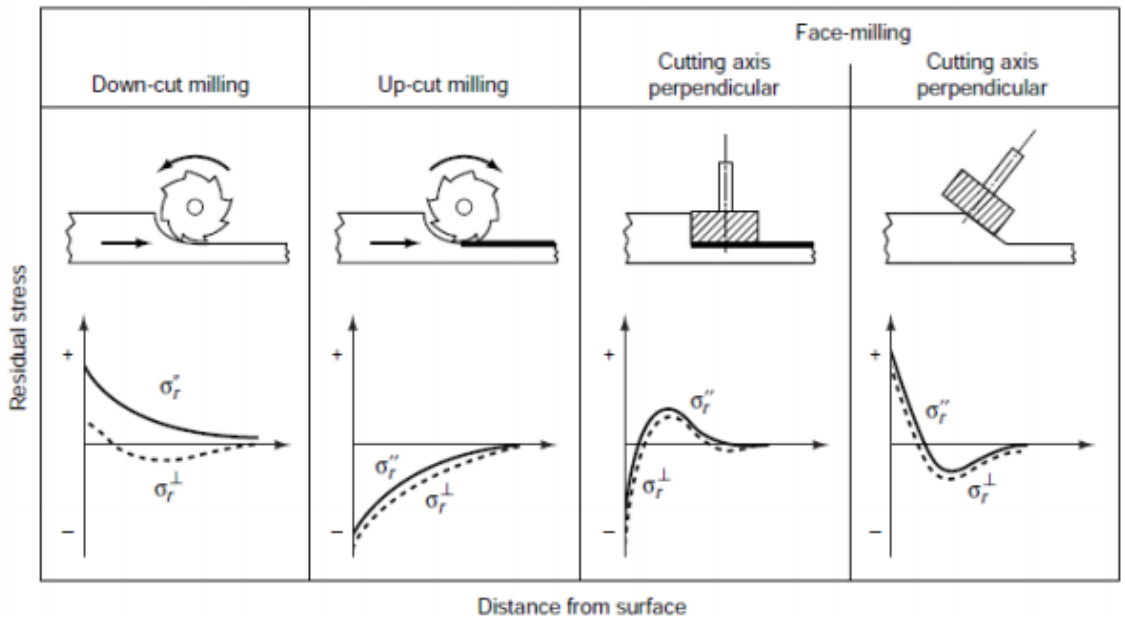

Figure 15: Variation of residual stresses in different milling operations (Totten et al., 2002).

The study (Marusich and Askari, 2001) concluded that machining parameters such as speed and chip load have no significant effect on residual stress in the orthogonal cutting process. The residual stresses from milling operation are near-surface within the depth of 250 μm (Denkena et al., 2007). Their (Dahlman et al., 2004) research describes that the rake angle largely influences the residual stresses in the hard turning process, increasing feed rate

resulting in higher compressive stresses. They (Totten et al., 2002) claimed that higher grinder power could result in higher residual stresses.

As there is growing use of additive manufacturing processes in industries, there are broader areas to explore residual stresses in additive manufacturing. Wire and arc additive manufacturing produce a larger grain size and higher residual stresses and distortions. High-pressure rolling can be employed in such parts to alleviate the residual stresses (Colegrove et al., 2013). The rapid heating and cooling cycle in the additive manufacturing process generates residual stresses analogous to the welding process (Kou, 2002).

Using bigger size specimens and optimal offsetting can avoid post-mining distortions (Cerutti and Mocellin, 2016). Dislocations can be reduced in the additive manufacturing process using post-heat treatment techniques (Tomus et al., 2016, Li et al., 2017). Study (Li et al., 2018) suggests mechanical control, scanning strategy control, thermal gradient control, and in-situ feedback control techniques can be used to minimize the machining induced issues. Mechanical peening can reduce tensile residual stresses and add up the compressive stresses, which assists in preventing crack and thus decreasing the chances of failures (Withers, 2007). Laser shock peening can help improve the near-surface microstructure and improve fatigue life by relieving residual stress (Kattoura et al., 2017).

2.5.2 Residual Stresses from Welding

The inherent problem of welding is that it can lead to the evolution of welding residual stresses, shrinkage, and distortion in the weldment and nearby areas in addition to the microstructural variation (Ueda et al., 2012). The residual stresses in the welding process can be induced by (a) volumetric changes relating to some change of phase, (b) difference in coefficient of thermal expansion of the joining material, and (c) temperature gradient leading to differential expansion (in the heating cycle) and contraction (in the cooling cycle). Due to the volumetric change of the same material in a different state (liquid, solid, gaseous), the material can have locked-in stresses. Suppose the joining material has a different thermal expansion coefficient. In that case, the material expands or contracts at different rates at the same temperature, resulting in uneven expansion and contraction, resulting in locked-in stresses. The residual stresses in weldment can arise because of restraint action experienced

by weld metal due to temperature gradient. The difference in temperature at various locations gives rise to a different rate of expansion and contraction, thereby altering the dimensions and producing residual stresses (Messler, 2008).

The mechanical behavior of welded joints is influenced by three factors resulting from welding operation: residual stress, stress concentration, and fatigue strength reduction. The heating and cooling process in welding led to residual stresses in the welding joints and surrounded areas. The welding process leads to change in the geometric shape of connecting regions, giving rise to stress concentration areas. Moreover, welding-induced defects and reduction in material properties cause a reduction in fatigue strength (Ding et al., 2016).

2.5.2.1 Cause and Effect of Weld Induced Residual Stresses

Structural mismatching while joining causes the larger size part of contracting because of compressive force acting on it. The shorter part tries to expand due to the tensile force acting on it, as illustrated in the figure below (Connor et al., 1991).

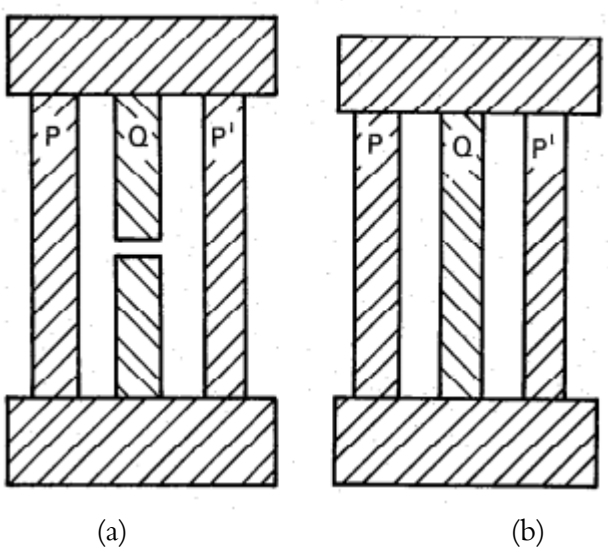

Figure 16: Different sizes of bars when forcibly joined result in residual stresses. (a) Bars in a free state, and (b) Stressed state

Non-uniform heating of material results in thermal stresses and strains. The thermal strain comprises of elastic strain components (ε_x', ε_y', and γ_{xy}') and plastic strain (ε_x'', ε_y'', and γ_{xy}'') components. The welded structure tries to distort in response to thermal stresses, but the residual stresses are formed if the structure is restrained from distortion. For plane stress

residual stress ($\sigma_z = 0$), the residual stress exists when the incompatibility (R) is not zero (Connor et al., 1991).

$$R = -\frac{d^2\varepsilon_x''}{dy^2} + \frac{d^2\varepsilon_y''}{dx^2} + \frac{d\gamma''_{xy}}{dxdy} \quad (2.5.2)$$

Residual stresses are local stress which affects fracture performance in the residual stress field only. Fatigue, Brittle fracture, and stress corrosion cracking occur at low applied stress and are significantly affected by residual stresses. When the applied stress is above the yield strength of the material, then the residual stress does not affect the performance of the welded structure. Higher applied stress results in the yielding of the welded structure as the residual stresses will be overwhelmed by applied stresses. Residual tensile stress is more detrimental than residual compressive stress if it is present in the flaw tip. The residual tensile stress adds up to the applied stress increasing the stress intensity factor and assists in the growth of the flaw leading to the brittle fracture. Compressive residual stress reduces the buckling strength of the welded structure. The compressive residual stress, if present on the surface of welded structures, increases the fatigue cycle. Suppose the residual stresses in a structure are present in an adverse environment. In that case, the structure undergoes stress corrosion cracking even in the absence of applied load; for instance, the presence of nitrites, hydroxides, and hydrogen sulfide in an environment where the low alloy steel structure is exposed leads to stress corrosion cracking.

2.5.3 Methods to Reduce Residual Stresses and Distortions in Weldments

Weld-induced residual stress and distortion significantly vary with scenarios, and it is always desirable to keep it minimum. The American Welding Society (AWS) recommends mainly three ways to reduce residual stresses and distortions, which are: (a) Proper selection of welding process, procedure, sequencing, and fixturing, (b) selecting proper stress-relieving techniques such as annealing, normalizing, tempering, and so on, and (c) using relevant design details and materials.

Employing a hot-non-fusion process can eliminate the volumetric shrinkage. Using smaller root openings with proper grooves, preferably small size, can minimize the residual stresses

(Connor et al., 1991). Thermal treatment, for example, preheats, can assist in alleviating the level of residual stresses and distortion by lowering the thermal gradients in the weldment. Preheat is helpful to reduce the chances of cracking in the weld metal and reducing the size of the heat-affected area. Post-weld heat treatment can be employed for thermal stress relaxation. Uniform heating of weldment at a suitable temperature, usually below a critical temperature, for a certain period followed by uniform cooling, reduces the yield strength of the base material and permits stress relaxation by undergoing plastic deformation and creep (Messler, 2008, Khan, 2007).

Thermal and mechanical straightening can be used for the suitable weldment to initiate plastic deformation to undistort the distorted member. Elastic straightening methods such as wedges to eliminate angular distortions at the expense of transverse shrinkage may be an appropriate choice when angular distortions must be avoided.

An efficient weld design involving a minimum amount of weld metal can help in minimizing distortions by eliminating the over the welding. Angular distortion can be minimized with the selection of an appropriate joint preparation strategy. Considering the compensation of the distortion in final weldment well ahead of welding is also an excellent choice to reduce distortions. For the structure involving many welding joints, assembling to the nominal size and tolerance and then applying restraints can help in mining the distortions in the final weld piece (Connor et al., 1991). On a study (Seyyedian Choobi et al., 2012) suggest that symmetrical welding of the workpiece starting at the center and moving towards the edge of the workpiece can also help minimize the angular distortions.

2.6 Residual Stress Measurement Methods

In this section, experimental and computational methods for estimating residual stress are discussed. The following figure summarizes the different techniques of residual stress measurement that are practiced widely in industries.

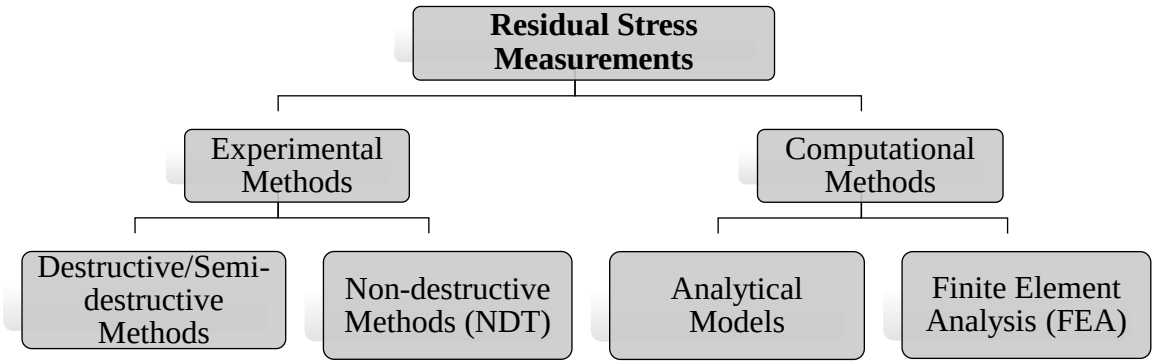

Figure 17: Residual stress measurement methods.

2.6.1 Experimental Methods

2.6.1.1 Destructive Methods

2.6.1.1.1 Sectioning method:

It is one of the destructive techniques used for decades to evaluate residual stresses in welded components and structural parts. This technique was initially invented in 1888 to measure longitudinal stresses in the bar by slashing longitudinal strips and determining length deformation (Tebedge et al., 1973a). The stress examination is done by considering minimal transverse stress, and the cutting process is not alone responsible for significant yield gain.

The slitting method is fragile; meanwhile, it ought not to present heat or plasticity in the cut examples keeping the first residual stress without the impact of external factors. These strains are measured using mechanical or electrical strain gauges (Rossini et al., 2012, Withers PJ, 2008). To find residual stresses in a plate, sample preparation must usually be done, depending upon residual stress gradient, the number of longitudinal strips to be cut according to it. In the places where mechanical strain gauges are not suitable for the sectioning process, device is not attached directly to the workpiece (Huang X, 2013). Over a specific cross-section, the required stress distribution can be found by finding the deformation in each strip's length and with the help of Hook's Law (Howell et al., 2013).

Advantages and disadvantages

For welded joints, this technique is commonly preferred. For example, in the box section of high-strength steel, using fillet welds in A36 steel and panels of thin Al 5456 (Howell et al., 2013). Sectioning is an accurate, adequate, and economical method to find residual stresses in structural member because of its reliability and versatility (Howell et al., 2013).

It cannot be used to test in-service structures and is usually costly and time consuming. Sometimes, a repeated number of experiments are required.

2.6.1.1.2 Contour method

In 2000, A new residual stress measurement technique was proposed as Contour Method (CM) (Prime and Gonzales, 2000). It works on the principle of superposition throughout the relaxation of residual stresses by considering that the structural material behaves elastically. By considering the following schematic figure of contour method, it can be summarized that relaxation of internal stresses is measured by displacements and are compared to the longitudinal stresses and flat surface contours (Lu, 1996).

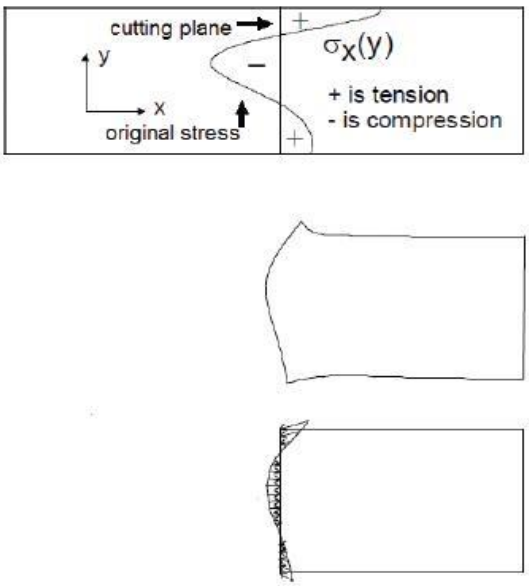

Figure 18: Contour Method Schematic Principles (Montanari et al., 2017).

As the sectioning method is simpler to decide residual stress over weld cross-areas as practically there is no requirement of computations, CM gives an advanced longitudinal goal (1 mm dividing).

Averaging the contours on the two parts to eliminate shear stress impacts requires another suspicion: the stiffness is similar on the cut's different sides. In homogeneous materials, this supposition is fulfilled when a symmetric part is sliced accurately down the middle. Practically, the part should be symmetric inside the area where the stiffness significantly affects the distortions of the cut surface, which can be assessed as reaching out from the cut exterior by close to 1.5 occasions the Saint Venant's trademark distance (Prime and Gonzales, 2000).The trademark distance is frequently the part thickness yet is all the more moderately taken as the most extreme cross-sectional measurement. On the off chance that the part is lopsided, a FE examination can be utilized to gauge potential blunders, which will, in general, be little until the part is topsy-turvy.

Advantages and disadvantages

The contour method is almost exceptional in its capacity to gauge a two-dimensional cross-sectional guide of leftover anxieties in uniform enormous parts (Howell et al., 2013). This method's performance is best for larger parts; a Bulge error can be further eliminated using the Finite element method (Withers et al., 2016).

While choosing an estimation procedure for stress disseminations that are fundamentally 1-D, improved exactness can almost certainly be accomplished by using other techniques, such as incremental slitting (Rossini et al., 2012). Until now, the contour strategy has just been used in utilizing wire EDM to get it done, which restricts the submission to metals and a couple of different ingredients that can be cut with EDM (Tsai et al., 1999).

2.6.1.2 Semi-destructive Methods

2.6.1.2.1 Hole drilling method

Hole Drilling Method (HDR) is a standard semi-destructive method used for finding the residual stresses. The principle, anticipated over 80 years prior by Ruud (Ruud, 1982), depends on how relaxation happens when approximate material is taken out from a section with interior residual

stresses. It very well may be assessed using the incited nearby deformation (Lu, 1996, Howell et al., 2013, Finch, 1994).

At the midpoint of a suitable model and rosette strain gauge, a hole is bored in the specific section to find the internal stresses using strain statistics. (Schajer, 1981) presents the incremental method to find the non-uniform residual stresses that allow deciding the number of step depth and a number of steps as this process is created on the incremental distortion as a result of drilling. A new hole shape was developed by Kockelmann (Bokuchava, 2018), along with the characteristics hole attained by high-speed milling. The most well-known fields of HDM application are the assessment of residual stress prompted by welding measures. Indeed, residual stress could influence the employable strength of the part, stress corrosion strength, and fatigue life. In as-welded conditions, regularly residual stress is near yield stress, and mechanical or thermal medicines are important to decrease it. Redistribution of the residual stresses occurs due to the removal of stressed material around the hole in the remaining material. There are localized deformations (Howell et al., 2013), as illustrated in Figure 19.

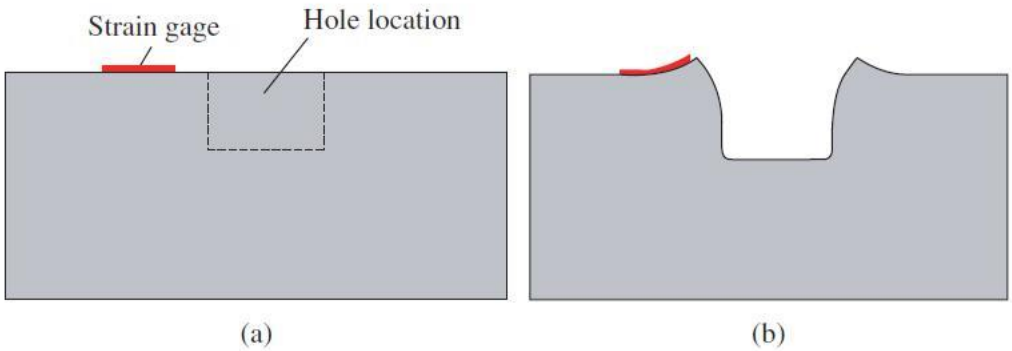

Figure 19: Comparison of before-hole drilling and after-hole drilling (Howell et al., 2013).

There is a schematic illustration of tensile residual stresses of deformation around a hole drilled into the material. When HDM results are compared with that of ultrasonic for residual stresses, the following graph is observed.

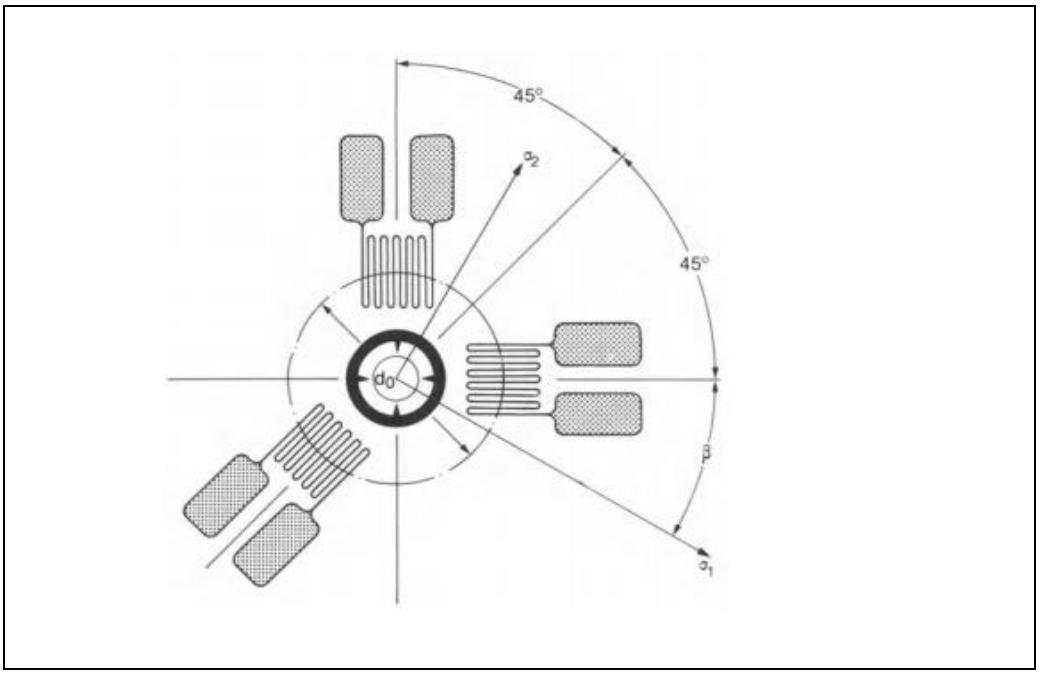

Figure 20: Three-element strain gauge rosette for use in the hole-drilling method. angular positioning and diameters, according to ASTM-Standard. (Radaj, 1992)

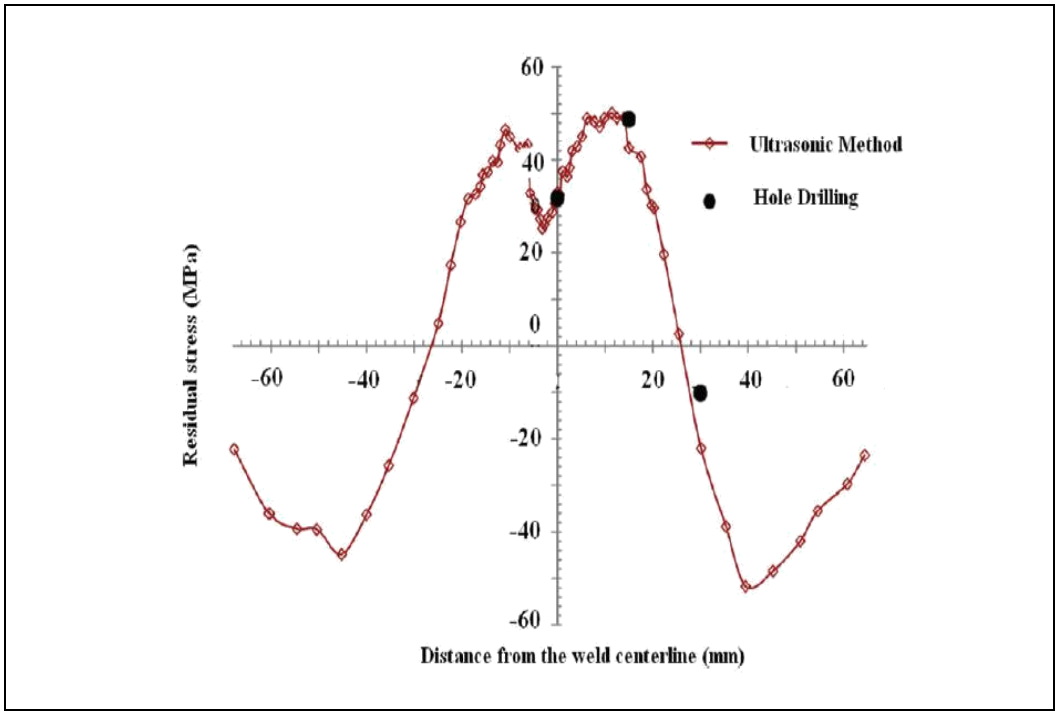

Figure 21: Comparison of residual stress variation measured by ultrasonic and hole drilling technique (Montanari et al., 2017).

Advantages and disadvantages

For non-specific specimen shapes, the hole drilling method is commonly used. This method is much more suitable for larger specimens, i.e. (100-1000mm) (Huang X, 2013).

The hole Drilling method is not able to evaluate the entire specimen depth. Another important factor is accuracy, as low accuracy is obtained due to the destruction of the specimen (Kesavan et al., 2005). Limited Resolution and low accuracy in case of inhomogeneous material stresses. The strength of material decreases due to the removal of material by hole drilling (Tebedge et al., 1973b).

2.6.1.3 Non-destructive Methods

2.6.1.3.1 Neutron diffraction method

The neutron diffraction method is a non-destructive method of measuring residual stress by elastic scattering of neutrons. Penetrating Radiation is commonly used in this method. Although the nucleus of an atom interacts directly, the value of diffracted intensity is different from X-rays as it interacts with electrons. It is additionally frequently the situation that light atoms (low atomic number, Z) contribute similarly as firmly to the neutron deflected intensity as do huge Z particles. In this manner, neutrons enter similarly well into high Z material as low Z. From isotope to isotope the scattering characteristics vary rather than linearly with respect to atomic number (Howell et al., 2013).

Advantages and disadvantages

Neutron energies of wavelength value between 0.7 to 3 angstroms are mainly used in Neutron diffraction stress measurement. This method is commonly used in measuring residual stresses in rolled rods, weldment, rocket case forgings, plastically deformed plates, and many other valuable components (Montanari et al., 2017).

The measurements are costly and require more time to calculate and analyze the results (Finch, 1994). At the point of strain measurement, the unstressed lattice spacing must be known as it cannot be easily measured with the synchrotron method. In addition to this, other limitations include that the component should bring to a neutron foundation for every single strain evaluation as it requires few seconds to an hour (Howell et al., 2013).

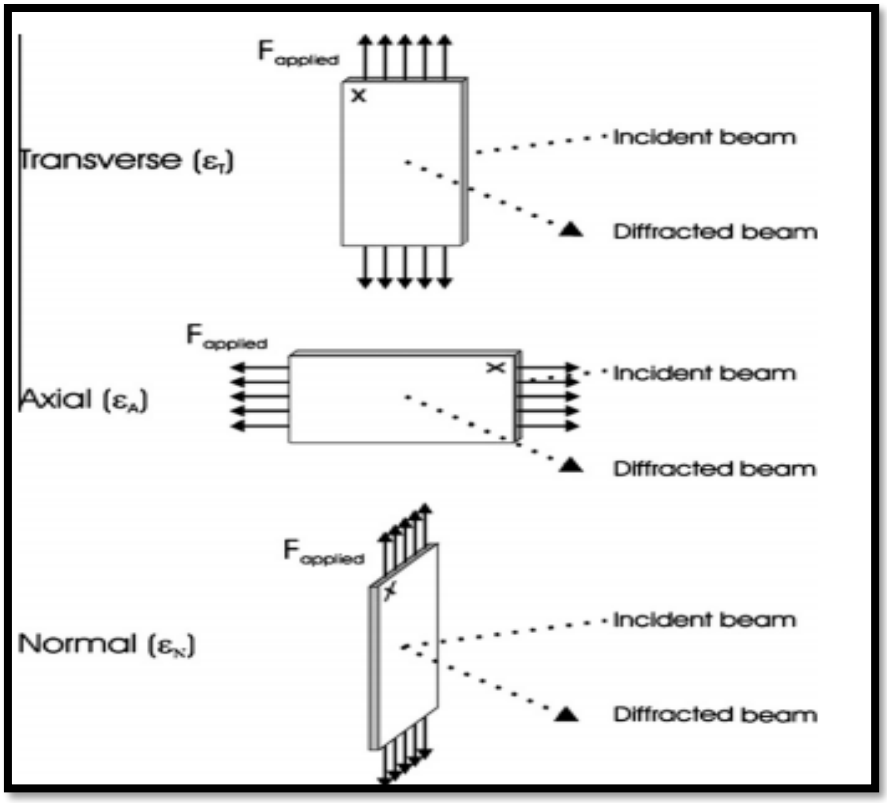

Figure 21: Transverse strain, axial strain, and normal strain measured in three different orientations. Applied load direction (Fapplied) and direction of the incident and diffracted beam of neutrons shown. (Rossini et al., 2012)

2.6.1.3.2 X-ray diffraction:

It is one of the non-destructive testing methods responsible for finding the inter-atomic lattice arrangement, revealing strain in the irradiated area. X-Ray Diffraction (XRD) is a method in which few microns penetrate in X-ray radiations. This shallow profundity obliges the presumption that the stress perpendicular to the surface is zero (Tebedge et al., 1973b). So, the gauge volume or irradiated volume is taken to be in a state of plane stress. This disorder considers rearrangements of the stress-strain equations and evades the requirement for exact assurance of the unstressed cross-section plane measurement. In this manner, worked on equations utilizing the distinction between explicit cross-section planes at a few angles to the surface plane are utilized to extrapolate the strain condition to a vector in the plane of the surface (Howell et al., 2013, Lu, 1996).

Advantages and disadvantages

Instrumentation for fetching XRD estimations from the lab climate to handle applications has progressed quickly over the most recent twenty years, particularly toward expanded convey ability, speed of activity, and conservativeness. A few seconds or less measure time in spatial analysis of less than $1mm^2$ is possible using the XRD technique.

The unstressed lattice factors can be exaggerated by phase alloy content, composition, and many other aspects. Stress evaluation in the X-Ray Diffraction technique was obtained only to some depth of about 0.025mm.

2.6.1.3.3 Ultrasonic testing:

Another useful NDT method is the ultrasonic technique, which works by altering the ultrasonic waves. It can be associated with the residual stress state by using the elastic constant of the material presented by Kandil(Kandil et al., 2001). Its measurement depends upon the linear relation between material stresses and the velocity of ultrasonic waves, and the relation between velocity and stress is as follows:

$$V = V_0 + K\sigma \tag{2.6.1}$$

The acoustoelastic constant is denoted by K, while V and Vo are the values of the velocities in the stressed and stress-free region. (Javadi et al., 2013) did a progression of intriguing examinations on the ultrasonic technique. They contrasted with contact and drenching ultrasonic estimations of residual welding stress in unique joints. A blend of FE welding recreation and Lcr ultrasonic waves was utilized to arrive at the objective and explore exploratory outcomes. They reasoned that both techniques could quantify the residual stress with adequate exactness. The choice between them relies upon the geometry and dimensions of the tried design and the accessible test gadgets.

2.6.1.4 Comparison between Destructive and Non-destructive Methods

The following figure presents a comparison between various residual stress measurement techniques in reference to their surface penetration. Figure 22 sums up a few strategies for

their spatial goal and their capacity to make residual stress estimation. Few elements should be painstakingly thought of and adjusted to settle a suitable residual stress estimation technique for a given application. In the comparison below, it is clear that sectioning and ultrasonic methods are the most expensive; even magnetic and eddy current method are expensive for more penetration results as it deals in micros. However, the overall best methods are X-ray diffraction and Neutron Diffraction as they are least expansive and can cover a wide range of penetration. The experimental method may not be suitable for measuring residual stresses as it poses limitations on the size and location of measurement. Therefore, analytical and numerical methods are indispensable for outgoing the limitations of the experimental techniques. For example, the large structural components such as wind vanes can not be tested if it poses a small crack under challenging locations.

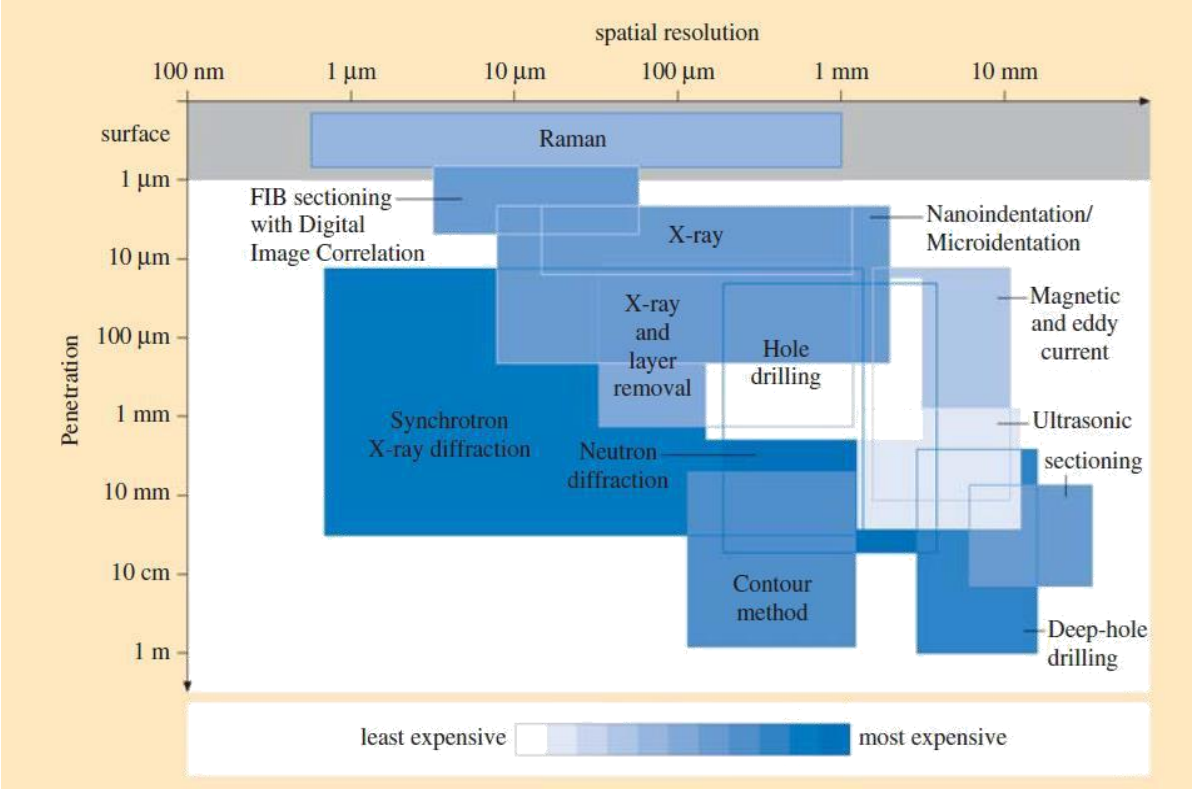

Figure 22: Spatial resolution vs. Measurement penetration for various residual stress measurement (Howell et al., 2013)

2.6.2 Analytical Methods to Measure Weld Induced Residual Stresses

Temperature gradients in the workpiece due to welding result in high thermal stresses beyond yielding, causing localized plastic deformation and residual stresses. The study of residual stress due to welding started in the early 1940s. The study (Boulton and Martin, 1936) suggested longitudinal stress in edge-welded mild steel plate using plastic analysis and verified it by experimental measurements. Research by (Rodger and Fletcher, 1938) also analyzed edge-welded plate and predicted the residual stress measuring temperature histories while welding. Rodger and Fletcher considered temperature-dependent mechanical properties such as Young's modulus, thermal expansion coefficient, and constant thermal properties using the superposition principle to establish the residual stress distribution. A residual stress investigation procedure was proposed in a similar leu (Rosenthal, 1940, Tall, 1961) proposed a step-by-step method to compute residual stresses considering temperature-dependent material properties and constant thermal properties assuming equilibrium during cooling at different periods. Tall proposed an analytical solution of the residual stresses to the as-welded thick plates concluding that the higher thickness of weld piece leads to more compressive residual stresses (Tall, 1961). A literature study (Abambres and Quach, 2016) presents a study on analytical expressions of longitudinal residual stresses for a structural shape such as plates, I, H, L, and T sections. These analytical models do not account for the heat loss, geometric properties and are limited for the reasonable prediction of longitudinal residual stress considering constant material properties (Song, 2012). The important material properties which influence the longitudinal and transverse residual stress distribution can be examined with 1D thermoplastic idealization (Dong, 2005).

2.6.2.1 One-bar Model

One-bar model is a simple method to study the residual stress developments, and its analytical solution is easy to obtain. Consider a fully restrained bar at room temperature (θ =0) subjected to uniform heating and cooling. The bar's temperature increases with time till it reaches melting temperature ($\theta = \theta_m$) and then decreases linearly to ambient temperature. Also, assume that the bar shown in Figure 23(a) obeys stress-strain behavior of elastic perfectly plastic material as in Figure 23(b), and yield strength is a function of temperature shown in Figure 23(c). Then the total strain increment based on incremental

plasticity theory is given as the sum of elastic, plastic, thermal, and phase transformation produced strain increment values (Dong, 2005, Ma et al., 2016).

$$\Delta\varepsilon = \Delta\varepsilon_e + \Delta\varepsilon_p + \Delta\varepsilon_t + \Delta\varepsilon_{Tr} \tag{2.6.2}$$

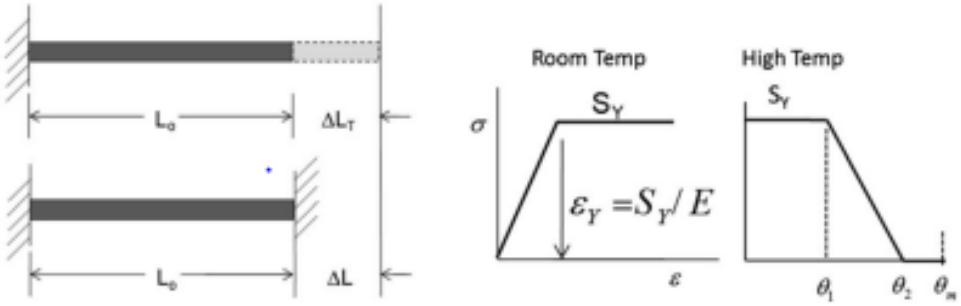

(a) (b)

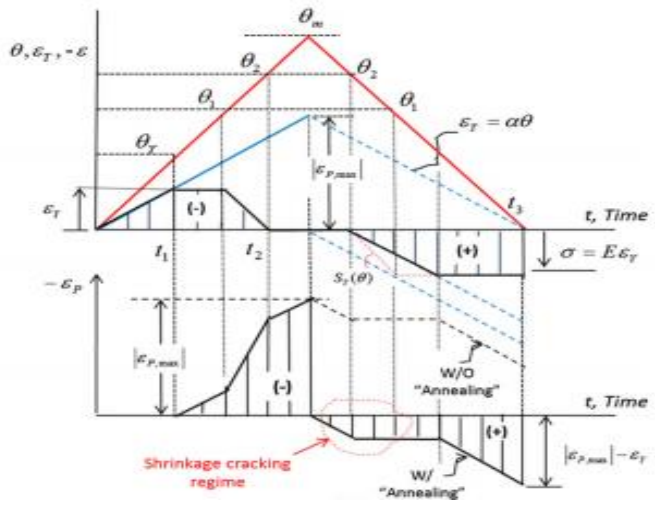

(c)

Figure 23: Analytical solution of one-bar model (a) one-bar model, (b) stress-strain relationship at room temperature (left), variation of yield strength at different temperature (right), (c) plot of four different types of strains as mention above with time (Dong, 2018).

When the bar is fully constrained, total incremental strain must be zero throughout the heating and cooling cycle. Total incremental strain depends solely on the thermomechanical process and resulting strains. For example, only thermal and elastic strains are generated during the early stage of a heating cycle. At this time, equation (2.6.2) becomes, $\Delta\varepsilon_e = -\Delta\varepsilon_t$ or $\Delta\sigma = -\alpha\theta E$ in terms of stress which is shown in the upper part of figure Figure

23. For Simplicity, the thermal expansion coefficient (α) and Young's modulus coefficient (E) are supposed to be constant for all heating and cooling cycles (Dong, 2005).

The continuous increase in temperature during the heating cycle results in higher compressive stress than the yield strength of the bar material. $EY = S_Y/E$ gives the yield strength. The temperature at those corresponding stresses can be written as $\theta_Y = \varepsilon_Y/\alpha$. When the temperature rises from θ_Y to θ_1, there will be no change in stress and elastic strain. Nevertheless, the increase in temperature results in thermal strains equal to compressive plastic strains.

Further increase in temperature from θ_1 to θ_2 causes a linear decrease in yield strength of the material and finally vanishes to zero. The plastic strain at this point is the difference between a total thermal strain and elastic strain (Figure 23c). The plastic strain goes to the maximum when the temperature rises from θ_2 to θ_m. When $\theta_2 = \theta_m$, either the material changes from solid to liquid due to zero plastic strain or returns to the original state upon cooling, referred to as plastic strain annihilation (Brust et al., 1997). When the cooling cycle begins from θ_m, thermal strain vanishes to zero elastic strain position, and the shrinkage phase starts. Until the temperature falls to θ_2, shrinkage strains become plastic strains due to zero strength of the material. If melting is considered at θ_m to recover material to its original state, a completely different plastic strain is obtained. Therefore, the strain accumulation effect must be addressed adequately while simulating weld deposition in addition to accounting for remelting effect in the case of a multi-pass weld. The final residual stress value is at yield, where $\sigma = S_y = E\varepsilon_y$ and tensile plastic strain is equal to $\varepsilon_{pmax} - \varepsilon_y$ (Dong, 2018).

2.6.2.2 Three-bar Model

Another method of simplifying the residual stress problem in different thermal processes is possible with the three-bar model. For example, his study (Dong, 2018) explains residual stress development for repair welding of the butt-welded plate. Also, (Song et al., 2019) uses a three-bar model to demonstrate the residual stress formation mechanism in the selective laser melting process by analyzing the evolution of thermal stresses during thermal cycles.

In this model, the welding piece is assumed to be composed of three-bars of equal length and unit thickness (Figure 24a). Bar 2 represents the welding region where fusion occurs, whereas bar1 and bar 3 have an equal area (A1=A3=A) at an equal distance (d) from the welding center and represent the region outside bar 2. In this case, bar1 and bar3 represent

the comparatively cooler section, which acts as a constraint for bar2 when exposed to a thermal cycle. When bar 2 is heated, it tries to expand, but its expansion is restricted by the relatively cold region (bar 2 and bar 3), and hence bar 2 experiences compressive stress and other bar experience tensile stresses.

The displacement conditions due to the rigid link and symmetry when bar2 is heated can be expressed as (Dong, 2018):

Deformation on bar 1 (δ_1) = deformation on bar 3 (δ_3) = δ and

Deformation on bar 2 (δ_2) = $\Delta L_T - \delta$;

Equilibrium condition at weld centerline in y-direction are:

$\sum F_y = F_1 - F_2 - F_3 = 0$ and $\sum M_2 = F_1 d - F_3 d$

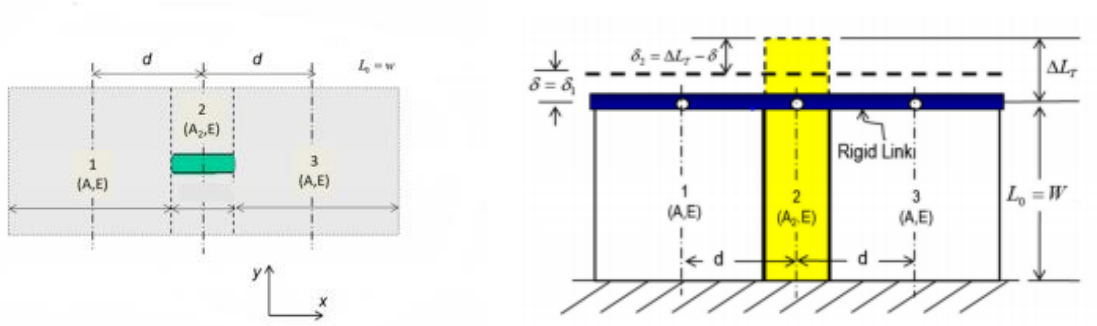

Figure 24: (a) Representation of workpiece plate as 3D bar model, (b) 3D bar during the heating cycle (Dong, 2018).

Solving the above equation using bar theory results deformation as:

$\delta_1 = \delta_3 = \delta = \frac{A_2 \Delta L_T}{2A + A_2}$; $\delta_2 = \frac{A_2 \Delta L_T}{2A + A_2}$, and the corresponding strain is given by $\varepsilon_2 = \frac{2\alpha\theta A}{2A + A_2}$.

Further increase in temperature in the middle bar causes yeilding, and thus the developed stress decreases. Stresses during this process under equilibrium are as follows.

$$\sigma_1 = \sigma_3 = \sigma = \frac{A_2 S_Y}{2A + A_2} ; \ \sigma_2 = -S_Y \tag{2.6.3}$$

At melting point temperature, there is no built-up stress. However, during the cooling process, restriction in a contraction of bar 2 by the other two surrounding bar results in compressive stress in bar2 and tensile stress in the other two end bars, as shown by equation (2.6.3) when bar 2 is cooled to ambient temperature these stresses remain in the material as residual stresses (Song et al., 2019). Upon returning to an ambient temperature, yield magnitude residual stress develops if a $2\theta_Y$ temperature difference is attained. The plastic strain forms with assistance from an increment thermal strain when the temperature difference is above $2\theta_Y$. In the absence of a rigid link, bar 1 and bar 3 experience no plastic deformation during thermal cycles, and therefore, bar 1 and bar 2 return to the initial position.

Nevertheless, if the temperature difference crosses $2\theta_{Y,}$ bar 2 will be shortened, and rigid link conditions are applied. Residual stress when the rigid link is attached is below(Song et al., 2019). Upon returning to an ambient temperature, yield magnitude residual stress develops if a $2\theta_Y$ temperature difference is attained. The plastic strain forms with assistance from an increment thermal strain when the temperature difference is above $2\theta_Y$. In the absence of a rigid link, bar 1 and bar 3 experience no plastic deformation during thermal cycles, and therefore, bar 1 and bar 2 return to the initial position. Nevertheless, if the temperature difference crosses $2\theta_{Y,}$ bar 2 will be shortened, and rigid link conditions are applied. Residual stress when the rigid link is attached is given as below.

$$\sigma_1 = \sigma_3 = \sigma = \frac{-A_2 S_Y}{2A + A_2} ; \ \sigma_2 = S_Y \tag{2.6.4}$$

Bar 2 is subjected to tensile residual stress equivalent to yield strength and the compressive stress on the region outside the middle bar. The equation above 2.6.2.3 and 2.6.2.4 describes residual stress distribution on the bar (Dong, 2018).

2.6.2.3 Analytical Calculation for the Three-bar Model

The following material properties are considered to calculate yield point temperature, transverse residual stress, and displacement caused by the welding process.

The area of the middle bar and outer bar is pi and four★pi, respectively.

linear expansion coefficient, $\alpha = 1.47 \times 10^{-5} \, °C^{-1}$

Yield strength of the material, σ_y = 206 Mpa

Modulus of Elasticity of the bar material, E= 206 GPa

Then we can find the Yield point temperature using

$\Delta T_Y = \frac{2\left(\frac{A}{A_2}\right)+1}{2\left(\frac{A}{A_2}\right)} * \frac{\sigma_y}{E*\alpha} = 76.53\,^{\circ}C$ for bar2. The value of yield point temperature is utilized to find yield level residual stress.

Residual stress in bar1 and bar3 ($\sigma_{1,3}$) = $E\star(\frac{A_2\alpha}{2A*E}\star \Delta T_Y)$. On simplification it becomes

$$\sigma_{1,3} = \frac{1}{9}\star(-E\star\alpha\star\Delta T_Y) = -\frac{206*1000*1.47*10^{-5}*76.53}{9} = -25.75\ Mpa$$

The final transverse residual stress in bar1 and bar3 is 25.75 Mpa, compressive.

Similarly, we can also find transverse residual stress on the middle bar ($\sigma_{2)}$ where the heat is inputted.

$$\sigma_2 = \frac{8}{9} * (E * \alpha * \Delta TY) = \frac{8*206*1000*1.47*10^{-5}*76.53}{9} = 206 \text{ Mpa.}$$

The resulting residual stress in bar2 is tensile in one complete heating and cooling cycle. Transverse residual stress in the middle bar is eight times the residual stress in the outer bar caused by the welding process for one-fourth area ratio. The induced transverse residual stress is in the opposite direction.

The maximum possible deflection or shrinkage can be calculated analytically with the following equation.

$$\delta = \frac{A_2 L_0 \sigma_y}{2A*E} = \frac{pi*10*206}{2*4*pi*206*1000} = 0.00125 \text{ mm}$$

This shows that the deflection is caused due to the continuous heating and cooling cycles in the welding process. The large deflection leads to major structural problems leading to the failure of the structure.

2.6.3 Finite Element Method to Predict Weld Induced Residual Stresses and Distortions

In welding, the material properties such as thermal conductivity, heat capacity, elastic modulus, yield stress, and Poisson's ratio vary sensitively with temperature as the temperature change ranges from atmospheric temperature to melting point temperature of the metal (Paik and Technology, 2018). The thermal transition period leads to the phase change of metal from solid-Liquid-solid, leading to a change in material properties and specific volume. Therefore, it is challenging to obtain an analytical solution of stresses and temperature fields. The recent advancement of finite element analysis tools can provide detailed information on transition temperature, displacement, strain, and stress. The temperature-dependent properties can be stated, and properties such as phase change and the welding state can be modelled.

The advancement in computer technology facilitates researchers and scientists to simulate the physical model and fully control all the process parameters. This allows the researchers to view the process as it evolves. Computational modelling requires less cost than establishing a laboratory setup for the experimental residual stress measurement limited by size, complexity, and accessibility. However, it does not eliminate the experimental test requirement but can be useful to examine and visualize the process as it evolves. These finite element model observations are validated with an experimental result that helps analyze and obtain the optimal parameters for the process. The use of simulation and the tests (described in the previous chapter) enables the evaluation of residual stresses that affect the life of the welded structure and the deformations that may hinder the functionality of the component (Lindgren, 2007). Finite element analysis is the most popular computational method in industries and the researcher's community to assess residual stresses. It can yield plausible results with some considerations and is beneficial for addressing some of the shortcomings of other methods.

The coupling of thermal, mechanical, and metallurgical aspects in welding analysis is computation intensive. The 3D FEA model for residual stress and distortion analysis, although generates comparatively better result than 2D FEA, is complex and time-

consuming, demanding more technological up-gradation in the FEA tools such as ABAQUS, ANSYS. To minimize the computing time in three-dimensional models, the composite shell of the particular kind was developed by Dong (Dong, 2001), and a three-dimensional model consisting of only one part of the welded structure was employed by (Hossain et al., 2006). Lumped pass technique is in everyday use among researchers while using the 3D model to reduce the computational time. While on the other hand, much time can be saved by considering 2D analysis instead of 3D. This can also be done by considering the axisymmetric model (Dong, 2001, Jiang et al., 2005). These studies showed that axisymmetric and complete 2D models could provide acceptable residual stresses and temperature results with a drastic reduction in computational time. Therefore, using 2D thermo-elastic plastic FEA with appropriate assumptions can yield approximate results; hence, it is still widely used to analyze residual stresses and distortions.

In the following paragraph, we will briefly review the contributions by some researchers to the finite element method for understanding the finite element method application and further analyze welding-induced residual stress and distortion issues.

The research by (Mackerle, 1996, Mackerle, 2002) provides a bibliographical review of modelling of welding processes, geometrical influence, heat transfer and fluid flow in a weld, residual stress deformations in weld plates, and other structural components. A study (Masubuchi et al., 1968) proposed a computer program to estimate the longitudinal residual stresses using a line heat source. The 2D finite element analysis was employed in thermal stress analysis in the early 1970s. Research (Iwaki and Masubuchi, 1971) performed thermo-elastic analysis on orthographic plastic using finite element analysis. The study was extended to study the thermal stress variation due to welding using a thermal elastic-plastic model (Ueda and Yamakawa, 1971b). They focused on variations in Modulus of elasticity, yield stress, and coefficient of linear thermal expansion with temperature. Thermal stress history was obtained for the butt and fillet weld under moving electrode. In the following year, the same author used finite element analysis for thermal stress analysis of metal considering the temperature-dependent mechanical properties (Ueda and Yamakawa, 1972). Extensive research (Fujita and Nomoto, 1971, Fujita et al., 1972, Ueda and Yamakawa, 1971a) characterized the welding-induced cracks based on welding-generated stresses. Using a finite element procedure, thermo-mechanical analysis of the welding process was carried out (Friedman, 1975). Improvement in modelling approaches with the use of computer graphics (Requicha et al., 1983, Kela. et al., 1984) also led the researcher to focus on improvement of finite element mesh grading and generation techniques (M.S. and K.H., 1984, Kela. et

al., 1984, McDill et al., 1987). In the late 1980s, researchers focused on enhancing the finite element model considering the welding process, energy sources, and heat flow (Goldak et al., 1984b). Many researchers (Watt et al., 1988, Khoral, 1992, David and Babu, 1995) focused on the microstructural effect induced by welding. A study (Lindgren, 2001) suggests that increased complexities in the welding process should be accounted for in finite element modelling and simulation of the welding process for a better understanding of welding-induced residual stresses. As the welding process is associated with the complex thermomechanical phenomena, which can be dissected into a solvable problem with the help of recent advancement in computational simulation techniques (Dong, 2005), modelling of welding can be dissected into four domain such as heat and fluid flow, heat-source metal interaction, weld solidification microstructure, and phase transformations (Zacharia et al., 1995). Understanding heat transfer equation, modelling of heat source, thermal and mechanical analysis procedure with pertinent boundary conditions are very crucial in finite element modelling. Therefore, next section focuses on discussion of aforementioned points.

2.6.3.1 Governing Equation for Transient Heat Transfer in Welding

Rosenthal developed the analytical approach to forecasting the temperature history during the fusion welding process. The Rosenthal equation indebted its legitimacy to its straightforwardness and extensive pertinence. Besides, this solitary equation fits foreseeing temperature-time step history as a component of solidification rate, temperature gradient, cooling rate, and time. Rosenthal equation is as follows:

$$T = T_0 + \frac{\lambda P}{2\pi kr} exp\left[\frac{V(r+\xi)}{2\alpha}\right] \tag{2.6.5}$$

In the above equation, the temperature at a location away from the upper surface is denoted by T_o, V is the velocity of scanning, k is thermal conductivity, α for thermal diffusivity, and distance from the heat source is denoted by 'r' (Jiang et al., 2005, Kee Paik and Min Sohn, 2012, Montanari et al., 2017). There is a difference in the thermal behavior of the FEA model and results obtained from Rosenthal equations as examined in the past, shown by Figure 25. The required energy input is obtained by altering the laser power and keeping the scanning velocity constant.

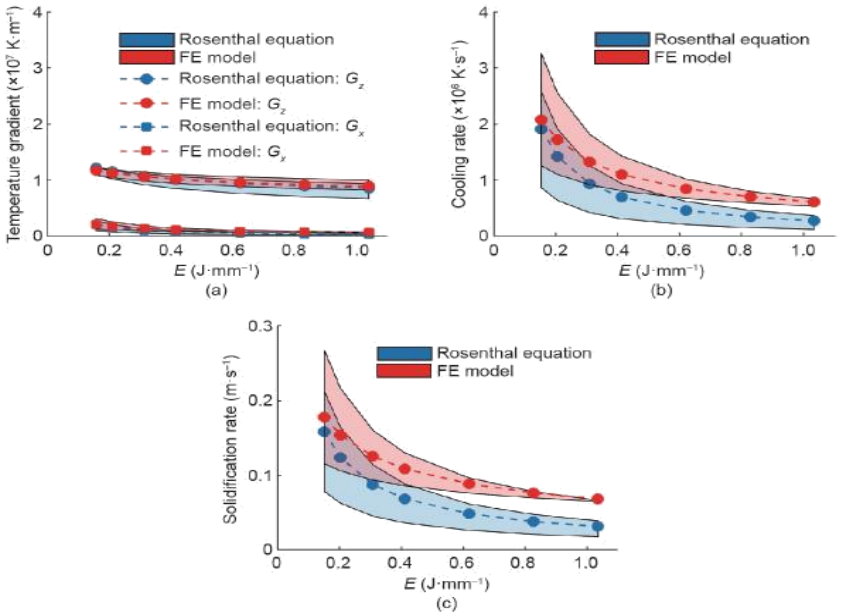

Figure 25: (a) Comparison of Temperature Gradient (b) Comparison of Cooling Rate (c) Comparison of Solidification rate. Note: This comparison is between the Rosenthal equation and FE model, where the shaded area shows the sensitivity to absorptivity; also, dashed lines depict the values of fitted absorptivity (Promoppatum et al., 2017).

A few assumptions are considered in the above results, i.e., using fixed scanning velocity and altering the laser power to achieve a required energy input.

3D heat conduction equation is applicable in the case of welding to characterize the governing parameters, which is as follows:

$$\frac{\partial}{\partial x}\left(K\frac{\partial T}{\partial x}\right)+\frac{\partial}{\partial y}\left(K\frac{\partial T}{\partial y}\right)+\frac{\partial}{\partial z}\left(K\frac{\partial T}{\partial z}\right)+\dot{Q}_v = \rho C_p\frac{\partial T}{\partial t} \qquad (2.6.6)$$

A volumetric heat source in a particular welding process is incorporated using the heat generation term in the above equation.

The convective flow of heat distribution is neglected. The material flow in a small weld pool is neglected, then the assumption of surface heat flux is not sufficient to accurately estimate the heat input.

2.6.3.2 Heat Source Modelling

Understanding heat source modelling is essential for an appropriate description of the input energy distribution. Each joining process has a unique input energy source. The magnitude

and distribution of input energy of the heat source affect the weld shape, and weld generated residual stresses and distortions, cooling rate, metallurgical structure (Glickstein and Friedman, 1993), and welding defects such as porosity, hot tearing, and cold cracking (Lundin, 1983). Therefore, using appropriate heat source modelling is a must for adequately predicting welding residual stresses and distortions.

In finite element simulation of welding, a simplified mathematical model/weakly coupled model represents the actual heat generation wherein the energy is applied to the finite area of the model.

For design-driven application, (Karlsson et al., 2011) presents a block dumping heat source strategy in place of a conventional moving heat source model to reduce the computational time for the design.

Various heat source model, beside variable-length heat source (VLHS), instantaneous line heat source (ILHS) and moving heat source (MHS), has been developed in order to incorporate the heat flux distribution in the weld-geometry and are briefly listed below.

1. Circular or disc shape heat source
   In the disc shape heat source model is heat is distributed over the surface of the geometry.
2. Ellipsoidal heat source model
   In an ellipsoidal heat source, heat is distributed over the geometry volume and is primarily used to model heat input of stationary welding processes.
3. Double-ellipsoidal heat source model
   In this model, the moving heat source model incorporates non-symmetrical energy distribution due to the welding velocity.
4. Quadruple-ellipsoidal heat source model
   Non-symmetric energy distribution due to various material properties, including welding velocity.
5. Conical heat source
6. Egg- configuration heat source
7. Hybrid heat source
8. Adaptive volumetric heat source model

A new procedure researcher utilized (Komanduri and Hou, 2000) non-dimensional integral to acquiring answers for point heat source, disc plate heat source model, and establish an

arrangement dependent on Gaussian appropriated circle heat source model. Notwithstanding, some heat flows in the complete thickness measurement since the dispersion is fractional and the admired line heat source is uncertain. For any given (point, area) heat source and material, the cooling rate is greatest at the center when the plate is exceptionally thick.

A few have endeavored to utilize a more sensible distributed area heat source; however, for a moving distributed heat source, no one has addressed the whole temperature field (Pavelic and KC, 1980). Lately, an overall type of the moving distributed heat source has been offered; however, computations of the thermal field were restricted and unexplained. Distributed volume heat source proposed by Paley and Hibbert (Friedman, 1975), where the density is consistent all through the fused region. This is ridiculous genuinely on the grounds that the mixing speed should rot to zero at the FZ limit and ascend to the most extreme during the interface of arc welding.

Fourier introduced the essential hypothesis of heat source in late 1930 for moving heat sources, and Rosenthal (Rosenthal, 1941) applied it in his work. Using mesh-based techniques, the arrangement of Rosenthal's model for moving heat passage issue requires modest strides just as the development of a fine or a versatile meshing to accomplish an exact portrayal of the situation of the spatial variation of heat flux and moving heat source. Every one of these prerequisites makes this sort of strategy computationally exorbitant.

Goldak (Goldak et al., 1984a) put forward another model for the heat source: the double ellipsoidal heat source model, which combines two semi-ellipsoidal heat source models. The double-ellipsoidal heat source can give more exact outcomes by looking at the exploratory evaluations, particularly in the low entrance welding measure.

Volumetric heat source modelling is the computationally intensive heat source modelling approach that considers the volume of material as the weld pool guided to traverse the model along with the weld bead. This weld pool is designed identical to the actual weld pool and heat flux received.

2.6.3.3 Thermal Modelling

Fourier's law for transient temperature field in space (x, y,z) and time (t) is expressed as

$$\nabla(k\nabla T) + \dot{q} - \rho cT = 0 \tag{2.6.7}$$

It can be written as

$$k\left(\frac{\partial^2 T}{\partial x^2} + \frac{\partial^2 T}{\partial y^2} + \frac{\partial^2 T}{\partial z^2}\right) + Qv = \rho c_p \frac{\partial T}{\partial t} \tag{2.6.8}$$

Qv is volumetric heat flux in $W.m^{-3}$, k(T) is the thermal conductivity as a function of temperature in $W.m^{-1}.K^{-1}$, Cp(T) indicates the specific heat in $J.kg^{-1}.k^{-1}$.

Newton's law of cooling is applicable for considering convection effects which can be written as

$$q_{conv} = -h_{conv}(T_s - T_\infty) \tag{2.6.9}$$

Where 'h' is the convective heat transfer coefficient, Ts is the surface temperature in K, and T_∞ is the surrounding temperature.

Stephen Boltzmann Law can be used to account for the radiation effects.

$$q_{rad} = -\sigma_{SB}\varepsilon_0[(T_s + 273.15)^4 - (T_\infty + 273.15)^4] \tag{2.6.10}$$

Rajput 2014 presented a model to present the MIG welding process in the double ellipsoidal heat source model. Heat density for front and rare are described by using the following equations:

For the front heat source:

$$Q_f(x,y,z) = \frac{6\sqrt{3}f_f Q}{a_f bc\pi\sqrt{\pi}} e^{-3\left(\frac{x^2}{a_f^2}+\frac{y^2}{b^2}+\frac{z^2}{c^2}\right)} \quad (2.6.11)$$

For the rear heat source:

$$Q_r(x,y,z) = \frac{6\sqrt{3}f_r Q}{a_f bc\pi\sqrt{\pi}} e^{-3\left(\frac{x^2}{a_r^2}+\frac{y^2}{b^2}+\frac{z^2}{c^2}\right)} \quad (2.6.12)$$

Q(x, y, z) indicates the value of thermal flow density in [W/m^3], Q is total source power. Also, a_r, a_f, b, c are useful parameters for that melting area.

2.6.3.4 Mechanical Analysis

The mechanical analysis includes utilizing the thermal narratives anticipated by the past thermal investigation for each time increase as a piece of information (thermal loading) to compute residual thermal stress and transient appropriations. In the thermal examination, the assessed mechanical and temperature investigations were directed to figure the weld twisting as the information data. A similar cross-section setup utilized in the thermal investigation is utilized in the mechanical examination, aside from the component type or boundary conditions. By and large, the complete strain increment can be communicated as the amount of the individual parts by thermal, plastic, and elastic strain and can be written as

$$\dot{\varepsilon} = \dot{\varepsilon}_e + \dot{\varepsilon}_p + \dot{\varepsilon}_{tp} + \dot{\varepsilon}_{ph} \quad (2.6.13)$$

Where the values of ε_{ph}, ε_{tp}, $\varepsilon_{p,}$ and ε_e are the values of phase transformation strain, thermal strain, plastic, and elastic strain and dot on top indicates the rate of respective strain. Using a thermal-elastic-plastic material formulation, residual analysis can be written as:

$$\sigma_v = \sqrt{\frac{1}{2}[(\sigma_1 - \sigma_2)^2 + (\sigma_2 - \sigma_3)^2 + (\sigma_3 - \sigma_1)^2]} \quad (2.6.14)$$

Where, σ_1, σ_2, and σ_3 are the values of principal stresses.

2.6.4 Limitations of residual stress measurement techniques in practice

The exploratory estimation of residual stress has pragmatic limitations. It is destructive as the opening drilling strategy. In any event, when non-destructive procedures are utilized (for example, diffraction strategy), residual stress can be estimated uniquely at discrete areas close to the weld surface. Because of the expense of doing welding experiments and time-intensive computational models, there is little data accessible about itemized residual stress circulation and its advancement in welds, including thicknesses more prominent than 50mm and the quantity of weld pass more noteworthy than 70mm.

The Lagrangian formulation has certain advantages over Eulerian for welding as complex geometry and non-linear equations can be easily solved using the Lagrangian approach. However, to use the Lagrangian approach to simulate the temperature field in welding phenomena, three main issues: Firstly, a very fine and neat mesh is required near and inside the weld pool to represent temperature gradient smoothly. Secondly, to minimize the numerical influence of welding, a large number of small time-step is required, which necessitates higher data storage capacity. Thirdly, to add the filler metal, for a moving weld pool, the geometry of the weld pool and mesh must be updated, which is very complex and expensive. So, mainly the addition of filler metal is usually ignored in Lagrangian finite element method simulations.

3 One-bar Model Demonstration using FEM in ABAQUS

3.1 Modelling Procedure

Step 1: Creating Model geometry

- The model database is created using the *standard/Explicit Model*.
- Deformable type wireframe 2D planar modelling space is used to create "One-bar model geometry".

- The approximate size of the grid is chosen as 2; this is always considered greater than the size of the part to be drawn for fitting our model inside the grid (dimension of the one-bar model is assumed as unit length and unit diameter). However, it is found that the approximate size of the grid does not affect the result of the analysis.
- Unit length Connected line is created using starting point of the line as axis value (X, Y) = (0, 0) and end point of the line as (X,Y) = (0,1).

Step 2: Storing Material Properties

- After the part has been created, material properties are stored.
- The *module* section of the Abaqus interface contains part, property, assembly, step, interaction, load, mesh, optimization, job, visualization, and sketch. A sequential process is followed to store the parameter values.
- Select a property module and create material properties with the name "Steel" The single material isotropic bar is assumed.
- Mechanical properties such as elastic, plastic are created. It is assumed that the bar material obeys stress-strain behavior of elastic -perfectly plastic-type, which implies that the linear relationship between stress and stress exists to the point of yield level. After the yield point, the material has stress equivalent to the yield strength of the bar material.
- Elastic properties of mild steel, i.e., young's modulus ($E = 206 * 10^3$ MPa) and Poison ratio (= 0.3), are inputted.
- Isotropic hardening with temperature-dependent plastic properties such as yield stress, the plastic strain of following values is used (Table 1).
- Isotropic linear expansion coefficient is set to ($\alpha = 1.47 \times 10^{-5}\ ^\circ C^{-1}$).
- Two cases are analyzed, with annealing and without annealing. When annealing is considered, the annealing temperature is set to melting point temperature of mild steel (θ_m = 1371 ◦C).

Table 1: yield stress and plastic strain properties at the corresponding temperature.

S. N.	Yield stress (Mpa)	Plastic strain	Temperature (◦C)
1	206	0	0
2	206	1	0
3	206	0	426
4	206	1	426
5	2.06	0	721
6	2.06	1	721
7	2.06	0	1371
8	2.06	1	1371

Step 3: Creating Section

- Once material properties are defined, a section is created.
- One-bar model is considered a truss section; therefore, select truss type section and press continue to define a cross-sectional area. The cross-sectional area of the bar is Pi/4 for the unit diameter bar.
- Temperature variation is considered constant through the thickness of the bar.
- The material properties are assigned to a bar section by selecting the *assign section* and clicking on any point of the bar drawn. Then press ok.

Step 4: Assembly section of a module

- Create instances from part drawn by going in the *assembly* section of the module. The instance type chosen here is mesh on part or dependent type instance.

Step 5: Creating step

- As our model is static, the initial step is created with the name "Apply temperature". The time period is set to 10 sec. One hundred increments are considered with initial, minimum, and maximum increment size as 0.1, 0.0001, 10, respectively.

The one-bar model has no contact properties as the bar is rigid at both ends. The interaction step is avoided.

Step 6: Defining loads

- Select *load* in module section and choose step as to applytemperature.
- A predefined field is created with the name "Temperature". The temperature step is applied to the bar by selecting the bar. Select direct specification distribution and the section variation as constant through the region. The temperature magnitude is selected as melting point temperature (1371 $^{\circ}$C for mild steel). The amplitude of temperature magnitude, which varies linearly over the step, is selected.
- Create tabular type amplitude, Amp-1, with the following time/frequency and amplitude data.

Table 2: time step and amplitude data for the predefined temperature field.

S. N.	Time/Frequency	Amplitude
1	0	0
2	5	1
3	10	0

Step 7: Defining boundary condition

- This step is performed by going into the *load* module.
- Create mechanical boundary conditions with the initial step type as encastre/symmetry/antisymmetry. Select two end points of the bar as the region of boundary condition and click done. Then select "ENCASTRE (U1 = U2 = U3 = UR1 = UR2 = UR3 = 0)" to apply rigid boundary condition at both ends of the bar. The term "U1, U2, U3 represents three possible translation motions, and UR1, UR2, UR3 denotes possible rotational motion.

Step 8: Meshing

- Select *Mesh* module and object as part (the created object name appears aside in the box, in this case, part-1 appears).
- Select see part and use approximate global size as 0.5. This indicates that the model has 3- nodes. The approximate global size defines the steps increment for each node for the length of the bar. With 0.5 increments, 3-nodes are generated.
- Select mesh part and click ok.
- Select the bar and then assign truss type mesh elements (T2D2: A 2-node linear 2-D truss).
- Verify the mesh.

Now, Field output can be selected. The desired output parameter is selected here. Generally, it is used to obtain contour plot, displaced shape plot, symbol plot, and X-Y plot. We select these options only as we are interested in elastic, plastic, thermal, and equivalent plastic strain components.

Step 9: Job creation

- Go to the *Job* module, create a job with the name "OneBar", and continue.
- Select job type as complete analysis and request output in ODB format.
- Go to the job manager section and submit the job.
- Go to job manager and select data check to see if there is any error notification. When the data check is completed, submit the job for analysis. The analysis time depends on the complexity of the job created.

- A similar procedure is repeated, or the previous job can be copied and modified for obtaining the job without annealing.

3.2 Post-processing/Results

- The results after the completion of the analysis are obtained in this section.
- Go to the *visualization* module, select contour plot, and plot the uniaxial stress contour.

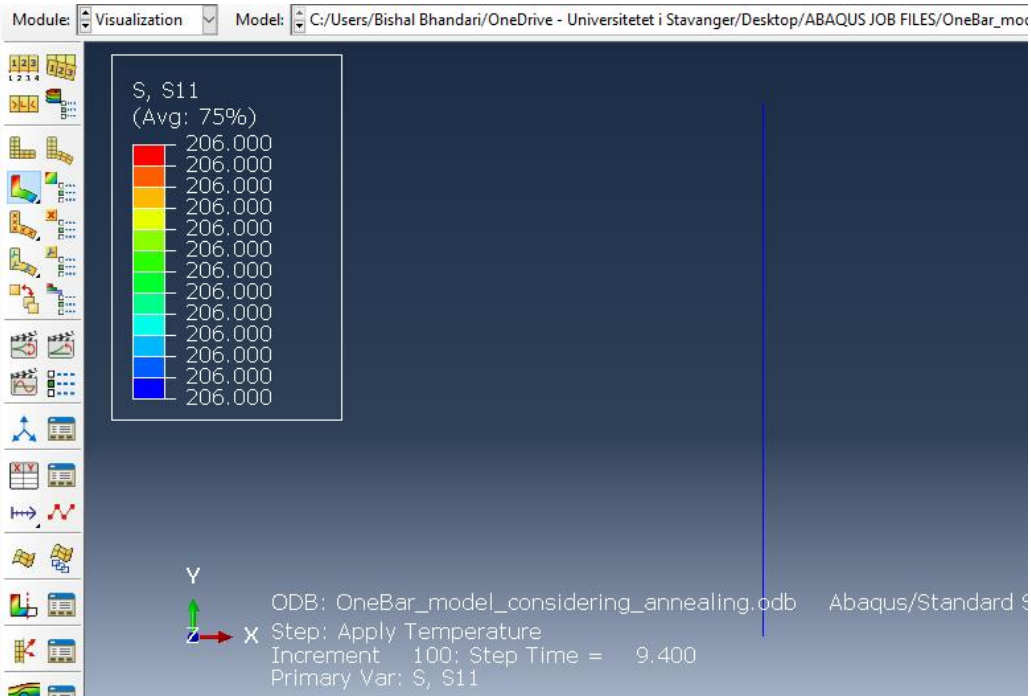

Figure 26: Contour plot showing uniaxial residual stress in the bar

- The von Misses stress contour plot shows that yield stress magnitude residual stresses are developed at the end of the thermal cycle. Here, we assumed the mild steel material with yield strength as 206 MPa in the one-bar model; therefore, we have obtained yield level residual stress of magnitude 206 MPa as shown by the above contour plot.
- Figure 27 shows the variation of elastic, plastic, thermal, and plastic equivalent strain with time. In the chosen study, the phase transformation effect is omitted. The total strain is then the sum of elastic, plastic, and thermal strain. However, this total strain depends on the type of strain increments involved in the thermomechanical process. Because the bar is fixed at both ends, the summation of incremental strain is always zero at different heating and cooling stages.

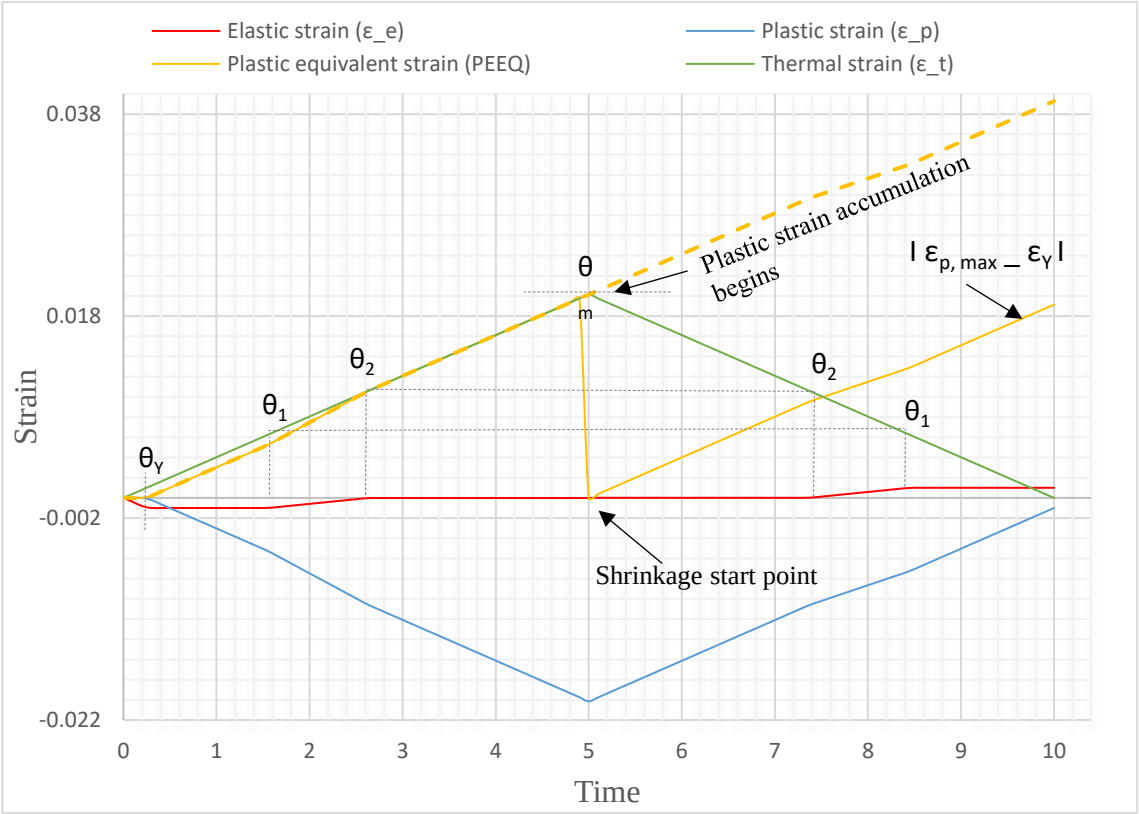

Figure 27: Variation of elastic, plastic, thermal, and plastic equivalent strain obtained from one-bar model generated. The effect of annealing is considered.

- At the initial stage of heating of the bar, only elastic and thermal strain are generated of the same value but opposite in sign as depicted in figure 21. The strength of the material decreases linearly as the temperature increases, and the yield level compressive residual stress is generated, as in figure 22. The elastic strain at this point is $\varepsilon_e = \sigma_y / E$ = (206 Mpa)/(206★10^3 MPa) = 0.001 and the temperature at which the one-bar reaches yield point is given by $\theta_y = \varepsilon_y / \alpha = 68.02\ ^{\circ}C$. $\theta_{max} \geq 2\theta_y$ is the sufficient temperature for generation of yield level residual stresses when the bar is fully restrained; therefore, yield level residual formation is common in most of the thermal processes such as forming, initial welding, repair welding, and so on as these processes easily attain the above-obtained temperature.
- The elastic strain and longitudinal residual stress have no change in values when the bar is further heated above θ_Y to θ_1, but the increase in temperature increases compressive plastic strain equivalent to an increase in thermal strain.
- Further increase of temperature from θ_1 to θ_2 leads to a continuous decrease in the value of yield strength and elastic strain approaching zero. However, at this point, the

compressive plastic strain and thermal strain keeps on increasing. The difference between a total thermal strain and elastic strain gives the value of equivalent plastic strain in this region.

- When the temperature of the bar rises from θ_2 to θ_m, the plastic strain reaches maximum. Nonetheless, an equivalent plastic strain of zero value is obtained at melting point temperature as the material changes from solid to liquid state when annealing is considered, or the material reaches its original state after cooling.
- When the annealing effect is not considered, the bar material retains its plastic strain history as it passes through melting point temperature.
- If the melting and re-melting process of the material displaying substantial strain hardening is not addressed, this may lead to overestimating residual stresses.
- While cooling from θ_m to θ_2, thermal strains decrease in addition to the beginning of the shrinkage phase. The shrinkage strain gets converted to the plastic strain before θ_2 is attained. The tensile plastic strain equivalent to the difference of maximum plastic strains and yield strains is obtained at the end of the cooling cycle.

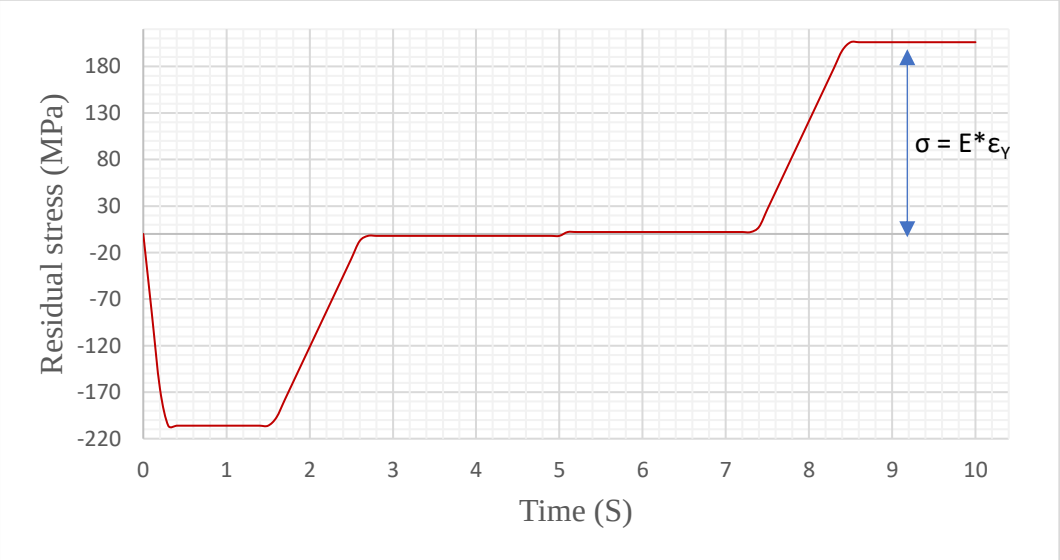

Figure 28: Residual stress variation in the one-bar model for the period of 10 s considering annealing effect.

- The residual stress plot shows that compressive residual stress of yield magnitude is generated in a uniform heating cycle, and tensile residual stress is produced at the cooling cycle. An initial increase in the bar's temperature during the heating cycle results in an increase in compressive residual stress of the bar material until $\theta_{Y,\,It}$ remains constant from θ_Y till θ_2, then gradually vanishes to zero at melting point temperature. In cooling further,

tensile residual stress gradually builds up and reaches a uniform value of yield stress magnitude.

3.3 Discussion

The one-bar model shows that plastic strain is commonplace in welding. During the heating cycle, the local plastic deformation starts as early as the yield point temperature (θ_Y = 68 $^{\circ}$C), and the $2\theta_Y$ temperature difference is enough to develop the yield magnitude residual stress upon cooling. Depending on the hardening behavior, the residual stress can be significantly higher than yield magnitude in a constrained direction. The melting and re-melting effect largely influences the equivalent plastic strain curve; therefore requires extensive knowledge on the exact annealing temperature and its influence. Inappropriate consideration can lead to an error-prone prediction of plastic equivalent strain because of plastic strain accumulation. This demonstration also helps to understand that the residual stress relaxation requires the minimum plastic deformation of the amount of yield strain and, in this case, is about 0.001 in permanent strain; thus, post-weld heat treatment methods can be used to relieve the residual stress. However, the one-bar model lacks information about the system's spatial residual stress distribution and final distortion behavior.

4 Demonstration of Residual Stress and Distortion using Three-bar Model in ABAQUS

The residual stress distribution in longitudinal and transverse directions can be obtained by constructing a three-bar model analogous to a welding plate. The deformation at different stages can also be obtained. This approach assumes central bar as welding centerline, and the other two bar surrounding the central bar is considered the plate section outside weld. If any one end of the bar is considered a weld bead line, then the problem is not axisymmetric, and the case is analogous to edge welding of the plate. The following modelling procedure assumes the symmetrical plate about the welding centerline, which means that the end bars have symmetrical geometrical properties and equidistance from the central bar.

4.1 Modelling Procedure

Step 1: Creating Model geometry

- The model database is created using the *standard/Explicit Model*.
- Deformable type wireframe 2D planar modelling space is used to create "Three-bar model geometry".
- Three-bar section having the following coordinates is constructed using connect lines.
    a) Central bar: start point (0,0) and end point (10,0)
    b) Left bar: start point (5,0) and end point (5,10)
    c) Right bar: start point (-5,0) and end point (-5,10)

Step 2: Input material properties

- *Storing the material properties* section of the one-bar modelling procedure is repeated to input the material properties.

Step 3: Create Section

- Two truss type section is created. Unit diameter bar is considered. The first section with the name Bar2 having cross-sectional area *pi* is assigned to a middle bar, and the second section with the name Bar13 having cross-sectional area 3*pi is assigned to the other two bars.
- Constant through-thickness temperature variation is selected.

Step 4: Assembly section of the module

- Part instance with instance type as mesh on part or dependent type instance is selected.

Step 5: Creating step

- General static type model having step name as "Three_bar" is created.

Step 6: Interaction

- Beam type multi-point constraint (MPC) with control point as middle bar and slave nodes on other two ends of the bar is created. MPC beam is assumed at the top of the bar, as shown in Figure 29.

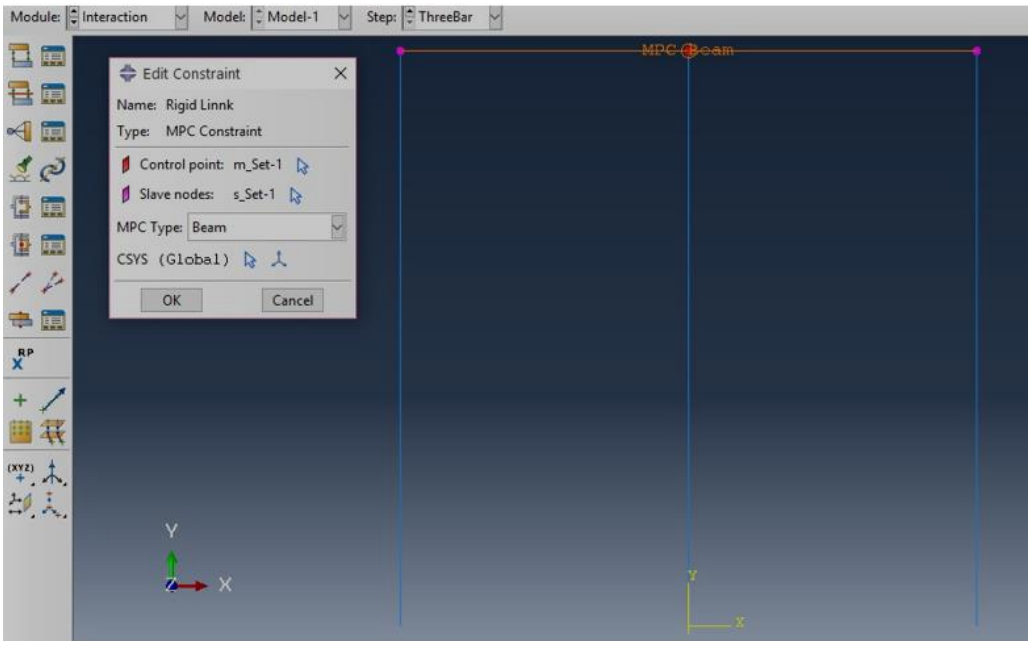

Figure 29: Beam type multi-point constraints

Step 6: Defining loads

- Temperature load is created with the name "Apply temperature". The same parameters as in the one-bar model are defined here with the same values.

  Step 7: Defining boundary condition

- The lower end of all the three-bars are fixed using ENCASTRE (U1 = U2 = U3 = UR1 = UR2 = UR3 = 0) boundary condition.

Step 8: Meshing

- Select *Mesh* module and object as part. Define global size equal to 5, which creates three nodes on all the bars, and then assign truss type mesh element T2D2 to all three-bars.

The required field outputs such as residual stresses, nodal temperature, and strain components can be selected in field output requests.

Step 9: Job creation

- Under the job module, a new job with the name "ThreeBarmodel" is created for the complete analysis, and output in Odb format is requested.
- Then the job is submitted, and data check is carried out to ensure the correctness of the data provided, and then the job is submitted.

4.2 Post-processing/Results

4.2.1.1 Strain Plot

The variation of elastic strain, plastic strain, thermal strain, and plastic equivalent strain in a middle bar during the heating and cooling cycle of the three-bar model as in Figure 30. The nature of the plot is similar to the one-bar model. This graph illustrates that consideration of the annealing process avoids the accumulation of plastic strain during the cooling process in the simulation result.

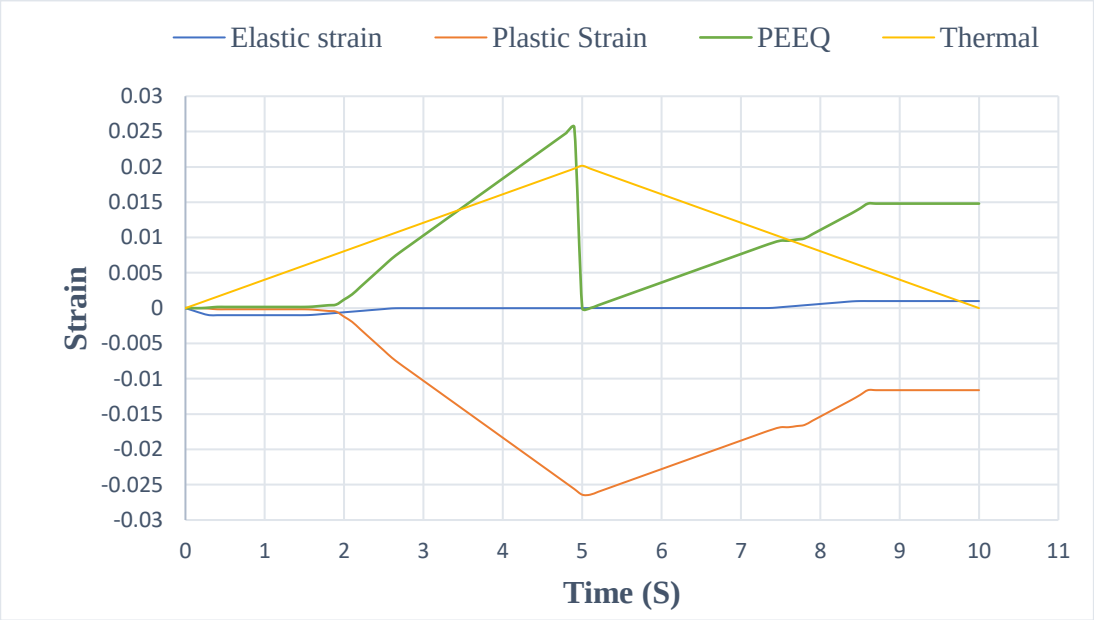

Figure 30: Variation of elastic, plastic, PEEQ, and thermal strain in the middle bar of the three-bar model during one complete heating and cooling cycle.

4.2.1.2 Transverse Residual Stress Variation

The bar's orientations in the y-direction in the three-bar model allow us to evaluate the transverse residual stress and distortions illustrated by Figure 31. The residual stress in the transverse direction is similar to longitudinal residual stress obtained in the one-bar model. During the heating cycle, compressive and tensile residual stress in the middle and outer bars increases until the yield point temperature is reached. As the heating cycle progresses, the maximum value of compressive transverse residual stress equivalent to yield strength is obtained. The tensile transverse residual stress on the surrounding bars is approximately equal to one-eighth of the transverse residual stress. The tensile and compressive residual stress on all the bars starts decreasing and vanishes to zero. No residual stresses are present till the material starts the solidification process that means when cooling begins, the residual

compressive and tensile stress on all the starts appearing. Now, the compressive stress on the outer bar and tensile stress on the heated bar increases. During the final stage of cooling, constant yield level tensile residual stress is developed in the middle bar while compressive stress on the outer bars of one-fourth of the yield value is produced.

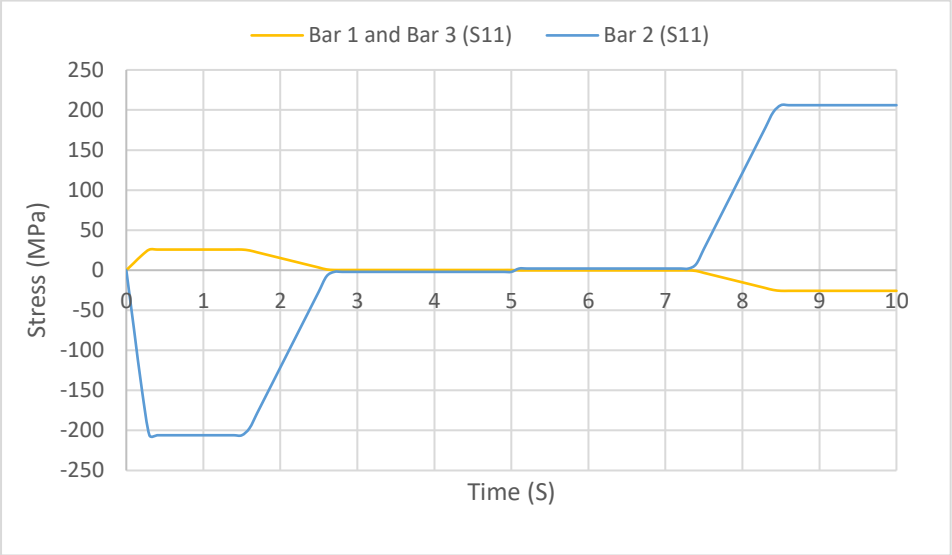

Figure 31: Development of compressive and tensile residual stress in the three-bar during a complete one thermal cycle

4.2.1.3 Displacement in the Bar due to Thermal Cycle

The three-bar model helps analyze the displacement of the bar because of the thermal cycle. The following contour plot suggests that the maximum possible displacement of 0.00125 mm occurred at time 0.3 s in all the bars. Other translational and rotational displacement in the bar is obtained zero due to the constrain applied at the bottom of the bar and the rigid link condition assumed. The displacement obtained due to the heating and cooling cycle is crucial in determining distortions' final state. If the distortions are too large, then there are high chances of failure of the structure.

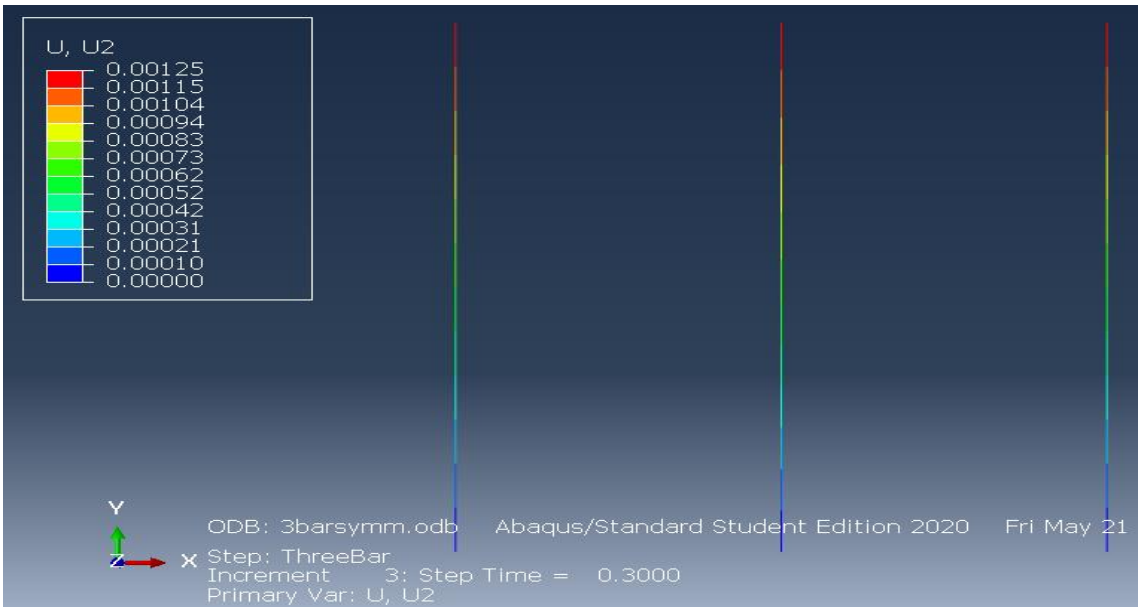

Figure 32: Displacement in the three-bar due to heating and cooling cycle.

4.3 Validation and Discussion

The final residual stress and displacement calculated by both residual stress measurement methods, i.e., analytical and finite element simulation methods, correspond to each other. The three-bar model is another simple model to demonstrate the residual stress and distortion measurement induced by the welding process. The welded plate is analogous to the three-bar model because the weld line is where the heat source is applied, and the remaining part is relatively cooler than the weld beads, which are represented as sidebars in the 3-bar model. The constrained action caused by the cooler section in the hotter section initiated the residual stress in the bar and is influenced by the consecutive heating and cooling cycle. This process caused a deflection in the bars.

5 Thermo-mechanical Analysis using FEM in ABAQUS

5.1 Problem Description

Consider a 5mm thick low carbon steel plate subjected to a specified temperature profile (depending on x only), as illustrated in Figure 33, along a plate width cross-section A-A. The same temperature distribution is assumed to be constant along the plate length direction (i.e., y). The temperature distribution is approximated using equation (5.1.1). It is further assumed that all relevant material properties are independent of temperature, namely E=206

GPa, yield stress S_Y=206 MPa, and coefficient of thermal expansion α = 0.0000147 mm/mm/°C.

$$Equation\ T(x) = 1000\exp\left(-\left(\frac{x}{20}\right)^2\right) \quad (5.1.1)$$

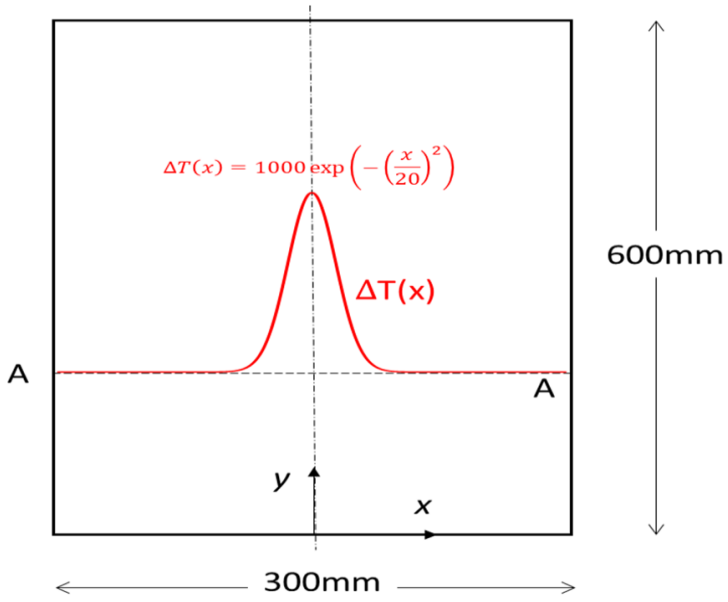

Figure 33: Full-size 2D axisymmetric model of the plate. The center axis line (y-axis line) is supposed as a welding line. The symmetrical plate requires only a quarter part to be analyzed. This dramatically reduces the number of nodes and computational time required for a thermomechanical simulation plate.

5.2 Objectives

- Create a plane stress element model with the anticipated plastic zone region modelled with an element size of about t/2.
- Perform elastic-plastic (assuming no hardening) thermomechanical simulation for determining the following:

  (a) Plot and analyze residual stress distribution and resulting distortion

  (b) Plastic deformation zone size w_p ("peeq">0) and shrinkage zone size w_p' ("peeq" $\geq \varepsilon_y$).

5.3 Modelling Procedure

Step 1: Creating Model geometry and storing properties

- 2D planar deformable shell model is created with the name "QuarterPlate" and an approximate grid size of 1000.
- The dimension of the quarter size plate is specified while creating the part with coordinates (0,0), (150,0), (150,300), (0,300).
- Material properties are stored with the name "Steel". Elastic properties with young's modulus $206*10^3$ MPa and poison's ratio 0.3 are specified. Rate independent plastic properties of yield stress 206 MPa and zero plastic strain are stored.
- A thermal expansion coefficient of value $1.47*10^{-5}$ $°C^{-1}$ is considered.

Step 3: Creating Section and assigning to the model

- Creating a section and assigning this section to the part created is the next step in the Abaqus modelling procedure.
- The homogeneous solid section having steel properties with plane stress/strain thickness of 5 is specified in the "sectionplate" section. This indicates that the study is focused on longitudinal and transverse residual stress in a 2D plate.
- Created section properties are assigned to the quarter plate model. In the next step, after going in the assembly model, a part instance is created for the model.

Step 4: Step module

- Create "Applytemperature" step of static, general procedure type. Hundred of increments are specified from the start point of 0.1 to the end value of 1 for this step. Another step representing the cooling cycle of the thermal process is also created. As the interactions are not present, the next step is to load the module and specify the boundary conditions of the problem.

Step 5: Boundary conditions and Predefined field input

- Go to create boundary condition section under load module.
- Create mechanical boundary conditions with the initial step type as encastre/symmetry/antisymmetry. Select y-axis line of plate model and press done. Then select "XSYMM (U1 = UR2 = UR3 = 0)" to apply rigid boundary condition in the welding centerline.
- Similarly, another mechanical boundary is created to apply the "YSYMM (U2 = UR1 = UR3 = 0)" boundary condition to the x-axis of the plate model.

- Temperature type predefined field in apply temperature step with the magnitude one and temperature distribution of equation T(x) = 1000*e^(-(x/20) ^2) is created. This analytical expression of the temperature field is selected in the heating cycle of the thermal process.
- The zero-magnitude temperature as per the temperature distribution equation is applied in the cooling step created.

Step 6: Mesh generation

- Go to mesh module, select the part and click on seed part to create global seeds of approximate seed size of 2.5. This means that the element size of about thickness t/2 thickness is chosen.

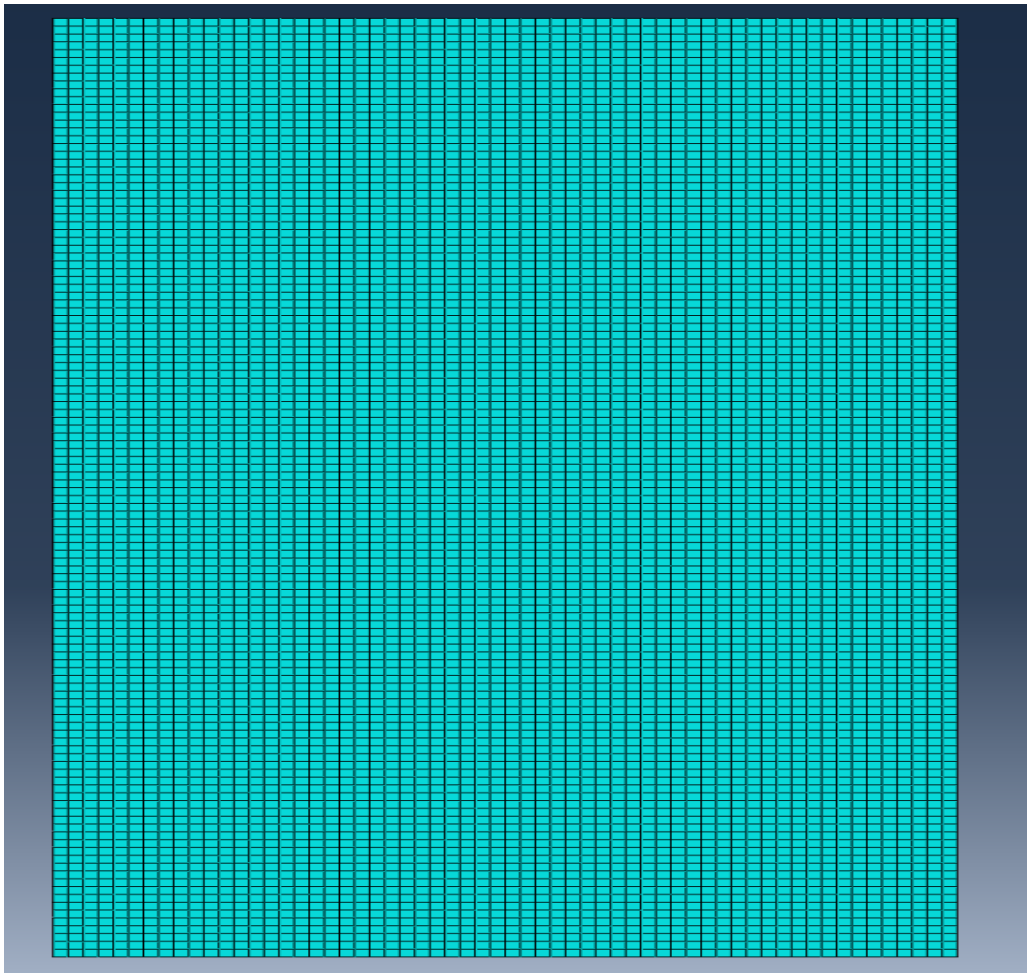

Figure 34: 2D axisymmetric quarter plate meshed with four-node bilinear plane stress quadrilateral element (CPS4R)

- Then the quarter plate model is meshed as in figure 34 with a four-node bilinear plane stress quadrilateral element (CPS4R) without reduced integration.

Field output and history output are requested for Nodal temperature (NT), stress (S), Strains, and reactions during heating and cooling cycles.

Step 9: Job module

- Create a job by going in the job module with the name "quarterplate". Data check is initiated, and upon successful data check, the job is submitted to the solver. This is the last step of pre-processing in Abaqus.

5.4 Post-processing/Results

5.4.1 Stress Contour Plot

The stress contour plot at the final point of the thermal process of the problem described is shown in Figure 35, Figure 35, and Figure 37. The stress contour plot of the quarter plate model in Figure 35 shows that one of the components of residual stress in the transverse direction to the welding centerline. The tensile residual stress of maximum value of 213 MPa and compressive stress of largest value 250 Mpa is obtained at the final increment of the heating cycle. The contour plot indicates that the welding plate experiences the tensile and compressive residual stress at a time. The larger residual stress at the top end weld centerline is highly influenced by tensile stress and a region slightly right to that experience's maximum compressive stresses. However, at the end of the cooling cycle, the region which suffered the maximum tensile residual stress in the previous stage (at the end of the heating cycle) is influenced by compressive stress. This causes a shrinkage in the top end point of the welding centerline, as depicted in Figure 35(right). Then the region a little far to the right end of the quarter plate suffers tensile residual stress in comparably lesser areas.

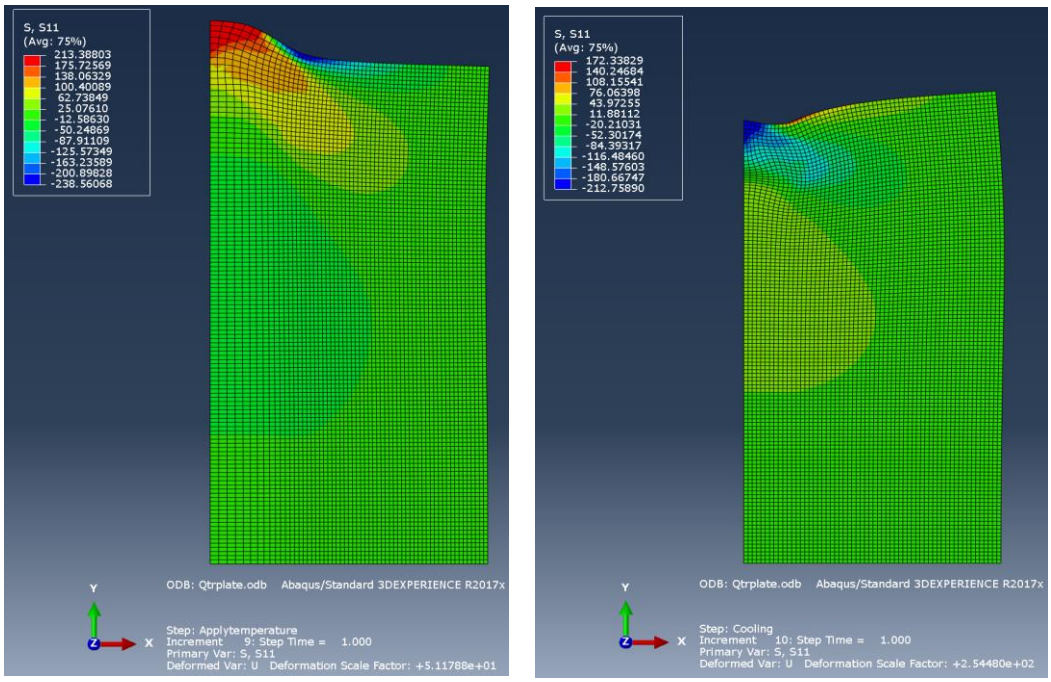

Figure 35: Stress contour plot (S11) at the final increment of the heating cycle (left) and the end of the cooling cycle (right).

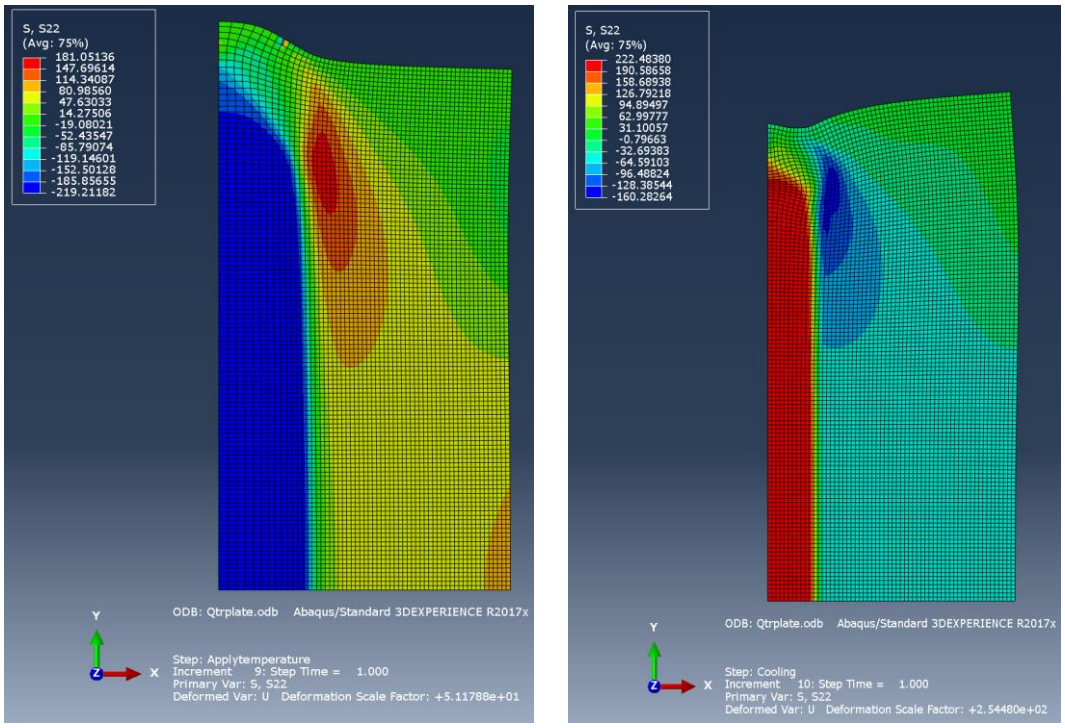

Figure 36: Stress contour plot (S22) at the end of the heating cycle (left) and the end of the cooling cycle (right).

Another component of residual stress in the transverse direction to the welding centerline is shown in Figure 36. The left contour plot shows that the maximum tensile stress is experienced by a region located at almost the upper-mid-left side of the quarter plate. In contrast, the welding centerline experiences the largest compressive residual stress at the end

of the heating cycle. The right figure shows that the maximum tensile residual stress influences the welding centerline at the end of the cooling cycle. In contrast, the region which suffered maximum tensile stresses at the end of the heating cycle is influenced by maximum compressive stresses when one thermal cycle completes.

The third component of transverse residual stress (S33) is zero because the 2D plane stress condition is assumed; therefore, this component is obtained zero in the contour plot.

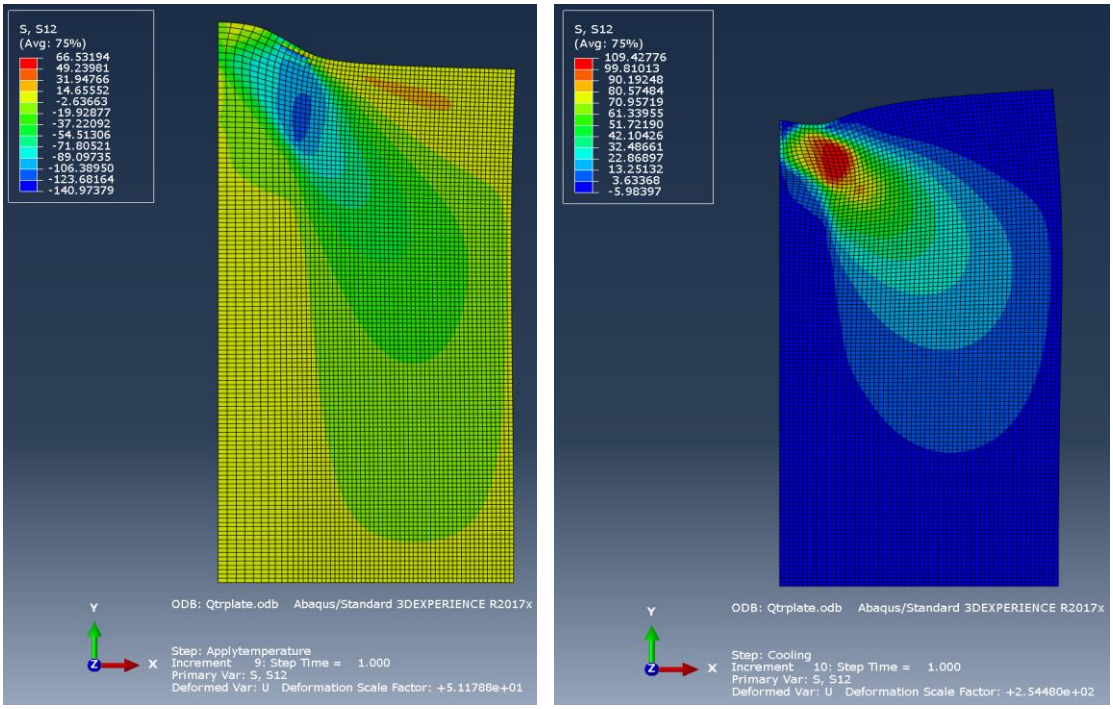

Figure 37: Shear stress component (S12) of residual stresses at the end of the heating cycle (left) and the end of the cooling cycle(right)

The shear component of residual stress is attached in Figure 37, which describes the variation of the shear component in the two-dimensional plate. The compressive shear stress dominates the plate surface at the end of the heating cycle, as shown in the left figure. However, a small region exists at the top-middle end of the plate where the positive value of shear stress is seen. Unlike the mapped residual stress at the end of the heating cycle of the thermal process, the maximum value of 109 MPa is observed at the top left corner of quarter plate mode; usually, this region largely suffers shrinkage phenomena. There is minimal shear residual stress on most of the plate at the end of the cooling cycle.

5.4.2 Residual Stress Vs. Distance from Weld Centre

Figure 38: S11 component of residual stress across the length of the quarte plate

Figure 38 presents the transverse residual stress distribution across the length of the quarter plate. S11 component of residual stress starts increasing slowly as we move towards the right side of the quarter plate; however, after a certain distance is reached, this component of residual stress starts decreasing and reaches zero at the bottom right corner of the quarter plate. This figure clearly describes that the s11 component of transverse residual stress is negligible in the direction perpendicular to the welding centerline.

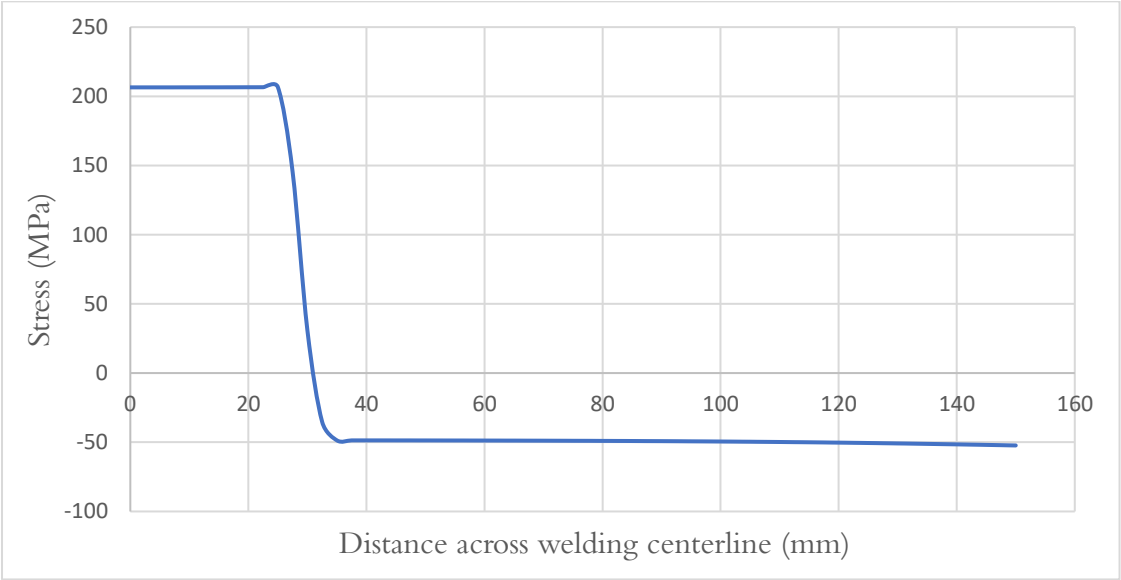

Figure 39: S22 across welding centerline

Tensile residual stress of approximate yield strength value is observed for a certain distance which then starts decreasing sharply over a small distance, and small compressive stress of 50 Mpa is developed across the length of the plate.

From Figure 38 and Figure 39, it can be concluded that there is a significant amount of residual stress present near the origin. However, finally, there will only exist compressive residual stress of approximately one-fourth of the yield stress value of the plate material.

Variation of residual stress along the welding centerline of the axisymmetric plate model is plotted in Figure 40—both components (S11, S22) of residual stress exhibit the same trend. S11 component of residual stress has a maximum value at the origin of the welding centerline, which remains constant for almost the entire length of the welding line; however, this stress sharply reduces and reaches a negligible compressive stress value at the end of the welding centerline. Contrary to the S11 component, the S22 component of residual stress experiences increases in the value of tensile residual stress. Almost at the same point where the s11 component started decreasing its value, this component also decreases and finally reaches a compressive value of yield strength. This plot suggests that when a plate is exposed to a thermal cycle, the plate is under continuous stress influences, whether it be tensile in nature or compressive. Finally, the plate primarily suffers from compressive stresses along the welding centerline, resulting in the shrinkage of the plate model at the top end of the welding centerline or the stop position of the welding process.

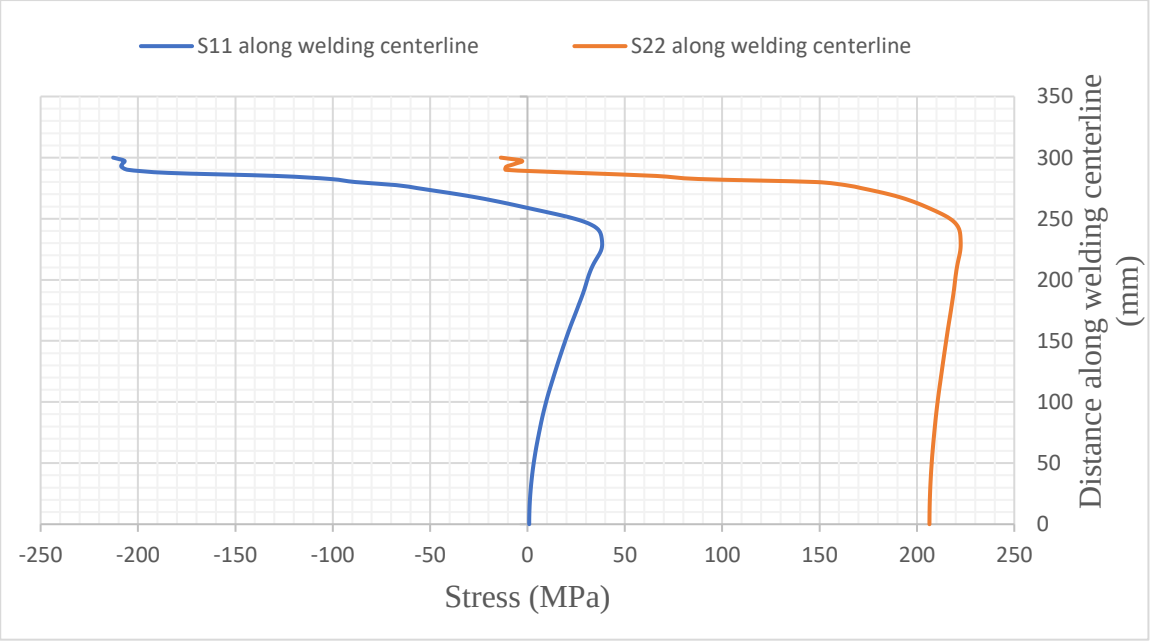

Figure 40: Variation of residual stress components along the welding centerline

5.4.3 Nodal Temperature Plot

Figure 41 explains the nodal temperature distribution in the quarter part of the welding plate at the end of each thermal process. At the end of a heating cycle, the temperature distribution contour plot shows that the welding centerline experiences the largest increase in temperature. The region experiencing this is called a heat-affected zone. The area outside the heat-affected zone has suffered significantly less increase in the temperature. The temperature contour plot is shown in Figure 41 (right) shows that the welding centerline experiences comparatively less temperature region at the end of the heating cycle. Region away from welding centerline also experiences comparatively less temperature region than in heating cycle.

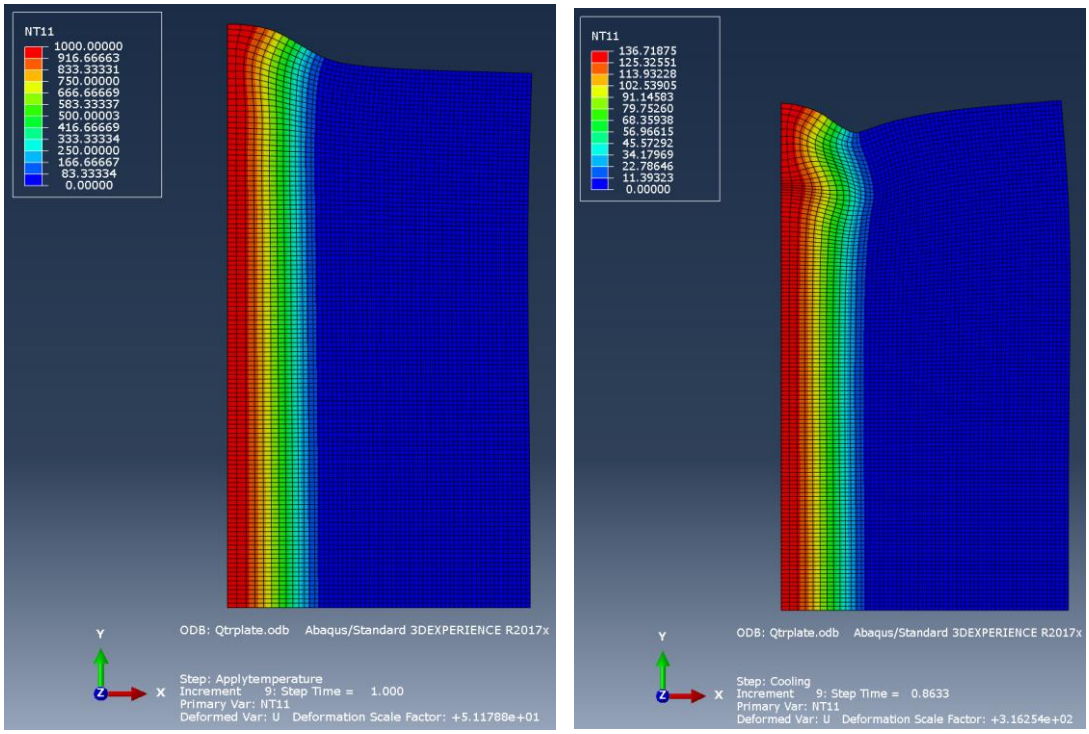

Figure 41: Temperature distribution across the welding plate at the end of the heating and cooling cycle in left and right, respectively.

5.4.4 Displacement Plot

The nodal temperature esteems determined during the thermal examination were utilized as a predefined field for the mechanical investigation to determine the distortions state initiated by welding. It is safe to expect that the mechanical reaction of the test specimens relies on the thermal stacking, while there is no inverse reliance. This is because the heat produced because of the mechanical dissemination is insignificantly little when contrasted

with the heat energy provided by the heat source. Figure 42 shows the contour deformation plot along and across the welding line. The deformed shape is mapped over the original shape so that the longitudinal and transverse shrinkages are visible. The left contour plot shows that the plate has positive deformation across the plate, whereas significant negative deformation (shrinkage) along the centerline. Larger negative values of displacement component define that a significant amount of shrinkage at the top left corner of the quarter plate occurs due to the thermal cycle.

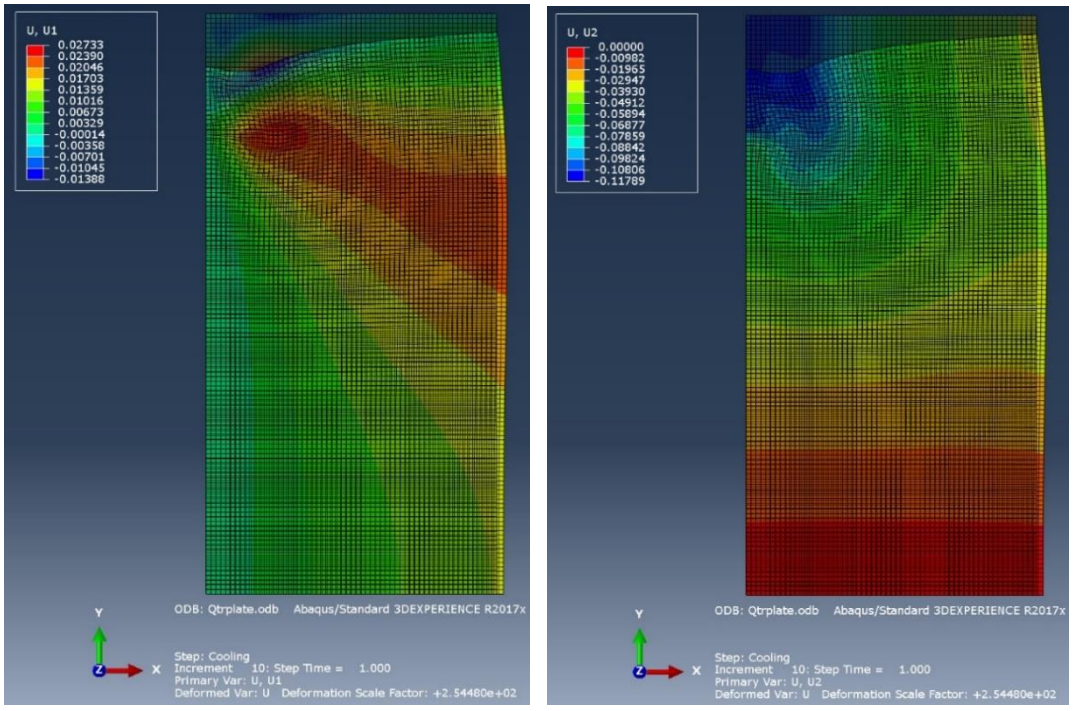

Figure 42: Displacement contour plots along and across the weld centerline. U1 represents longitudinal shrinkage along the length of the welding centerline, and U2 describes transverse shrinkage across the welding line.

5.4.5 Plastic Strain Zone and Shrinkage Strain Zone

The temperature distribution plot across the welding centerline shows a gradual decrease in nodal temperature in relation to the distance away from the heat application line. The welding centerline experiences the maximum magnitude of temperature as described by the temperature distribution equation used in the predefined field. ss

The temperature distribution and PEEQ plot shown in Figure 43 is used to examine the yield point temperature, plastic deformation zone (W_p) and, shrinkage zone (W_p'). The intersection of the nodal temperature plot and a horizontal line extended from yield strain value (= 0.001) is used to find the plastic deformation zone. The intersection of the plastic equivalent strain graph with a horizontal line drawn from yield strain value defines the

shrinkage zone. The horizontal distance from the weld centreline to these intersection points is used to calculate the plastic deformation zone and shrinkage zone. The plastic deformation zone (Wp) size is 63.2 mm, and the shrinkage zone size (W_p') is 54.8 mm measured from the welding centreline.

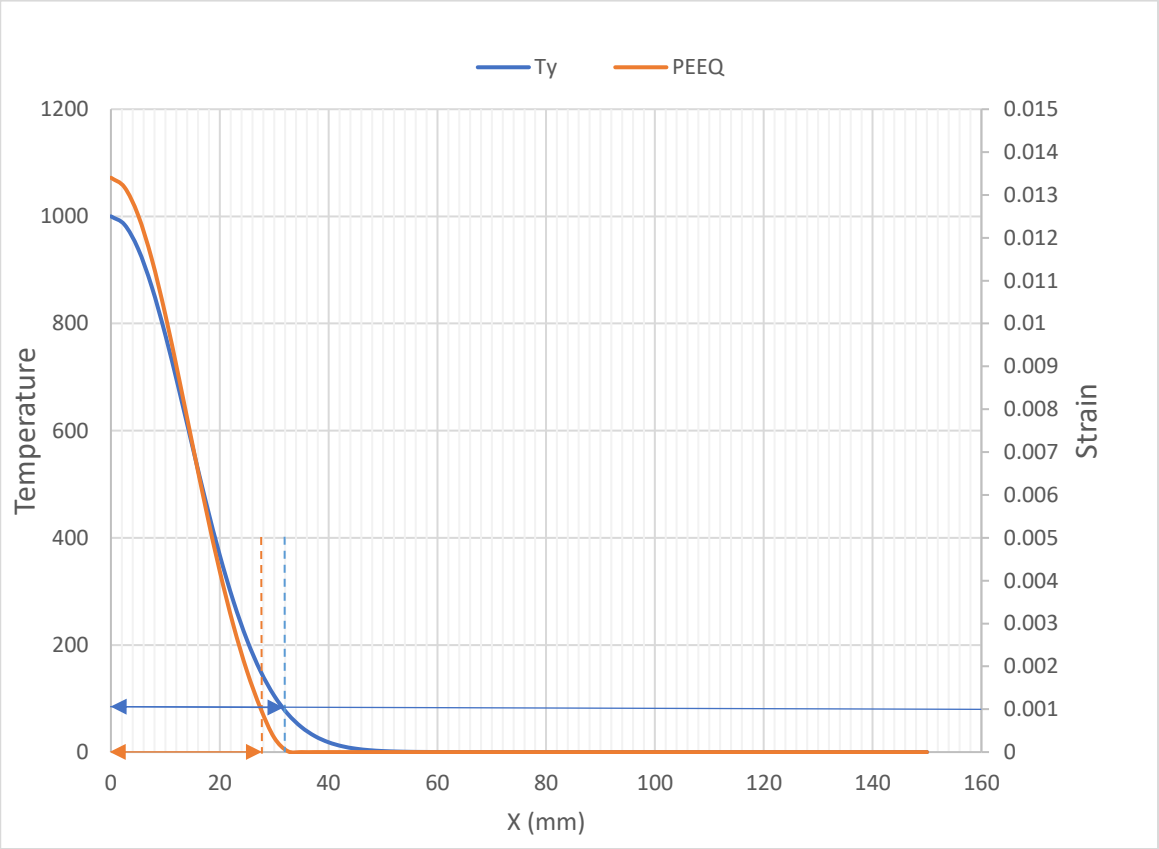

Figure 43: Temperature distribution and plastic equivalent strain variation across the welding centerline

The radius of the shrinkage zone, the plate's width, yield strain, and thermal expansion coefficient are used to calculate the yield point temperature. Table 3 below shows the calculation of Plastic strain zone size (W_p) and Shrinkage zone size (W_p'), and yield point temperature (ΔT_y).

Table 3: Yield temperature, plastic strain zone, and shrinkage zone result comparison.

<table>
<tr><th>X (mm)</th><th>Temperature(°C)</th><th>Plastic strain zone size (W_p) and Shrinkage zone size (W_p')</th><th>Yield point temperature</th></tr>
<tr><td>25</td><td>209.611</td><td rowspan="2">W_p= 2rp = 63.2</td><td rowspan="4">$\Delta T_y = \frac{W*\varepsilon y}{\alpha\,(W-ry)}$ = 83.23 °C</td></tr>
<tr><td>27.5</td><td>150.977</td></tr>
<tr><td>30</td><td>105.399</td><td rowspan="2">W_p' = 2ry = 54.8</td></tr>
<tr><td>32</td><td>71.3167</td></tr>
</table>

5.5 Application of Shrinkage Strain Method on Illustrative Case Study using FEM

5.5.1 Objective

- Based on the shrinkage zone size identified in the thermo-mechanical process, perform a shrinkage strain-based residual stress estimation.
- Compare transverse residual stress distributions, displacements.

5.5.2 Modelling Procedure

Step 1: Creating model geometry and storing properties

- 2D planar deformable shell model is created with the name "QuarterPlate_SS".
- The dimension of the quarter size plate is specified while creating the part with coordinates (0,0), (150,0), (150,300), (0,300).
- With partition face sketch in the part module, offset line is drawn with respect to the y-axis, and offset value of 27.4 mm (shrinkage zone value for the quarter plate) is specified. The shrinkage size should be known in advance to use the shrinkage strain method to analyze residual stress and distortions.

- Material properties are stored with the name "Steel". Elastic properties with young's modulus $206 \star 10^3$ MPa and poison's ratio 0.3 is specified. Rate independent plastic properties of yield stress 206 MPa and zero plastic strain are stored.
- A thermal expansion coefficient of value $1.47 \star 10^{-5}$ $°C^{-1}$ is considered.

Step 3: Creating Section and assigning to the model

- The homogeneous solid section having steel properties with plane stress/strain thickness of 5 is specified in the "sectionplate" section. This indicates that the study is focused on longitudinal and transverse residual stress in a 2D plate.
- Created section properties are assigned to the quarter plate model. In the next step, after going into the assembly model, the part instance is created for the model.

Step 4: Step module

- Create "Applytemperature" step of static, general procedure type. Hundred of increments are specified from the start point of 0.1 to the end value of 1 for this step. Another step representing the cooling cycle of the thermal process is also created. As the interactions are not present, the next step is to load the module and specify the boundary conditions of the problem.

Step 5: Boundary conditions and Predefined field input

- Go to create boundary condition section under load module.
- Create mechanical boundary conditions with the initial step type as encastre/symmetry/antisymmetry. Select y-axis line of plate model and press done. Then select "XSYMM (U1 = UR2 = UR3 = 0)" to apply rigid boundary condition in the welding centerline.
- Similarly, another mechanical boundary is created to apply the "YSYMM (U2 = UR1 = UR3 = 0)" boundary condition to the x-axis of the plate model.
- Go to a predefined field under the load module and create a predefined temperature field, and name that step as "shrinkage_strain_step". The temperature value specified in this is -83.23 $^{\circ}C$ (a negative sign is used to define the temperature resulting in shrinkage in the plate).

Step 6: Mesh generation

- Go to mesh module, select a part and click on seed part to create global seeds of approximate seed size of 2.5. This means that the element size of about thickness t/2 thickness is chosen.
- Then the quarter plate model is meshed as in figure 34 with a four-node bilinear plane stress quadrilateral element (CPS4R) without reduced integration.

Field output and history output are requested for Nodal temperature (NT), stress (S), Strains, and reactions during heating and cooling cycles.

Step 9: Job module

- Create a job by going to the job module with the name "quarterplate_shrinkaghe_strain". Data check is initiated, and upon successful data check, the job is submitted to the solver.

5.5.3 Post-Processing/Results

5.5.3.1 Stress Contour Plot

The stress contour plot in Figure 44 maps the residual stress induced over the surface of the plate when a temperature field /heat source is applied to it. A significant amount of compressive stress (221 MPa) influences the top left corner of the plate where the end point of welding is. However, most of the plate is influenced by the tensile component of residual stress having significantly smaller values. S22 component of residual stress is more concentrated along the welding centerline, while compressive residual stresses are generated beside the welding centerline. On the top half upper part of the plate, shear components of residual stress are generated having comparably lesser value than the tensile and compressive stresses components shown in Figure 44 (a), (b), and (c).

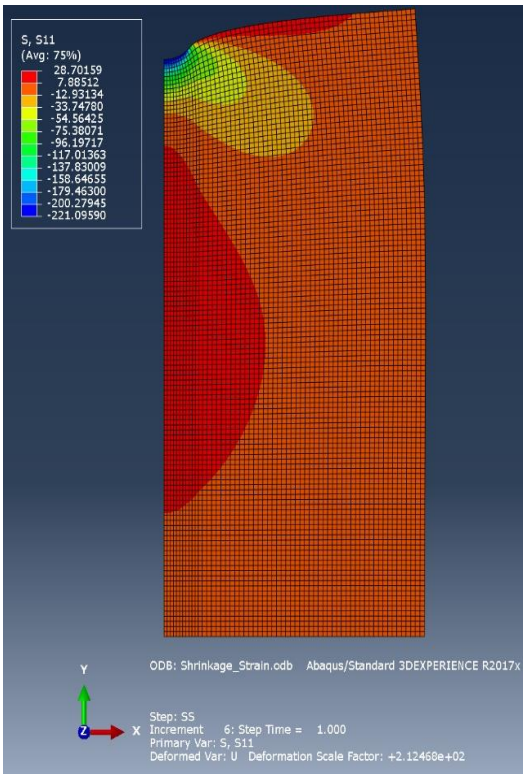

(a)

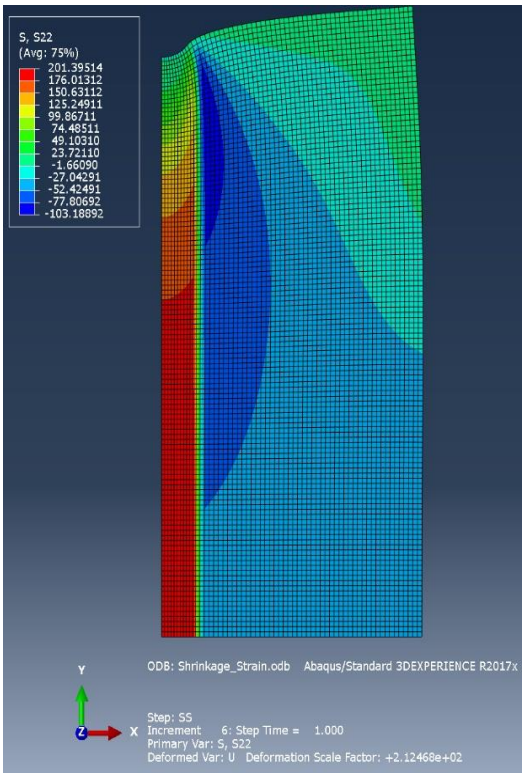

(b)

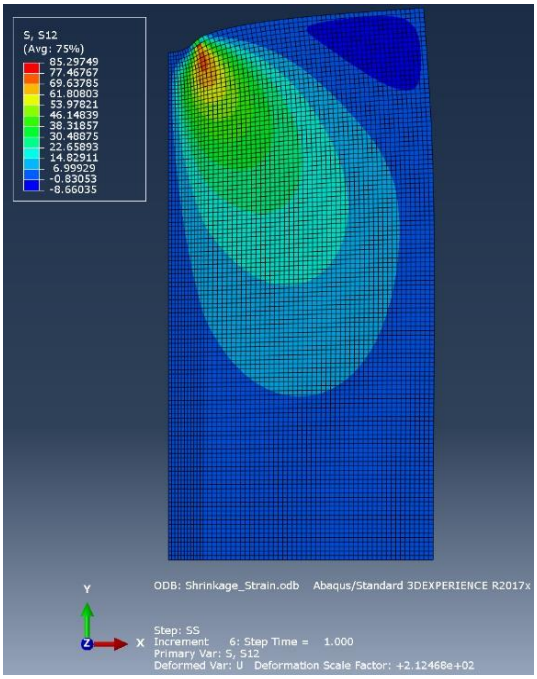

(c)

Figure 44: Stress contour plot obtained by shrinkage strain method (a) S11 component (b) S22 component (c) S12 or shear component

5.5.3.2 Displacement Contour Plot

The displacement contour plot, U1 component, and U2 component resulted from the shrinkage strain method describe the significant amount of longitudinal shrinkage along the axis of the welding line and transverse shrinkage across the length of the quarter plate. The contour plot of the deformed shape is mapped over the original plate, as shown in Figure 45. From the images, it can be seen that there is not much effect of thermal cycle on displacement contour at the bottom and mid point of welding line; however, the top left end of the welding plate along the welding line experiences a significant amount of distortions and resulting in transverse shrinkage. Moreover, the top part of the quarter plate across the welding line experiences shrinkage distortions, although in smaller amounts compared to the top-left end of the quarter plate. The shrinkage distortion is significant at the top-left end of the quarter plate and reduces across the right end of the quarter plate. Transverse shrinkage of decreasing value from the top-right end of the plate to the bottom right end of the plate is observed in both of the contour plots of displacement components.

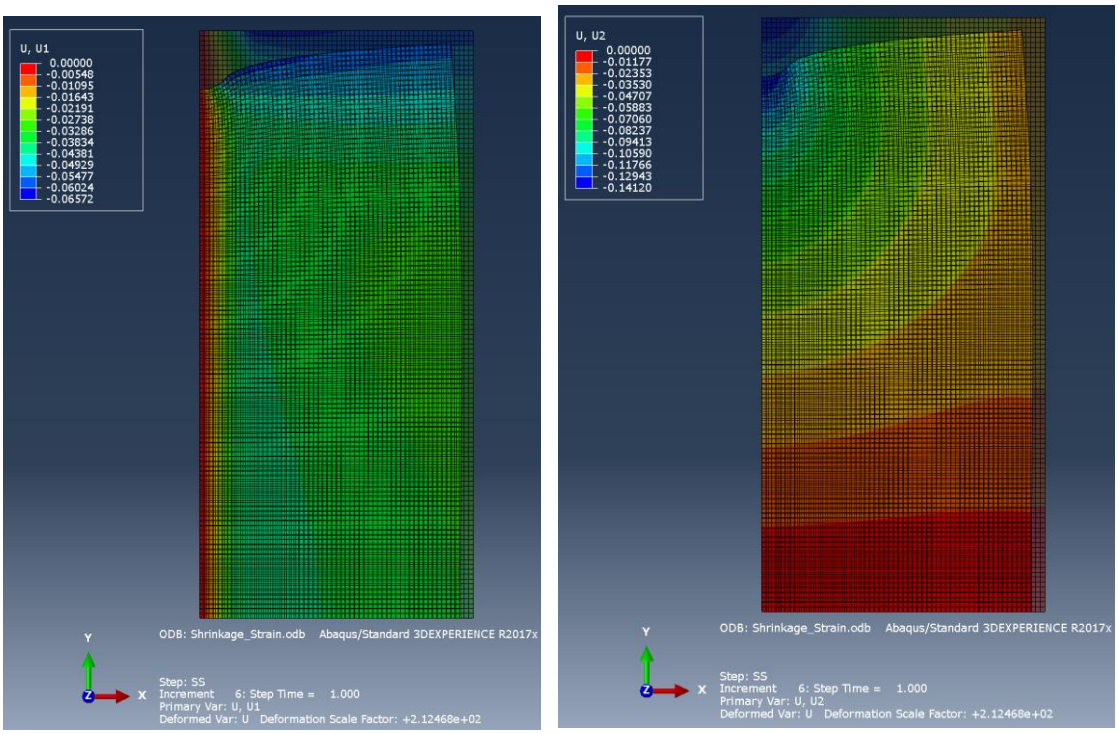

Figure 45: Deformed and undeformed (original) state contour plot for displacements along and across the welding line due to thermal cycles from shrinkage strain method (a) U1 component of displacement (b) U2 component of displacement

5.6 Comparison of Results from Thermomechanical and shrinkage strain method

5.6.1 Stress Vs. Distance Along and Across The Weld Centerline

From a thermo-mechanical analysis and a shrinkage method analysis, two components of residual stress, parallel and perpendicular, to the welding direction are obtained. The first component of the residual stress (S22) is plotted across and along the welding centerline in Figure 45 and Figure 46, respectively.

Figure 45 shows that both methods yield comparatively similar results. From zero to 20 mm, the tensile residual stress values are close to yield stress values. Both graphs see a sharp decline in the interval of ca. 20 - 30 mm, after which the curves flatten out and remain constant over the width of the plate, which means that the final compressive residual stress value is approximately one-fourth of the yield stress value across the weld centerline.

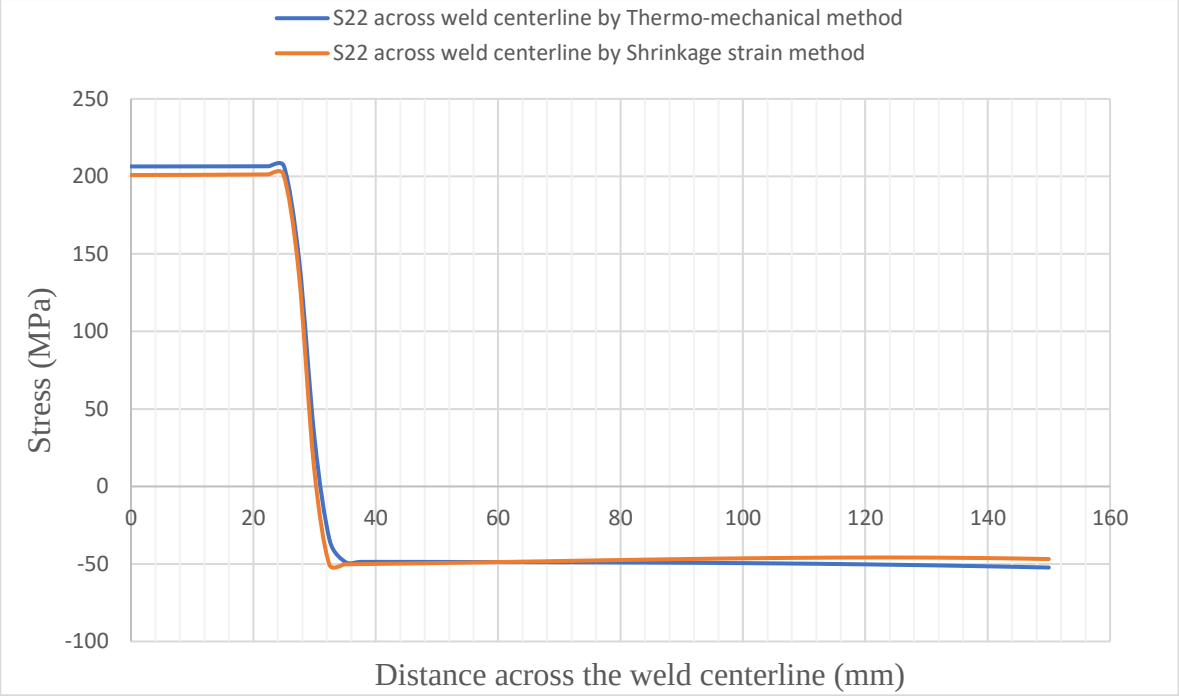

Figure 46: Comparison of S22 component of residual stress across the welding centerline from thermo-mechanical method and shrinkage strain method

Figure 46 shows the variation of the S22 component of residual stress along the welding axis. As per thermo-mechanical analysis, yield level residual stress is generated initially, which slowly increases and reaches a maximum value of 222.35 MPa at 235 mm distance

along the length of the plate. Then the value of residual stress decreases steeply over the remaining length of the plate and finally reaches a negligible value of compressive. The shrinkage strain method yields a slightly lesser tensile residual stress value than the thermo-mechanical method, measured along the weld direction initially. However, the difference in values obtained from both the study increases as the distance increases from the weld starts position till 250 mm, although the gap is reduced afterwards and finally reaches a similar compressive residual stress value.

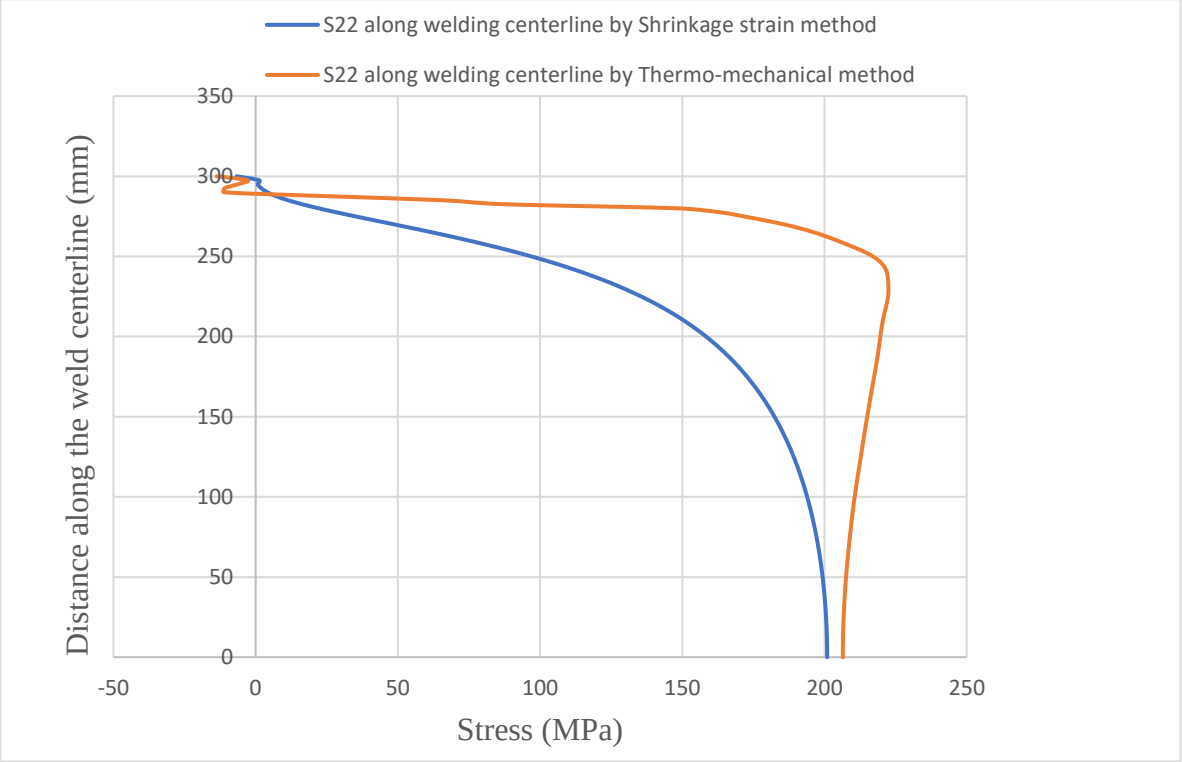

Figure 47: Comparison of S22 component of residual stress along the welding centerline from thermo-mechanical method and shrinkage strain method

Figure 50 compares the residual stress component (S11) obtained from the thermo-mechanical and shrinkage method along the welding centerline. In the shrinkage method, the tensile residual stress increases slowly along the welding direction till 225 mm, decreases steeply, and reaches a compressive yield strength at the end of the weld centerline. However, thermo-mechanical analysis shows that the S22 component of residual stress increases linearly and reaches a maximum value at 237 mm from the weld start position. At this point, there is a slight discrepancy in the residual stress obtained from these two methods. Thermo-mechanical study shows a higher value of tensile residual stress than shrinkage strain method. Finally, the shrinkage strain method also yields approximately the same value of compressive residual stress at the weld stop position.

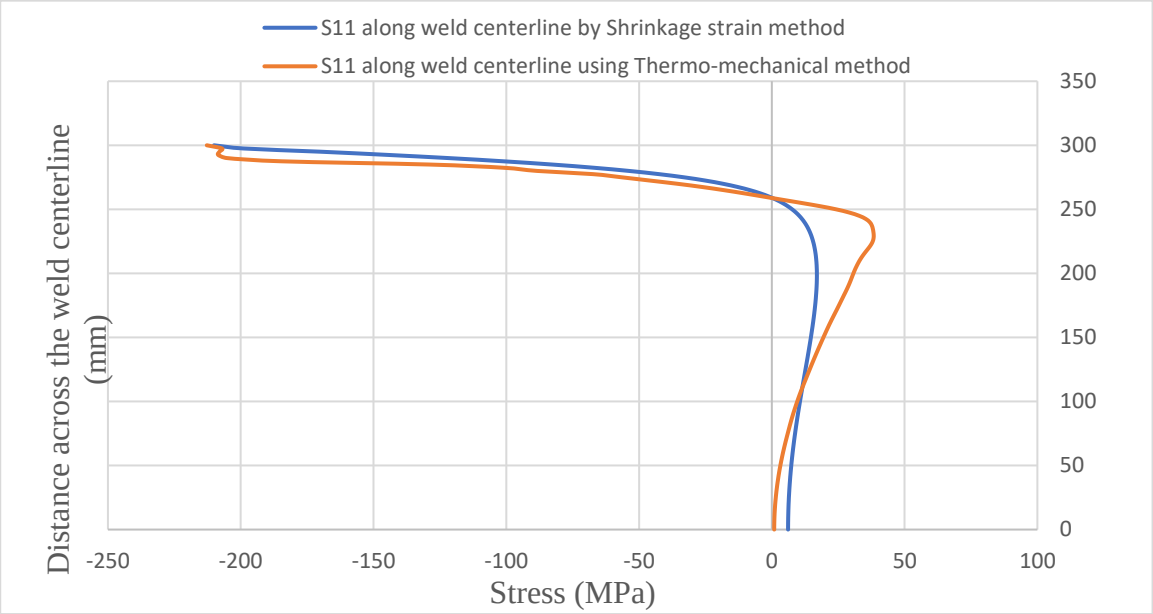

Figure 48: Comparison of S11 component of residual stress along the welding centerline from thermo-mechanical method and shrinkage strain method

The transverse residual stress component (S11) across the welding centerline measured from the thermo-mechanical study differs from the result obtained from the shrinkage strain method at the beginning, which is shown in Figure 49. Although the distance across the welding centerline increases, the transverse residual stress value decreases, and the value obtained from both methods is closer. Finally, the S11 component of transverse residual stress ceases to zero at the plate's bottom-right edge.

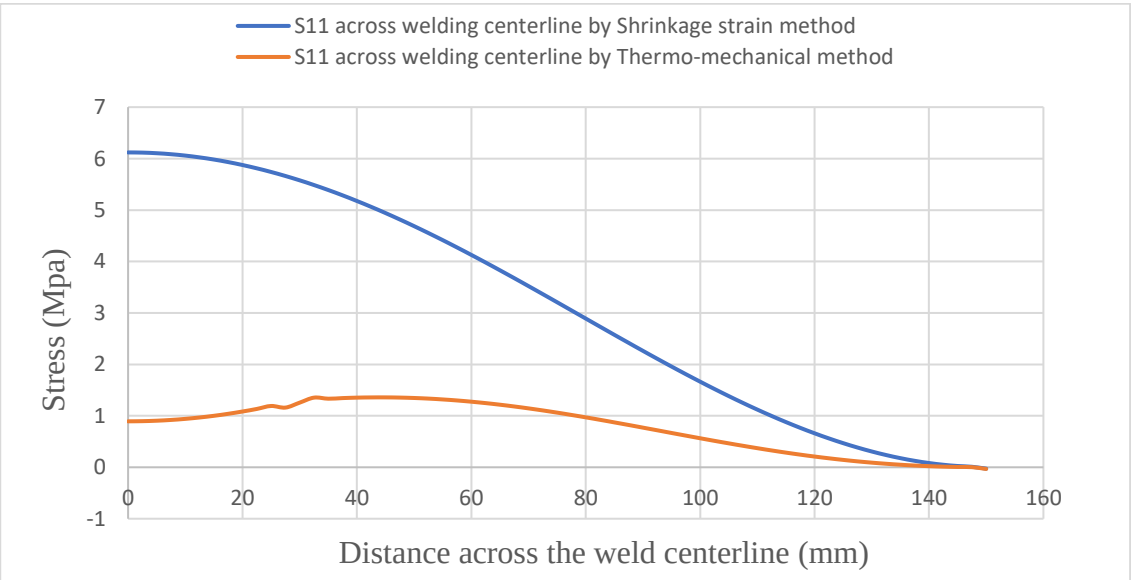

Figure 49: Comparison of S11 component of residual stress along the welding centerline from thermo-mechanical method and shrinkage strain method

5.6.2 Displacement Contour Plot Comparison

The displacement contour plots obtained from thermal-mechanical analysis and shrinkage strain method are shown in Figure 50 and Figure 51. U1 component of contour plot indicates lateral expansion in thermal and mechanical analysis contrary to no lateral expansion seen in shrinkage strain method and same is valid in case of U2 component of deformation across the welding centerline.

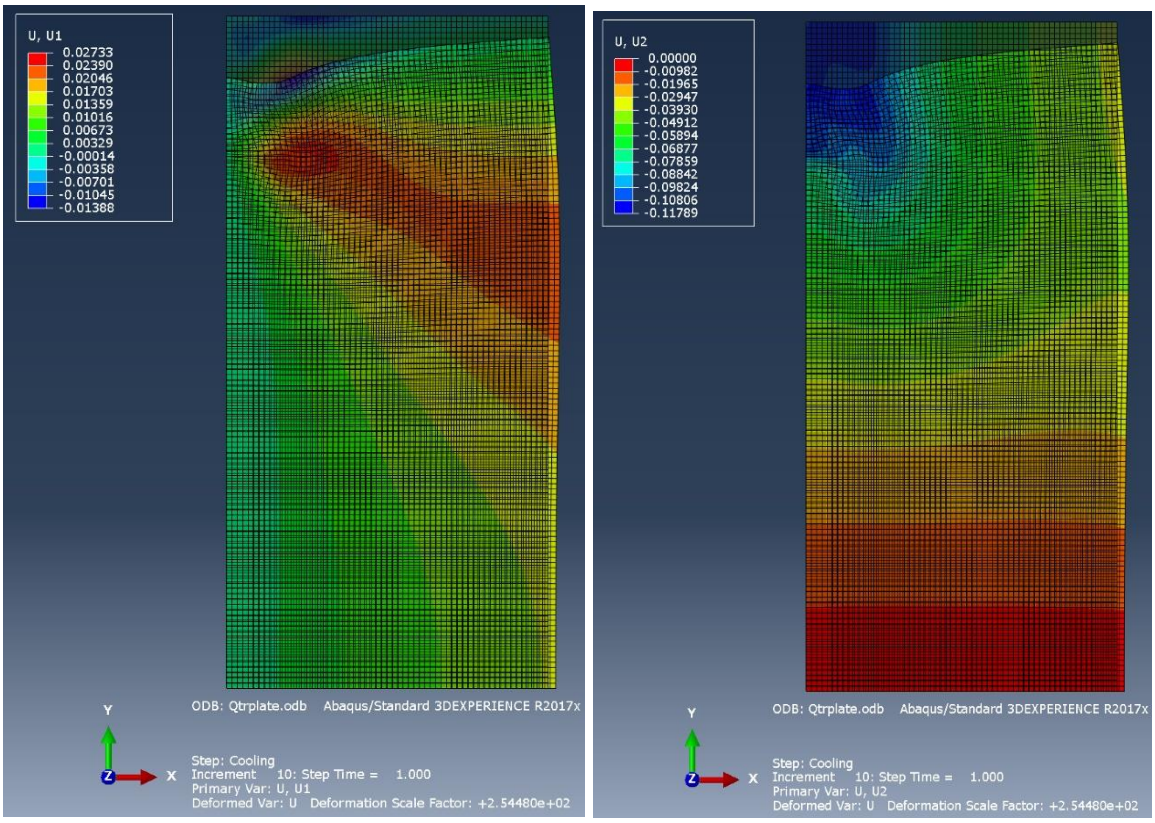

Figure 50: Displacement contour plots along and across the weld centerline using the thermo-mechanical method. U1 represents longitudinal shrinkage along the length of the welding centerline, and U2 describes transverse shrinkage across the welding line.

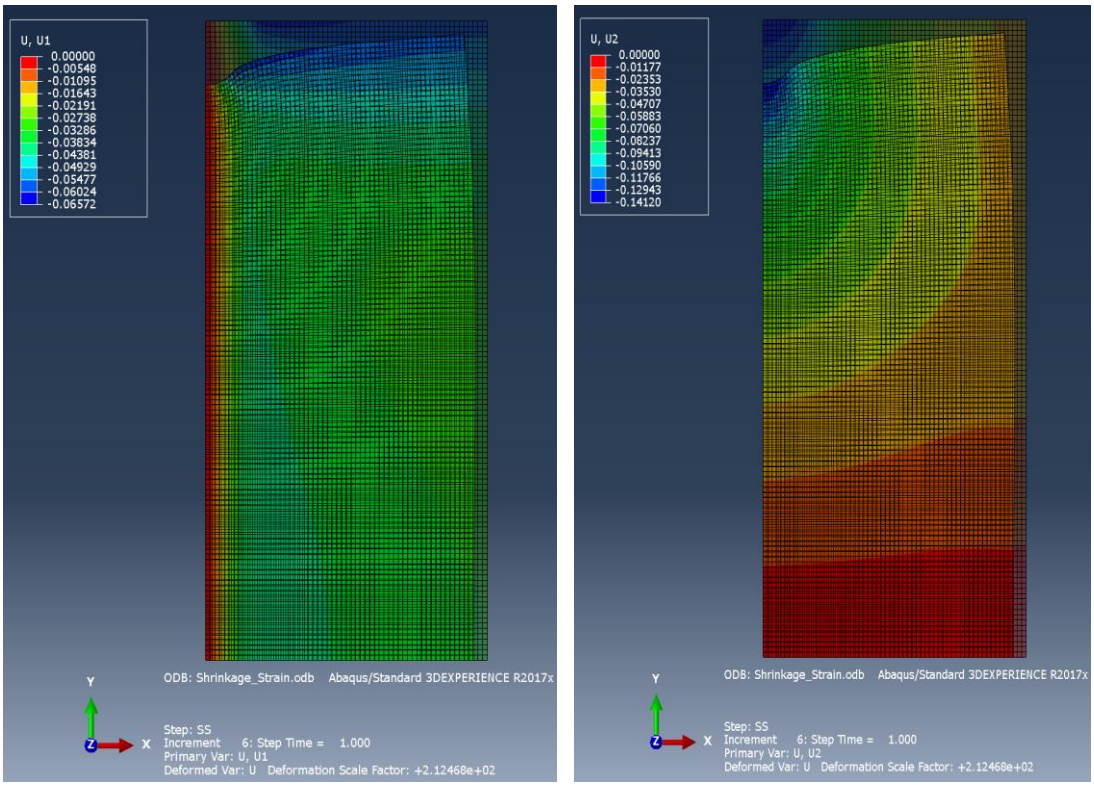

Figure 51: Displacement contour plots along and across the weld centerline using shrinkage strain method. U1 represents longitudinal shrinkage along the length of the welding centerline, and U2 describes transverse shrinkage across the welding line.

6 Conclusion

Weld subjected to high restraint conditions experiences residual stress in longitudinal and transverse directions. One-bar and three-bar models were used to demonstrate the residual stresses using analytical and finite element simulation methods. Three-bar models have been used to demonstrate the distortions occurring during the thermal cycle due to the limitations posed by the one-bar model. Results from the one-bar model show the presence of yield level tensile residual stress. Similarly, the three-bar model shows yield level tensile residual stress in the middle bar (representing weld centerline). However, sidebars (representing the remaining areas) show compressive residual stress. The compressive transverse residual stress on the sidebars is approximately equal to one-eighth of the transverse residual stress at the final stage. Since the middle bar area is around one-third of the sidebars, the residual stress is likely dependent on geometric properties.

Thermo-mechanical analysis and shrinkage strain method was also used to analyze the transverse and longitudinal stresses induced by the welding process and distortions in the welded structure. The predefined temperature field is applied to the welding axis of the quarter plate to observe

and analyze the residual stresses and distortion, using contour plots and line graphs. Thermo-mechanical analysis shows that the tensile residual stress nearly equivalent to the yield stress of the plate material is present along and across the welding centerline. Finally, the plate suffers from compressive stresses approximate to the yield strength value along the welding centerline. In contrast, nominal tensile transverse residual stress is observed across the welding centerline at the end of the thermal cycle. Longitudinal and transverse shrinkages are observed due to the tensile and compressive stresses present in overall plate geometry.

The results from the shrinkage strain method showed residual stress values closer to the results obtained from the thermo-mechanical study. Yield level residual stress calculated by analytical one-bar and three-bar models corresponded to the numerical results of the one-bar, three-bar model, thermo-mechanical simulation, and shrinkage strain method. Therefore, it can be concluded that the yield level residual stresses are induced in the thermal cycle associated with welding.

The plastic zone obtained from the thermo-mechanical analysis is larger than the shrinkage zone. Yield temperature calculated using the shrinkage zone is applied as a predefined temperature in shrinkage strain analysis. Both the shrinkage strain method and thermo-mechanical study suggest that the longitudinal shrinkage is present at the top of the plate. The transverse shrinkage value mapped in the contour plot, however, differs in two methods. The thermo-mechanical study showed lateral expansion, and the shrinkage strain method showed transverse shrinkage.

7 Further Prospects

- Consideration of rate-dependent plastic properties such as yield strength, poison's ratio, thermal conductivity, specific heat capacity, and thermal expansion coefficient is suggested in the future study. Therefore, considering these properties to generate a model can result in a more realistic model representing the actual scenario. Hence, these parameters could be considered for further study.
- The solid-state phase transformation effect can be considered to extend the research. A thermo-mechanical-metallurgical model can provide the details of microstructural changes caused by the thermal process during and after the welding process. The results obtained when including these changes can deliver more precise information about the residual stresses developed in the welded structure, which can further reinforce the material's structural integrity.

References

ABAMBRES, M. & QUACH, W.-M. 2016. Residual stresses in steel members: a review of available analytical expressions. *International Journal of Structural Integrity,* 7**,** 70-94.

ANTONINI, J. M. 2014. 8.04 - Health Effects Associated with Welding. *In:* HASHMI, S., BATALHA, G. F., VAN TYNE, C. J. & YILBAS, B. (eds.) *Comprehensive Materials Processing.* Oxford: Elsevier.

BHADESHIA, H. & HONEYCOMBE, R. 2017. Chapter 13 - Weld Microstructures. *In:* BHADESHIA, H. & HONEYCOMBE, R. (eds.) *Steels: Microstructure and Properties (Fourth Edition).* Butterworth-Heinemann.

BHADESHIA, H. & SVENSSON, L. J. M. M. O. W. P. 1993. Modelling the evolution of microstructure in steel weld metal. 1**,** 109.182.

BHIDE, S., MICHALERIS, P., POSADA, M. & DELOACH, J. J. W. J. 2006. Comparison of buckling distortion propensity for SAW, GMAW, and FSW. 85**,** 189-195.

BOKUCHAVA, G. J. C. 2018. Neutron RTOF Stress Diffractometer FSD at the IBR-2 Pulsed Reactor. 8**,** 318.

BOULTON, N. S. & MARTIN, H. E. L. 1936. Residual Stresses in Arc-Welded Plates. 133**,** 295-347.

BRUST, F. W., DONG, P. & ZHANG 1997. A constitutive model for welding process simulation using finite element methods. 51-56.

CAPELLO, E. 2005. Residual stresses in turning: Part I: Influence of process parameters. *Journal of Materials Processing Technology,* 160**,** 221-228.

CERUTTI, X. & MOCELLIN, K. 2016. Influence of the machining sequence on the residual stress redistribution and machining quality: analysis and improvement using numerical simulations. *The International Journal of Advanced Manufacturing Technology,* 83**,** 489-503.

COCHRANE, R. C. 2012. 6 - Phase transformations in microalloyed high strength low alloy (HSLA) steels. *In:* PERELOMA, E. & EDMONDS, D. V. (eds.) *Phase Transformations in Steels.* Woodhead Publishing.

COLEGROVE, P. A., COULES, H. E., FAIRMAN, J., MARTINA, F., KASHOOB, T., MAMASH, H. & COZZOLINO, L. D. 2013. Microstructure and residual stress improvement in wire and arc additively manufactured parts through high-pressure rolling. *Journal of Materials Processing Technology,* 213**,** 1782-1791.

CONNOR, L. P., O'BRIEN, R. L. & SOCIETY, A. W. 1991. *Welding Handbook: Welding processes,* American Welding Society.

DAHLMAN, P., GUNNBERG, F. & JACOBSON, M. 2004. The influence of rake angle, cutting feed and cutting depth on residual stresses in hard turning. *Journal of Materials Processing Technology,* 147**,** 181-184.

DAVID, S. & BABU, S. 1995. Microstructure modelling in weld metal. Oak Ridge National Lab.

DAVID, S. A., BABU, S. S. & VITEK, J. M. 2003. Welding: Solidification and microstructure. *JOM,* 55**,** 14-20.

DEBROY, T. & DAVID, S. A. 1995. Physical processes in fusion welding. *Reviews of Modern Physics,* 67**,** 85-112.

DENG, D. 2009. FEM prediction of welding residual stress and distortion in carbon steel considering phase transformation effects. *Materials & Design,* 30**,** 359-366.

DENKENA, B., REICHSTEIN, M. & DE LEON GARCIA, L. J. S. S. 2007. Milling induced residual stresses in structural parts out of forged aluminium alloys, proceedings of the 6th international conference on HSM 2007.

DING, Y.-L., SONG, Y.-S., CAO, B.-Y., WANG, G.-X. & LI, A.-Q. 2016. Full-Range S-N Fatigue-Life Evaluation Method for Welded Bridge Structures Considering Hot-Spot and Welding Residual Stress. *Journal of Bridge Engineering,* 21**,** 04016096.

DONG, P. 2001. Residual stress analyses of a multi-pass girth weld: 3-D special shell versus axisymmetric models. *J. Pressure Vessel Technol.,* 123**,** 207-213.

DONG, P. 2005. Residual stresses and distortions in welded structures: a perspective for engineering applications. *Science and Technology of Welding and Joining,* 10**,** 389-398.

DONG, P. J. W. I. T. W. 2018. On repair weld residual stresses and significance to structural integrity. 62**,** 351-362.

EL-KHABEERY, M. M. & FATTOUH, M. 1989. Residual stress distribution caused by milling. *International Journal of Machine Tools and Manufacture,* 29**,** 391-401.

FINCH, D. 1994. *A review of non-destructive residual stress measurement techniques*, ERA Technology Limited Surrey.

FRIEDMAN, E. 1975. Thermomechanical analysis of the welding process using the finite element method.

FUJITA, Y. & NOMOTO, T. Studies of thermal stresses in welding with special reference to weld cracking. First International Symposium on Cracking and Fracture in Welds, Tokyo, 1971.

FUJITA, Y., TAKESHI, Y., KITAMURA, M. & NOMOTO, T. J. I. D. X.-.-. 1972. Welding stresses with special reference to cracking.

GERY, D., LONG, H. & MAROPOULOS, P. J. J. O. M. P. T. 2005. Effects of welding speed, energy input and heat source distribution on temperature variations in butt joint welding. 167**,** 393-401.

GLICKSTEIN, S. S. & FRIEDMAN, E. 1993. Characterization and modelling of the heat source. United States: Westing house Electric Corp.

Bettis Atomic Power Laboratory.

GOLDAK, J., CHAKRAVARTI, A. & BIBBY, M. 1984a. A new finite element model for welding heat sources. *Metallurgical transactions B,* 15**,** 299-305.

GOLDAK, J., CHAKRAVARTI, A. & BIBBY, M. J. M. T. B. 1984b. A new finite element model for welding heat sources. 15**,** 299-305.

HOSSAIN, S., TRUMAN, C., SMITH, D. & BOUCHARD, P. 2006. Measurement of residual stresses in a type 316H stainless steel offset repair in a pipe girth weld.

HOWELL, L. L., MAGLEBY, S. P., OLSEN, B. M. & WILEY, J. 2013. *Handbook of compliant mechanisms*, Wiley Online Library.

HUANG, T. D., CONRARDY, C., DONG, P., KEENE, P., KVIDAHL, L. & DECAN, L. 2007. Engineering and Production Technology for Lightweight Ship Structures, Part II: Distortion Mitigation Technique and Implementation. *Journal of Ship Production,* 23**,** 82-93.

HUANG X, L. Z., XIE H 2013. Recent progress in residual stress measurement techniques.

ION, J. C., EASTERLING, K. E. & ASHBY, M. F. 1984. A second report on diagrams of microstructure and hardness for heat-affected zones in welds. *Acta Metallurgica,* 32**,** 1949-1962.

IWAKI, T. & MASUBUCHI, K. J. J. S. N. A. J. 1971. Thermo-elastic analysis of orthotropic plastic by the finite element method. 130**,** 195-204.

JAVADI, Y., NAJAFABADI, M. A. J. M. & DESIGN 2013. Comparison between contact and immersion ultrasonic method to evaluate welding residual stresses of dissimilar joints. 47**,** 473-482.

JIANG, W., YAHIAOUI, K., HALL, F. & LAOUI, T. 2005. Finite element simulation of multipass welding: Full three-dimensional versus generalized plane strain or axisymmetric models. *The Journal of Strain Analysis for Engineering Design,* 40**,** 587-597.

KANDIL, F., LORD, J., FRY, A. T. & GRANT, P. 2001. A review of residual stress measurement methods-a guide to technique selection.

KARAOĞLU, S. & SEÇGIN, A. 2008. Sensitivity analysis of submerged arc welding process parameters. *Journal of Materials Processing Technology,* 202**,** 500-507.

KARLSSON, L., PAHKAMAA, A., KARLBERG, M., LÖFSTRAND, M., GOLDAK, J., PAVASSON, J. J. J. O. M. O. M. & STRUCTURES 2011. Mechanics of materials and structures: a simulation-driven design approach. 6**,** 277-301.

KATTOURA, M., MANNAVA, S. R., QIAN, D. & VASUDEVAN, V. K. 2017. Effect of laser shock peening on residual stress, microstructure and fatigue behavior of ATI 718Plus alloy. *International Journal of Fatigue,* 102**,** 121-134.

KEE PAIK, J. & MIN SOHN, J. 2012. Effects of welding residual stresses on high tensile steel plate ultimate strength: nonlinear finite element method investigations. *Journal of offshore mechanics and Arctic engineering,* 134.

KELA., A., VOELCKER, H. & GOLDAK, J. A. 1984. Automatic generation of finite element meshes from CSG representations of solids. *International conference on accuracy estimates and adaptive refinements in finite element computations (ARFEC).* Lisbon: International Association of Computational Mechanies.

KESAVAN, K., RAVISANKAR, K., PARIVALLAL, S. & SREESHYLAM, P. J. E. T. 2005. Non destructive evaluation of residual stresses in welded plates using the Barkhausen noise technique. 29**,** 17-21.

KHAN, M. I. 2007. *Welding science and technology,* New Delhi, New Age International (P) Ltd., Publishers.

KHORAL, P. 1992. Coupling microstructure to heat transfer computation in weld analysis.

KIHARA, H. & MASUBUCHI, K. 1954. Studies on the shrinkage and residual welding stresses of constrained fundamental joint. *Society of Naval Architects of Japan,* 95**,** 181-195.

KOHANDEHGHAN, A. R. & SERAJZADEH, S. 2011. Arc welding induced residual stress in butt-joints of thin plates under constraints. *Journal of Manufacturing Processes,* 13**,** 96-103.

KOU, S. 2002. Fusion Welding Processes. *Welding Metallurgy.* 2nd ed. New Jersey: John Wiley & Sons, Inc.

KUMAR, K. S. J. P. M. S. 2014. Analytical modelling of temperature distribution, peak temperature, cooling rate and thermal cycles in a solid work piece welded by laser welding process. 6**,** 821-834.

LEGGATT, R. H. 2008. Residual stresses in welded structures. *International Journal of Pressure Vessels and Piping,* 85**,** 144-151.

LI, C., LIU, Z., FANG, X. & GUO, Y. J. P. C. 2018. Residual stress in metal additive manufacturing. 71**,** 348-353.

LI, C., WANG, Y., HAN, T., HAN, B. & LI, L. 2011. Microstructure and toughness of coarse grain heat-affected zone of domestic X70 pipeline steel during in-service welding. *Journal of Materials Science,* 46**,** 727-733.

LI, C., WHITE, R., FANG, X., WEAVER, M., GUO, Y. J. M. S. & A, E. 2017. Microstructure evolution characteristics of Inconel 625 alloy from selective laser melting to heat treatment. 705**,** 20-31.

LINDGREN, L.-E. J. J. O. T. S. 2001. Finite element modelling and simulation of welding part 1: increased complexity. 24**,** 141-192.

LINDGREN, L. E. 2007. *Computational Welding Mechanics: Thermomechanical and Microstructructural Simulations (Woodhead Publishing in materials),* Woodhead Publishing.

LONG, H., GERY, D., CARLIER, A., MAROPOULOS, P. J. M. & DESIGN 2009. Prediction of welding distortion in butt joint of thin plates. 30**,** 4126-4135.

LU, J. 1996. *Handbook of measurement of residual stresses,* Fairmont Press.

LUNDIN, C. D. 1983. Discontinuities in welds — Cause and effect. *Journal of Materials for Energy Systems,* 5**,** 123-130.

M. LARSSON, M. L. 2019. *Investigation of Material Property changes in HSLA Steel due to Weld Proximity.* Master of Science in Engineering and Materials(Mechanical Systems), University of Stavanger.

M.BENSON, P. R., J.WALLACE 2018. Weld Residual Stress Finite Element Analysis Validation. *Proposed Validation Procedure-II.* U.S.N.R.C.: Office of Nuclear Regulatory Research.

M.S., S. & K.H., L. 1984. The modified-quadtree mesh generator and adaptive analysis. *International conference on accuracy estimates and refinements in finite element computations (ARFEC).* Lisbon: International Association of Computational Mechanics.

MA, N., NAKACHO, K., OHTA, T., OGAWA, N., MAEKAWA, A., HUANG, H. & MURAKAWA, H. Inherent strain method for residual stress measurement and welding distortion prediction. ASME 2016 35th International Conference on Ocean, Offshore and Arctic Engineering, 2016. American Society of Mechanical Engineers Digital Collection.

MACKERLE, J. 1996. Finite element analysis and simulation of welding: a bibliography (1976 - 1996). *Modelling and Simulation in Materials Science and Engineering,* 4**,** 501-533.

MACKERLE, J. 2002. Finite element analysis and simulation of welding - an addendum: a bibliography (1996-2001). *Modelling and Simulation in Materials Science and Engineering,* 10**,** 295-318.

MARUSICH, T. & ASKARI, E. Modelling residual stress and workpiece quality in machined surfaces. Proceedings of the 4th CIRP International Workshop on Modelling of Machining Operations, Delft, The Netherlands, 2001. Citeseer, 105-109.

MASMIATI, N., SARHAN, A. A. D., HASSAN, M. A. N. & HAMDI, M. 2016. Optimization of cutting conditions for minimum residual stress, cutting force and surface roughness in end milling of S50C medium carbon steel. *Measurement,* 86**,** 253-265.

MASUBUCHI, K., SIMMONS, F. & MONROE, R. 1968. Analysis of thermal stresses and metal movement during welding. BATTELLE MEMORIAL INST COLUMBUS OHIO.

MASUBUCHI, K. J. W. J. 1960. Analytical investigation of residual stresses and distortions due to welding. 39**,** 525s-537s.

MCDILL, J., GOLDAK, J., ODDY, A. & BIBBY, M. J. C. I. A. N. M. 1987. Isoparametric quadrilaterals and hexahedrons for mesh-grading algorithms. 3**,** 155-163.

MESSLER, R. W. 2008. *Principles of Welding: Processes, Physics, Chemistry, and Metallurgy*, Wiley.

MONTANARI, R., FAVA, A. & BARBIERI, G. 2017. Experimental techniques to investigate residual stress in joints. *Residual Stress Analysis on Welded Joints by Means of Numerical Simulation and Experiments.* IntechOpen.

NAIDU, D. S., OZCELIK, S. & MOORE, K. L. 2003. Chapter 2 - Gas Metal Arc Welding: Modelling. *In:* NAIDU, D. S., OZCELIK, S. & MOORE, K. L. (eds.) *Modelling, Sensing and Control of Gas Metal Arc Welding.* Oxford: Elsevier Science Ltd.

NATSUME, S., GOTOH, A. & NAKAGAWA, T. 1995. Submerged arc welding method for high strength Cr-Mo steel. Google Patents.

NORONHA, P. J., CHAPMAN, J. R. & WERT, J. J. 1973. Residual Stress Measurement and Analysis Using Ultrasonic Techniques. *Journal of Testing and Evaluation,* 1**,** 209-214.

NORRISH, J. 2006. 7 - Gas metal arc welding. *In:* NORRISH, J. (ed.) *Advanced Welding Processes.* Woodhead Publishing.

PAIK, J. J. W. J. O. E. & TECHNOLOGY 2018. Three-dimensional thermo-elastic-plastic finite element method modelling for predicting weld-induced residual stresses and distortions in steel stiffened-plate structures. 6**,** 176-200.

PAVELIC, V. & KC, T. 1980. WELD PUDDLE SHAPE AND SIZE CORRELATION IN A METAL PLATE WELDED BY THE GAS TUNGSTEN ARC PROCESS.

PILIPENKO, A. 2001. *Computer simulation of residual stress and distortion*

of thick plates

in multi-electrode submerged arc welding.

Their mitigation techniques. PhD, Norwegian University of Science and

Technology (NTNU).

PRIME, M. & GONZALES, A. 2000. The contour method: simple 2-D mapping of residual stresses. Los Alamos National Lab., NM (US).

PROMOPPATUM, P., YAO, S.-C., PISTORIUS, P. C. & ROLLETT, A. D. 2017. A comprehensive comparison of the analytical and numerical prediction of the thermal history and solidification microstructure of Inconel 718 products made by laser powder-bed fusion. *Engineering,* 3**,** 685-694.

RADAJ, D. 1992. Welding residual stress and distortion. *Heat Effects of Welding: Temperature Field, Residual Stress, Distortion.* Berlin, Heidelberg: Springer Berlin Heidelberg.

REQUICHA, A. A., VOELCKER, H. B. J. I. C. G. & APPLICATIONS 1983. Solid modelling: Current status and research directions. 3**,** 25-37.

RODGER, E. & FLETCHER, R. J. W. J. R. S. 1938. The Determination of Internal Stresses from the Temperature History of a Butt Welded Pipe. 17**,** 4-7.

ROSENTHAL, D. 1941. Mathematical theory of heat distribution during welding and cutting. *Welding journal,* 20**,** 220-234.

ROSENTHAL, D. J. W. 1940. Temperature distribution and shrinkage stresses in arc welding. 19**,** 323-331.

ROSSINI, N., DASSISTI, M., BENYOUNIS, K., OLABI, A.-G. J. M. & DESIGN 2012. Methods of measuring residual stresses in components. 35**,** 572-588.

RUUD, C. J. N. I. 1982. A review of selected non-destructive methods for residual stress measurement. 15**,** 15-23.

SCHAJER, G. 1981. Application of finite element calculations to residual stress measurements.

SEYYEDIAN CHOOBI, M., HAGHPANAHI, M. & SEDIGHI, M. 2012. Effect of welding sequence and direction on angular distortions in butt-welded plates. 47**,** 46-54.

SHI, Y. & HAN, Z. 2008. Effect of weld thermal cycle on microstructure and fracture toughness of simulated heat-affected zone for a 800MPa grade high strength low alloy steel. *Journal of Materials Processing Technology,* 207**,** 30-39.

SHOME, M. 2007. Effect of heat-input on austenite grain size in the heat-affected zone of HSLA-100 steel. *Materials Science and Engineering: A,* 445-446**,** 454-460.

SHOME, M., GUPTA, O. P. & MOHANTY, O. N. 2004. Effect of simulated thermal cycles on the microstructure of the heat-affected zone in HSLA-80 and HSLA-100 steel plates. *Metallurgical and Materials Transactions A,* 35**,** 985-996.

SMITH, P. 2007. CHAPTER 6 - Fabrication, Assembly, and Erection. *In:* SMITH, P. (ed.) *The Fundamentals of Piping Design.* Gulf Publishing Company.

SONG, J., ZHANG, L., WU, W., HE, B., NI, X., XU, J., ZHU, G., YANG, Q., WANG, T. & LU, L. 2019. Understanding processing parameters affecting residual stress in selective laser melting of Inconel 718 through numerical modelling. *Journal of Materials Research,* 34**,** 1395-1404.

SONG, S. 2012. *Analysis and Characterization of Residual Stresses in Pipe and Vessel Welds.* PhD, University of New Orleans.

SUMAN, S. & BISWAS, P. J. M. T. P. 2020. Thermo-mechanical study of single and multi-pass welding of CSEF steel for residual stresses and deformations considering solid state phase transformation. 28**,** 789-795.

TALL, L. Residual stresses in welded plates - a theoretical study, No. 235 (64-1). Presented at the Spring Meeting of the AWS in Dallas, (September 1961). 1961.

TANG, Z. T., LIU, Z. Q., PAN, Y. Z., WAN, Y. & AI, X. 2009. The influence of tool flank wear on residual stresses induced by milling aluminum alloy. *Journal of Materials Processing Technology,* 209**,** 4502-4508.

TEBEDGE, N., ALPSTEN, G. & TALL, L. 1973a. Residual-stress measurement by the sectioning method. *Experimental Mechanics,* 13**,** 88-96.

TEBEDGE, N., ALPSTEN, G. & TALL, L. J. E. M. 1973b. Residual-stress measurement by the sectioning method. 13**,** 88-96.

TOMUS, D., TIAN, Y., ROMETSCH, P. A., HEILMAIER, M., WU, X. J. M. S. & A, E. 2016. Influence of post heat treatments on anisotropy of mechanical behaviour and microstructure of Hastelloy-X parts produced by selective laser melting. 667**,** 42-53.

TOTTEN, G. E., HOWES, M. A. H. & INOUE, T. 2002. *Handbook of residual stress and deformation of steel / [E-Book],* Materials Park, OH, ASM International.

TSAI, C., PARK, S. & CHENG, W. J. W. J.-N. Y.-. 1999. Welding distortion of a thin-plate panel structure. 78**,** 156-s.

UEDA, Y., MURAKAWA, H. & MA, N. 2012. Chapter 1 - Introduction to Welding Mechanics. *In:* UEDA, Y., MURAKAWA, H. & MA, N. (eds.) *Welding Deformation and Residual Stress Prevention.* Boston: Butterworth-Heinemann.

UEDA, Y. & YAMAKAWA, T. Mechanical characteristics of cracking of welded joints. Proc. of The 1st Int. Symp. of the Japan Welding Society, Tokyo, 1971a.

UEDA, Y. & YAMAKAWA, T. J. J. W. S. T. 1971b. Analysis of thermal elastic-plastic stress and strain during welding by finite element method. 2.

UEDA, Y. & YAMAKAWA, T. J. M. B. O. M. 1972. Thermal stress analysis of metals with temperature dependent mechanical properties. 10-20.

WAHAB, M. A. 2014. 6.03 - Manual Metal Arc Welding and Gas Metal Arc Welding. *In:* HASHMI, S., BATALHA, G. F., VAN TYNE, C. J. & YILBAS, B. (eds.) *Comprehensive Materials Processing.* Oxford: Elsevier.

WATT, D., COON, L., BIBBY, M., GOLDAK, J. & HENWOOD, C. J. A. M. 1988. An algorithm for modelling microstructural development in weld heat-affected zones (part a) reaction kinetics. 36**,** 3029-3035.

WEMAN, K. 2012. 9 - Manual metal arc (MMA) welding with coated electrodes. *In:* WEMAN, K. (ed.) *Welding Processes Handbook (Second Edition).* Woodhead Publishing.

WITHERS, P., BHADESHIA, H., WITHERS, P. & BHADESHIA, H. 2016. Residual stress. Part 1–Measurement techniques Residual stress Part 1–Measurement techniques. vol.

WITHERS PJ, T. M., EDWARDS L, BOUCHARD PJ, BUTTLE DJ 2008. Recent advances in residual stress measurement. *International Journal of Pressure Vessels and Piping***,** 118-127.

WITHERS, P. J. R. O. P. I. P. 2007. Residual stress and its role in failure. 70**,** 2211.

YANG, Y., LI, M. & LI, K. J. T. I. J. O. A. M. T. 2014. Comparison and analysis of main effect elements of machining distortion for aluminum alloy and titanium alloy aircraft monolithic component. 70**,** 1803-1811.

ZACHARIA, T., VITEK, J. M., GOLDAK, J. A., DEBROY, T. A., RAPPAZ, M. & BHADESHIA, H. K. D. H. 1995. Modelling of fundamental phenomena in welds. *Modelling and Simulation in Materials Science and Engineering,* 3**,** 265-288.